DOE/ET-53088-595 IFSR #595

Arbitrary Mode Number Boundary Layer Theory for Non-Ideal Toroidal Alfvén Modes

H.L. BERK, R.R. METT, and D.M. LINDBERG
Institute for Fusion Studies
The University of Texas at Austin
Austin, Texas 78712

March 1993

Arbitrary Mode Number Boundary Layer Theory for Non-Ideal Toroidal Alfvén Modes

H.L. Berk, R.R. Mett, and D.M. Lindberg
Institute for Fusion Studies
The University of Texas at Austin
Austin, Texas 78712

Abstract

The present work generalizes the theory of toroidicity-induced Alfvén eigenmodes (TAE) and kinetic TAE (KTAE) to arbitrary mode numbers for a large aspect ratio low-beta circular tokamak with appropriate boundary conditions. The method divides the problem into an outer region, described by ideal magnetohydrodynamics (MHD) in cylindrical geometry, and an inner region, which includes the toroidicity and the nonideal effects of finite Larmor radius, electron inertia, and collisional effects. Eigenmodes are obtained by asymptotically matching the solutions over the entire radial extent of the plasma. The method systematically describes the rich spectrum of TAE and KTAE modes. The complete interaction between nearest neighbor TAE/KTAE is described by a three term recursion relation. The solubility of this relation leads to the dispersion relation for the eigenfrequencies. By using quadratic forms, the analytic description is proven to be intrinsically stable when nonideal effects outside the scope of the lowest order theory are neglected. The formulation also indicates how perturbation theory can be applied to include complex frequency shifts due to the neglected nonideal effects. For moderately small nonideal effects, simple analytic forms using WKB theory and parabolic cylinder functions (which may be approximately expressed

as gamma functions) are developed. The WKB approximations are extremely accurate over the entire frequency spectrum except very close to the edge of the gap. Here, the cylinder functions are most accurate, completing the analytic picture over the full range of frequencies. The analytic descriptions explicitly show the competition between the resistive damping and that due to radiation of kinetic Alfvén waves (KAW). The radiative damping is frequently found to dominate the damping of the TAE for moderate values of the nonideal parameter, but not the KTAE. For small nonideal effects, the KTAE modes are found to occur in pairs close to the odd eigenmodes of the homogeneous inner layer equation. For large nonideal effects, another analytic description is developed that reproduces the scaling found previously for the single gap case.

I. Introduction

There has been considerable interest in recent years in understanding the structure of Alfvén waves in toroidal geometry. Initial work noted that the Alfvén continuum can be intrinsically modified in toroidal geometry.[1,2] This modification gives rise to the Toroidicity-induced Alfvén Eigenmode (TAE).[3,4] In Ref. 3 there was further study of how resistivity gives rise to an additional set of damped Alfvén modes.

More recently, methods have been developed to estimate the continuum damping that is associated with TAE modes due to the overlap of eigenfunctions onto different resonant surfaces.[5–7] The method developed in Ref. 6, for localized high-n modes of a large aspect ratio low-beta plasma, was generalized somewhat in Ref. 8, to take into account the change in safety factor and plasma density across the radial extent of an eigenmode when the n-value is not too small. In the present work we show how the method is extended to systematically account for arbitrary n-values.

Mett and Mahajan[9,10] pointed out the significance of nonideal effects (finite parallel electric fields) on the TAE mode. They pointed out that it produces additional damping on the TAE mode and introduces a new family of Kinetic Toroidal Alfvén Eigenmodes (KTAE), which are related to the resistive modes reported earlier.[3] The additional damping of the TAE is a form of radiation damping. It is a component that is not linearly proportional to the dissipative effects, and for that reason Mett and Mahajan called it "non-perturbative." We shall call this component radiative damping or "tunneling" for reasons discussed below. The KTAE are important because they are weakly damped when realistic electron collisionality effects are taken into account. Mett and Mahajan's theory considers a single pair of poloidal harmonics interacting near one resonant surface. Consequently, the theory does not properly account for the eigenmode structure outside the gap region.

Candy and Rosenbluth[11] developed the nonideal theory in the high-n limit, taking into account that toroidal modes couple between the resonant surfaces. The problem is divided into an outer region, which is described by the MHD equations in slab geometry, and an inner region near the resonant surface, which is described by equations that contain toroidal and nonideal effects, including finite parallel electron conductivity and ion Larmor radius. They obtained a three-term recursion relation that is an extension of the one derived in Ref. 6. Their theory accounts for multiple TAE and KTAE resonant regions. In addition, they show that in the limit of weak nonideal effects, the placement of branch lines for the TAE modes in the complex ω-plane is determined by the nonideal theory. These lines are the limit of a set of poles in the complex ω-plane, with each pole associated with a KTAE mode.

The purpose of the present work is to generalize the description of TAE and KTAE modes to arbitrary n-number for the model of a large aspect ratio low-beta circular tokamak. The outer region is described by the MHD equations in the cylindrical limit. The solutions of these equations, which depend on boundary conditions and which must in general be numerically solved, are matched to the inner regions. One needs to extract from the external solutions a larger number of constants than was needed in the slab model used in the high-n limit of Refs. 6 and 8, and a comparison with the results of the previous theories will be given. Substantial differences can arise.

The theory for inner layer equations are developed in a manner similar to Ref. 11. Using suitable transformations, a set of inner layer equations can be obtained with the same symmetry structure as exhibited in Ref. 11 in the high-n limit. It turns out that the low-n corrections for the inner layer equations are usually small, even for $n = 1$. The solutions of the inner layer equations are performed numerically. In addition, an asymptotic evaluation of the solutions are made in appropriate limits, and improvements are achieved in the analytic results from those reported in Ref. 11. In particular, compact formulas are obtained

for describing the effect of radiation damping on TAE modes and for describing the analytic response of the KTAE mode. In addition, we formulate our problem in such a manner so that it is clearly apparent how to introduce the perturbative effects on the TAE and KTAE modes of additional currents (e.g. from energetic particles, other plasma kinetic effects such as ion Landau damping, etc.). In this formulation we obtain a concise variational form that leads to the three term recursion relation. From the variational formulation we are able to exhibit the intrinsic stability of the system when additional kinetic currents are absent. When these currents are included, the variational structure of the equation leads to the physical property that the imaginary frequency shift is determined by the condition that the time rate of change of wave energy of the zeroth order solution is equal to the rate of energy transfer from the kinetic current carriers to the electromagnetic field.

In order to calculate thresholds for instability, it is necessary to calculate the power transfer from energetic particles as well as from other stabilizing kinetic current sources. A detailed study of such threshold conditions will be presented in a forthcoming paper, using the formalism and numerical tools developed in this work. Some preliminary results of this calculation are given in Ref. 12.

For the purposes of this work, we will analyze in detail numerical results for the n=1 mode. In the important case of resonance at $q = 3/2$, involving the interaction of the $m = 1$ and $m = 2$ poloidal harmonics, the three term recursion relation reduces to a simple form that was given in Ref. 5. This simple form is compared with model of Mett and Mahajan,[9] and we show how the results correlate between the two models.

The paper is divided as follows. In Sec. II we derive the structure of the three-term recursion relation in terms of the constants $\overline{\Delta}$ and $\widetilde{\Delta}$ that are obtained from the outer MHD equations, and analytic functions $\alpha(\omega)$ and $\beta(\omega)$ that are obtained from the inner layer equations. In this section we also discuss how a perturbative theory can be developed to calculate frequency shifts due to additional kinetic currents. The theory for determining α

and β from the ideal theory is developed in Sec. III, and the corrections due to finite-n are obtained from the results of previous theories. In Sec. IV the theory for determining α and β with nonideal effects included is developed. In Sec. V we present some numerical results. This paper is augmented by a set of Appendices that discuss: (1) how the external constants $\overline{\Delta}$ and $\widetilde{\Delta}$ are numerically calculated, (2) a proof of the stability of the 3-term recursion relation, and how to obtain accurate approximations of the α and β values in appropriate domains using (3) gamma functions, (4) WKB theory, and (5) another approximation valid when the kinetic parameter is large.

II. Derivation of Equations

We start with the reduced MHD equation for a large aspect ratio, low beta, tokamak, together with contributions from small perturbing currents from kinetic effects. We use the form derived in Ref. 5,

$$\frac{d}{dr}\widehat{C}_{m,n}(r)-(m^2-1)\left(\Omega^2\rho(r)-k_{m,n}^2\right)\phi_{m,n}+\Omega^2 r\,\frac{\partial\rho(r)}{\partial r}\,\phi_{m,n}=\frac{-4\pi i\omega\, r^2}{c^2}\sum_j e_j\boldsymbol{\nabla}\cdot\int d^3v\,\mathbf{v}\delta h_{jm} \tag{1}$$

where $\Omega^2 = \omega^2 R_0^2/v_{A0}^2$, R_0 the major radius, v_{A0} the Alfvén speed at $r = 0$, $\rho(r) = n_i(r)/n_i(r=0)$ is the relative ion density, $k_{m,n}^2 = (m/q(r) - n)^2$ is the square of the normalized parallel wave number, δh_{jm} the mth poloidal component of the "non-adiabatic" part of the distribution function of species j, $\widehat{C}_{m,n}(r)$, which we refer to as the flux of the mth poloidal and nth toroidal harmonic, is given by

$$\widehat{C}_{m,n}(r) = r^3\left(\Omega^2\rho(r)-k_{m,n}^2\right)\frac{\partial(\phi_{m,n}/r)}{\partial r}+\widehat{\varepsilon}r^3\rho(r)\Omega^2\left(\frac{\partial(\phi_{m-1,n}/r)}{\partial r}+\frac{\partial(\phi_{m+1,n}/r)}{\partial r}\right) \tag{2}$$

with ϕ_{mn} the harmonic of the electrostatic potential (we will now suppress the subscript n, except when first introducing a subscripted parameter) and $\widehat{\varepsilon} = 5r/2R_0$. We take $q(r)$ to be monotonically increasing as a function of r and then $q_0 < q < q_a$ with $q_0 \equiv q(r{=}0)$

and $q_a \equiv q(r{=}a)$ with $r = a$ the plasma boundary. We take $\phi(r{=}a) = 0$ as our boundary condition.

The assumption of the TAE mode nearest neighbor model is that toroidal coupling is unimportant over most of the plasma. However, near a TAE resonance, where $r \approx r_{m,n}$ where $q(r_m) = q_{m,n} = (m + 1/2)/n$, and when $\Omega \simeq 1/(2q_m\rho^{1/2}(r_m)) \equiv \Omega_{m,n}$, the interaction between the m and $m + 1$ poloidal harmonic is important. Thus, each poloidal harmonic, m, has up to two narrow regions where toroidal coupling is important; $r \approx r_{m-1}$ where the m and $m - 1$ poloidal harmonics interact and $r \approx r_m$, where the m and $m + 1$ harmonics interact. Outside these regions $\phi_m(r)$ nearly satisfies Eq. (2) with $\hat{\varepsilon} = 0$. Thus, for $r < r_{m-1}$, $\phi_m(r)$ is approximately given by the function

$$\phi_m(r) \sim C_m^- \phi_m^{(a)}(r) \tag{3}$$

where $\phi_m^{(a)}(r)$ satisfies Eqs. (1) and (2) with $\hat{\varepsilon} = 0$ (without the kinetic term) and $\Omega^2 = \Omega_{m-1}^2$. Note that $\phi_m^{(a)}$ is well behaved at the origin and has the property that

$$\phi_m^{(a)}(r) \longrightarrow \ln\left[n(q_{m-1} - q)\right] + \pi\Delta_m^{(a)} \tag{4}$$

as $r \longrightarrow r_m$, where $\Delta_m^{(a)}$ is determined from the differential equation with $\hat{\varepsilon} = 0$. In Appendix A we indicate how $\Delta_m^{(a)}$ can be numerically determined. The amplitude C_m^- is asymptotically related to $\widehat{C}_m(r)$ as $r \longrightarrow r_{m-1}$,

$$\widehat{C}_m(r) \longrightarrow \frac{r_{m-1}^2\, q'_{m-1}}{q_{m-1}^2}\, n(1 + \lambda_{m-1}) C_m^- \tag{5}$$

where $\lambda_{m-1} = (1 + \delta_{m-1}/2)/2nq_{m-1}$, $\delta_{m-1} = q_{m-1}\frac{\partial\rho(r_{m-1})}{\partial q}\Big/\rho(r_{m-1})$ and $q'_{m-1} = q(r_{m-1})$.

Similarly for $r > r_m$, $\phi_m(r)$ is approximated by the function

$$\phi_m(r) \sim C_m^+ \phi_m^{(b)}(r) \tag{6}$$

where $\phi_m^{(b)}(r)$ satisfies Eqs. (1) and (2) with $\hat{\varepsilon} = 0$, $\Omega^2 = \Omega_m^2$ and the boundary condition at $r = a$ (in this work we use $\phi_m^{(b)}(a) = 0$ as the boundary condition). As $r \longrightarrow r_m$, $\phi_m^{(b)}(r)$ has

the form

$$\phi_m^{(b)}(r) \longrightarrow \ln\left[n(q-q_m)\right] + \pi\Delta_m^{(b)} \tag{7}$$

with $\Delta_m^{(b)}$ determined from the differential equation. The amplitude C_m^+, as $r \longrightarrow r_m$, is related to $\widehat{C}_m(r)$ by

$$\widehat{C}_m(r) \rightarrow -r_m^2 \frac{q_m'}{q_m^2}\, n(1-\lambda_m) C_m^+ \,. \tag{8}$$

For $r_{m-1} < r < r_m$, the approximate solution for $\phi_m(r)$ is given by the $\widehat{\varepsilon} = 0$ solution of Eq. (1), which has the form,

$$\phi_m(r) = C_m^- \phi_m^-(r) + C_m^+ \phi_m^+(r) \tag{9}$$

where $\phi_m^-(r)$ is for the frequency $\Omega = \Omega_{m-1}$ and is well-behaved for $r \approx r_m$ and logarithmically divergent near $r = r_{m-1}$, i.e.

$$\phi_m^-(r) \longrightarrow \begin{cases} \ln\left[n(q-q_{m-1})\right] + \pi\Delta_m^- \,, & q - q_{m-1} \rightarrow 0^+ \\ \pi\widetilde{\Delta}_m^- & q_m - q \rightarrow 0^+ \,. \end{cases} \tag{10}$$

Similarly $\phi_m^+(r)$ satisfies the differential equation given by Eq. (1) for $\Omega = \Omega_m$ with

$$\phi_m^+(r) \longrightarrow \begin{cases} \ln\left[n(q_m-q)\right] + \pi\Delta_m^+ \,, & q_m - q \rightarrow 0^+ \\ \pi\widetilde{\Delta}_m^+ & q - q_{m-1} \rightarrow 0^+ \,. \end{cases} \tag{11}$$

From these forms we can write that the jumps in $\phi_m(r)$ about $r = r_{m-1}$ and $r = r_m$ are given by

$$\Delta\Phi_m^- \equiv \left[\phi_m(r_{m-1}+\delta) - \phi_m(r_{m-1}-\delta)\right] \Big/ \pi = -\overline{\Delta}_m^- C_m^- + \widetilde{\Delta}_m^+ C_m^+ \tag{12}$$

$$\Delta\Phi_m^+ \equiv \left[\phi_m(r_m+\delta) - \phi_m(r_m-\delta)\right] \Big/ \pi = \overline{\Delta}_m^+ C_m^+ - \widetilde{\Delta}_m^- C_m^- \tag{13}$$

with $\overline{\Delta}_m^- = \Delta_m^{(a)} - \Delta_m^-$ and $\overline{\Delta}_m^+ = \Delta_m^{(b)} - \Delta_m^+$.

One can also observe another near equality. To the extent Ω_m is nearly equal to Ω_{m-1}, it follows from the Wronskian of the second order differential equation obtained by combining

Eqs. (1) and (2) in the $\widehat{\varepsilon}=0$ limit, that

$$r_{m-1}\,\frac{q'_{m-1}}{q^2_{m-1}}\,n(1+\lambda_{m-1})\widetilde{\Delta}^+_m = r_m\,\frac{q'_m}{q^2_m}\,n(1-\lambda_m)\widetilde{\Delta}^-_m + \mathcal{O}(\Omega_m-\Omega_{m-1})\ . \tag{14}$$

For this relation to be nearly satisfied we need both r_m and r_{m-1} to be in the plasma and that the position r^+_m be close to r_m (viz. $n|q_m-q(r^+_m)|\ll 1$), r^-_m is close to $r_{m-1}(n|q_{m-1}-q(r^-_m)|\ll 1$) where the second resonance points r^+_m and r^-_m are defined by

$$\begin{aligned}\Omega_{m-1}\,\rho^{1/2}(r^+_m) &= n - m/q\,(r^+_m)\\ \Omega_m\,\rho^{1/2}(r^-_m) &= \frac{m}{q(r^-_m)} - n\ .\end{aligned} \tag{15}$$

At the end of Appendix A we discuss how the theory is affected when these approximations fail.

We now introduce a variational method to compute the toroidal coupling. This variational method is used so that the kinetic contribution to the theory can be incorporated in a natural way. We also observe that Eq. (1), without the kinetic contribution, is clearly self-adjoint as the equation for the adjoint function, $\widetilde{\phi}_m(r)$, is identical to $\phi_m(r)$ (if Ω^2 is real, the complex conjugate, $\phi^*_m(r)$, is also the Hermetian adjoint function). If we multiply Eq. (1) by the adjoint function $\widetilde{\phi}_m(r)/r$ and integrate over the mth TAE gap region, between $-\delta+r_m<r<\delta+r_m$, where $\frac{\widehat{\varepsilon}_m}{4nq'_m}<\delta<\frac{1}{nq'_m}$ with $\widehat{\varepsilon}_m=\widehat{\varepsilon}(r_m)$ and $q'_m=q'(r_m)$, we find using that $\widehat{C}_m(r)$ is nearly constant and after a partial integration,

$$\begin{aligned}-r_m\,\frac{q'_m}{q^2_m}\,\pi n(1-\lambda_m)\Bigg[&\frac{\widetilde{\phi}_m(r)}{\pi}\,C^+_m(r_m)\Bigg|^{r_m+\delta}_{r_m-\delta}\\ -\,C^+_m(r)&\int^{r_m+\delta}_{r_m-\delta}\frac{dr'}{\pi}\,\frac{\partial\widetilde{\phi}_m(r')}{\partial r'}\Bigg] \doteq \frac{4\pi i\omega r_m}{c^2}\sum_j e_j\int dr\,\frac{\partial\widetilde{\phi}_m}{\partial r}\int d^3v\,\mathrm{v}\delta h_{jm}+\mathcal{O}(\delta)\ .\end{aligned} \tag{16}$$

On the left-hand side, for the first term, we use the solution obtained from the $\widehat{\varepsilon}=0$ equation, while for the second term we use the solution of the inner boundary layer equation. The

jump in the inner layer is obtained from the integral,

$$\Delta\widetilde{\Phi}_m^+ \equiv \int_{r_m-\delta}^{r_m+\delta} \frac{dr'}{\pi} \frac{\partial\widetilde{\phi}_m(r')}{\partial r'} ,$$

and the result will depend linearly on the fluxes C_m^+ and C_{m+1}^- that interact due to the toroidal coupling. Specific forms of the coupling will be evaluated in subsequent sections for the ideal, and nonideal (where $E_\parallel$ and ion FLR effects are accounted for) cases. In general, the jump can be written as,

$$\Delta\widetilde{\Phi}_m^+ \equiv \int_{r_m-\delta}^{r_m+\delta} \frac{dr'}{\pi} \frac{\partial\widetilde{\phi}_m(r')}{\partial r} = -\alpha_m^+(g_m)\widetilde{C}_m^+ - \beta_m^+(g_m)\widetilde{C}_{m+1}^- , \tag{17}$$

where $\widehat{\varepsilon}_m\, g_m = \frac{\omega^2}{\omega_m^2} - 1$. We also use the adjoint of Eq. (13) to obtain the jump in $\widetilde{\phi}_m$ in terms of $\widetilde{C}_m^+$ and $\widetilde{C}_m^-$. Thus, substituting into Eq. (16) we have the relation

$$\begin{aligned} -\frac{\pi q_m'}{q_m^2} n\, r_m\, (1-\lambda_m) \left[\left(\overline{\Delta}_m^+ + \alpha_m^+\right) C_m^+ \widetilde{C}_m^+ + \beta_m^+ \widetilde{C}_{m+1}^- C_m^+ - \widetilde{\Delta}_m^- C_m^+ \widetilde{C}_m^- \right] \\ = -\frac{4\pi i\omega\, r_m}{c^2} \int_{(m\text{th TAE structure})} \widetilde{\mathbf{E}}_m \cdot \delta\mathbf{j}_m\, dr \end{aligned} \tag{18}$$

with $E_m = -\frac{\partial\phi_m}{\partial r}$ the approximate electric field of the mth harmonic at the gap and $\delta\mathbf{j}_m$ is the mth harmonic of the kinetic current contribution.

An identical set of manipulations apply to $\widetilde{\phi}_{m+1}(r)$ in the vicinity of $r \simeq r_m$. We define

$$\Delta\widetilde{\Phi}_{m+1}^- \equiv \int_{r_m-\delta}^{r_m+\delta} \frac{dr'}{\pi} \frac{\partial\widetilde{\phi}_{m+1}(r')}{\partial r'} = \alpha_{m+1}^-(g_m)\widetilde{C}_{m+1}^- + \beta_{m+1}^-(g_m)\widetilde{C}_m^+ \tag{19}$$

and then find,

$$\begin{aligned} -\frac{\pi q_m' r_m n}{q_m^2} (1+\lambda_m) \left[\left(\overline{\Delta}_{m+1}^- + \alpha_{m+1}^-\right) C_{m+1}^- \widetilde{C}_{m+1}^- + \beta_{m+1}^- \widetilde{C}_m^+ C_{m+1}^- - \widetilde{\Delta}_{m+1}^+ \widetilde{C}_{m+1}^+ C_{m+1}^- \right] \\ = -\frac{4\pi i\omega\, r_m}{c^2} \int_{(m\text{th TAE structure})} \widetilde{\mathbf{E}}_{m+1} \cdot \delta\mathbf{j}_{m+1} dr \end{aligned} \tag{20}$$

We now construct a quadratic form by summing Eqs. (18) and (20) and then summing over all TAE structures. The result is,

$$-\sum_m \frac{\pi^2 R_0 c^2 q'_m r_m n}{q_m^2 \omega}$$

$$\left[\begin{array}{l}(1+\lambda_m)\, C^-_{m+1}\, \tilde{C}^-_{m+1} \left(\overline{\Delta}^-_{m+1} + \alpha^-_{m+1}\right) \\ +(1-\lambda_m)\, C^+_m\, \tilde{C}^+_m \left(\overline{\Delta}^+_m + \alpha^+_m\right) \\ +(1+\lambda_m)\, \beta^-_{m+1}\, \tilde{C}^+_m\, C^-_{m+1} \\ +(1-\lambda_m)\, \beta^+_m\, \tilde{C}^-_{m+1}\, C^+_m \\ -(1+\lambda_m)\, \tilde{\Delta}^+_{m+1}\, \tilde{C}^+_{m+1}\, C^-_{m+1} - (1-\lambda_m)\, \tilde{\Delta}^-_m\, C^+_m\, \tilde{C}^-_m\end{array}\right]$$

$$= i \sum_m \int_{(m)} d^3 r\, \tilde{\mathbf{E}} \cdot \delta \mathbf{j} \tag{21}$$

where (m) denotes each TAE structure.

We now note several specific properties (to be proved later) in the coefficients, α, β, that are common to the ideal and nonideal theories. These are

$$\alpha^+_m = \alpha^-_{m+1} \equiv \alpha_m$$

$$\beta^-_{m+1} = \left(\frac{1-\lambda_m}{1+\lambda_m}\right)^{1/2} \beta_m \tag{22}$$

$$\beta^+_m = \left(\frac{1+\lambda_m}{1-\lambda_m}\right)^{1/2} \beta_m$$

and the relations

$$\begin{aligned} &\alpha_m^2 - \beta_m^2 = -1 \\ &\text{Im}\ \alpha_m \leq 0\ , \qquad \text{for} \quad \text{Im}\ g_m \geq 0 \quad \text{when Re}\ \Omega > 0\ . \end{aligned} \tag{23}$$

The relation given by Eq. (23), together with the Wronskian relation given in Eq. (14) (to the accuracy of our theory we can, if desired, synchronize our evaluation of the $\tilde{\Delta}$'s to satisfy

this relation exactly) ensures that the quadratic form on the left-hand side of Eq. (21) is a self-adjoint structure. This symmetry guarantees that $\tilde{C}_m$ and C_m satisfy the same equation and are identical to each other. By extremizing this form, by taking the variation with respect to C_m^+ and C_m^- (neglecting the right-hand side of Eq. (21)), one can readily ascertain that one obtains the same relations as setting Eq. (13) equal to Eq. (17) and Eq. (12) equal to Eq. (19). We then find the relations

$$C_m^+ = \frac{\tilde{\Delta}_m^- C_m^- - \beta_m^+ C_{m+1}^-}{\overline{\Delta}_m^+ + \alpha_m^+} \tag{24}$$

$$C_m^- = \frac{\tilde{\Delta}_m^+ C_m^+ - \beta_m^- C_{m-1}^+}{\overline{\Delta}_m^- + \alpha_m^-} \,. \tag{25}$$

Equations (24) and (25) can be combined to form a three-point recursion relation

$$\begin{aligned} &\left(\frac{1+\lambda_m}{1-\lambda_m}\right)^{1/2} \frac{\beta_m \tilde{\Delta}_{m+1}^+ C_{m+1}^+}{\overline{\Delta}_{m+1}^- + \alpha_m} + \left(\frac{1-\lambda_{m-1}}{1+\lambda_{m-1}}\right)^{1/2} \frac{\beta_{m-1} \tilde{\Delta}_m^- C_{m-1}^+}{\overline{\Delta}_m^- + \alpha_{m-1}} \\ &+ C_m^+ \left[\overline{\Delta}_m^+ + \alpha_m - \frac{\beta_m^2}{\overline{\Delta}_{m+1}^- + \alpha_m} - \frac{\tilde{\Delta}_m^+ \tilde{\Delta}_m^-}{\overline{\Delta}_m^- + \alpha_{m-1}}\right] = 0 \end{aligned} \tag{26}$$

where we have used the first relations defined in Eq. (22) (note that the explicit λ_m dependence can be removed with a straightforward renormalization of the $\tilde{\Delta}$ values).

The solution to Eq. (26) determines the eigenfrequency ω_0, and the relative flux amplitudes C_m^+, with C_m^- determined from Eq. (25). The effect of the perturbing kinetic currents can then be obtained from considering Eq. (21).

We now indicate the procedure that can be used to evaluate frequency shifts when perturbing currents are accounted for. We are particularly interested in the cases where these currents are destabilizing, and calculating the conditions for marginal stability. We start from Eq. (21) and write it in the schematic form,

$$\sum_{m,n} \tilde{C}_m \mathcal{L}_{mn}(\omega) C_n = \varepsilon \sum_{m,n} \tilde{C}_m P_{mn} C_n \tag{27}$$

with $\varepsilon \ll 1$. We have the self-adjointness property, $\mathcal{L}_{mn} = \mathcal{L}_{nm}$ with the left-hand side in general complex for ω real. Hence, in general, there is no real ω to make the left-hand side vanish. We can write $C_n = \mathcal{L}^{n,r}$ and $\widetilde{C}_n = \mathcal{L}^{r,n}$ (in our case $\mathcal{L}^{n,r} = \mathcal{L}^{r,n}$) where $\mathcal{L}^{n,r}$ is the cofactor of $\mathcal{L}_{mn}$ (i.e. $\sum_n \mathcal{L}_{mn}\,\mathcal{L}^{n,r} = |\mathcal{L}(\omega)|\delta_{mr}$ with $|\mathcal{L}(\omega)|$ the determinant of $\mathcal{L}_{mn}$ and δ_{mr} the Kroneker delta.)

In Appendix B, we prove that there are no roots of $|\mathcal{L}(\omega)| = 0$ for $\mathrm{Im}\ \omega > 0$ (i.e. stability of the 3-point recursion relation). Further, where $\mathrm{Im}\,|\mathcal{L}(\omega)| = 0$ there cannot be any real roots. However, we can seek the $\omega = \omega_0$ for real ω_0, which minimizes the absolute value of $|\mathcal{L}(\omega)|$. By assumption we take $|\mathcal{L}(\omega_0)| \approx \mathcal{O}(\epsilon)$. We now look for the perturbed solutions, which include the right-hand side of (27). Hence, with $\omega = \omega_0 + \delta\omega$, $C_n = \mathcal{L}^{m,r} + \delta C_n$, $\widetilde{C}_m = \mathcal{L}^{s,m} + \delta\widetilde{C}_m$, we find to first order in ε,

$$\delta\omega = \frac{\varepsilon \sum_{m,n} \widetilde{C}_n^{(0)}\, P_{n,m}\, C_m^{(0)}}{\sum_{m,n} \widetilde{C}_m^{(0)} \dfrac{\partial \mathcal{L}_{mn}(\omega_0)}{\partial\omega} C_n^{(0)}} - \gamma_d\ , \tag{28}$$

$$\gamma_d = \frac{-\sum_{m,n} \widetilde{C}_m^{(0)}\, \mathcal{L}_{mn}(\omega_0) C_n^{(0)}}{\sum_{m,n} \widetilde{C}_m^{(0)} \dfrac{\partial \mathcal{L}_{mn}(\omega_0)}{\partial\omega} C_n^{(0)}} \tag{29}$$

with $C_n^{(0)} = \mathcal{L}^{n,r}(\omega_0)$ and $\widetilde{C}_m^{(0)} = \mathcal{L}^{s,m}(\omega_0)$. We have written γ_d separately and note that rather than explicitly evaluating Eq. (29) there are numerically more efficient ways of evaluating γ_d when the perturbation method is justified (two obvious ways are to find the damped eigenvalue of $|\mathcal{L}(\omega)| = 0$ or to set $\gamma_d = -|\mathcal{L}(\omega_0)|/(\partial|\mathcal{L}(\omega_0)|/\partial\omega)$.

The explicit representation for the denominators in Eqs. (28) and (29) is

$$\sum_{m,n} \widetilde{C}_m^{(0)} \frac{\partial \mathcal{L}_{mn}}{\partial\omega} C_n^{(0)} = -\sum_m \frac{2\pi^2\, R_0\, c^2\, q'_m r_m n}{q_m^2 \widehat{\varepsilon}_m\, \omega_m^2}$$

$$\times\Bigg\{\left[(1+\lambda_m)\,C^-_{m+1}\,\widetilde{C}^-_{m+1}+(1-\lambda_m)\,C^+_m\,\widetilde{C}^+_m\right]\frac{\partial\alpha_m}{\partial g_m}$$

$$+\;\left[(1+\lambda_m)\,(1-\lambda_m)\right]^{1/2}\left(\widetilde{C}^+_m\,C^-_{m+1}+C^+_m\,\widetilde{C}^-_{m+1}\right)\frac{\partial\beta_m}{\partial g_m}\Bigg\}. \tag{30}$$

Solving for Im $\delta\omega = 0$, gives the marginal stability condition.

For interpreting the physical content of Eq. (28), we make an additional approximation. In the original sum for real ω, $\sum_{m,n}\widetilde{C}^{(0)}_m\,\mathcal{L}_{mn}\,C^{(0)}_n$, is assumed small at $\omega=\omega_0$. To fulfill this assumption the explicit imaginary terms in $\mathcal{L}_{mn}$ must be smaller than the real terms. Thus, for the indices where $\mathcal{L}_{mn}$ is predominantly imaginary, either $\mathcal{L}_{mn}$ is small or $C^{(0)}_n$ and $\widetilde{C}^{(0)}_m$ are small. We consider the matrix $\widehat{\mathcal{L}}_{mn}$ obtained by discarding the predominantly imaginary terms in the sum as well as the imaginary part of the predominantly real $\mathcal{L}_{mn}$ terms. We then take the cofactor $\widehat{\mathcal{L}}^{m,n}$ as the trial function for the $C^{(0)}_m$ appearing in the ε term of Eq. (28), and we also replace $\dfrac{\partial\mathcal{L}_{mn}}{\partial\omega}$ by $\dfrac{\partial\widehat{\mathcal{L}}_{m,n}}{\partial\omega}$. In the numerator we need only sum over the dominant amplitudes with the trial function for $C^{(0)}_m$. Then, the ε term in Eq. (28) has the following physical interpretation. The imaginary part of the numerator is the power transferred $-\,\mathrm{Re}\int d^3r\,\mathbf{E}^*\cdot\mathbf{j}$ from the particle to the wave, (this is obvious from Eq. (21)). The denominator is two times the wave energy, WE, excited by the shear Alfvén wave spectrum for $\omega^2\approx k^2_m v^2_A$ (i.e. $WE\simeq\int d^3r\,\dfrac{|B_\theta|^2}{4\pi}$ where we use $B_\theta\gg B_r$ in the gap region and the excited kinetic energy is nearly the same as the field energy). This assertion is readily ascertained by direct construction. The imaginary part of Eq. (21) then gives

$$\frac{\partial}{\partial t}\,WE=-\,\mathrm{Re}\int_{\left(\substack{\text{kinetic}\\ \text{currents}}\right)}\widetilde{\mathbf{E}}^*\cdot\delta\mathbf{j}\,d^3r-2\gamma_d\,WE\;. \tag{31}$$

Marginal stability occurs when the right-hand side vanishes. Note that Eq. (31) is slightly less accurate than Eq. (28).

III. Coupling Coefficients for Ideal Problem

To calculate the coupling coefficients α_m and β_m for the ideal problem, we note that for $r \approx r_m$, Eq. (1) can be approximately written as $\frac{d}{dr}\,\widehat{C}_m(r) = 0$, which on integration gives that $\widehat{C}_m$ is a constant which we write as

$$\widehat{C}_m(r) = -r_m^2\,\frac{q_m' n}{q_m^2}\,(1-\lambda_m)\;C_m^+ \tag{32a}$$

$$\widehat{C}_{m+1}(r) = r_m^2\,\frac{q_m' n}{q_m^2}\,(1+\lambda_m)\;C_{m+1}^- \tag{32b}$$

with C_m^+ and C_{m+1}^- constants. Now using Eq. (2), when $n|q-q_m| \ll 1$ and taking into account the interaction of the m and $m+1$ modes, we find

$$\left(x - \frac{\widehat{\varepsilon}_m}{4}\,\frac{g_m}{(1-\lambda_m)}\right)\frac{d\phi_m}{dx} - \frac{\widehat{\varepsilon}_m}{4(1-\lambda_m)}\,\frac{d\phi_{m+1}}{dx} = C_m^+ \tag{33a}$$

$$\frac{\widehat{\varepsilon}_m}{4\,(1+\lambda_m)}\,\frac{d\phi_m}{dx} + \left(x + \frac{\widehat{\varepsilon}_m\, g_m}{4\,(1+\lambda_m)}\right)\frac{d\phi_{m+1}}{dx} = C_{m+1}^- \tag{33b}$$

with $\widehat{\varepsilon}_m = \widehat{\varepsilon}(r_m)$ and $x = n(q-q_m)$.

Solving for $\dfrac{d\phi_m}{dx}$ and $\dfrac{d\phi_{m+1}}{dx}$ then gives

$$\frac{d\phi_m}{dx} = \frac{1}{\mathrm{Det}}\left[\left(x + \frac{g_m\,\widehat{\varepsilon}_m}{4(1+\lambda_m)}\right)C_m^+ + \frac{\widehat{\varepsilon}_m\,C_{m+1}^-}{4(1-\lambda_m)}\right] \tag{34a}$$

$$\frac{d\phi_{m+1}}{dx} = \frac{1}{\mathrm{Det}}\left[\left(x - \frac{g_m\,\widehat{\varepsilon}_m}{4(1-\lambda_m)}\right)C_{m+1}^- - \frac{\widehat{\varepsilon}_m\,C_m^+}{4(1+\lambda_m)}\right] \tag{34b}$$

with

$$\mathrm{Det} = \left(x - \frac{g_m\,\lambda_m\,\widehat{\varepsilon}_m}{4(1-\lambda_m^2)}\right)^2 + \frac{\widehat{\varepsilon}_m^2}{16(1-\lambda_m^2)}\left(1 - \frac{g_m^2}{1-\lambda_m^2}\right).$$

Now with the definitions

$$\Delta\Phi_m^+ \equiv \frac{1}{\pi}\int_{-\infty}^{\infty} dx\,\frac{d\phi_m(x)}{dx} \equiv -\left(\alpha_m^+\,C_m^+ + \beta_m^+\,C_{m+1}^-\right), \tag{35a}$$

$$\Delta\Phi_{m+1}^- \equiv \frac{1}{\pi}\int_{-\infty}^{\infty} dx\,\frac{d\phi_{m+1}(x)}{dx} \equiv \alpha_{m+1}^-\,C_{m+1}^- + \beta_{m+1}^-\,C_m^+, \tag{35b}$$

we substitute Eqs. (34) into Eqs. (35), and find

$$\alpha_m^+ = \alpha_{m+1}^- = -\frac{h_m}{(1-h_m^2)^{1/2}} \equiv \alpha_m \tag{36a}$$

$$\beta_m^+ \left(\frac{1-\lambda_m}{1+\lambda_m}\right)^{1/2} = \beta_{m+1}^- \left(\frac{1+\lambda_m}{1-\lambda_m}\right)^{1/2} = -\frac{1}{(1-h_m^2)^{1/2}} \equiv \beta_m \tag{36b}$$

where $h_m = g_m/(1-\lambda_m^2)^{1/2}$. Note that $\alpha_m^2 - \beta_m^2 = 1$. When h_m is nearly real and $|\,\mathrm{Re}\; h_m| > 1$, causality dictates that $(1-h_m^2)^{1/2} = -i(h_m^2-1)^{1/2}\mathrm{sgn}(\mathrm{Re}\; h_m)$.

IV. Derivation of Non-ideal Inner Layer Equation

With finite Larmor radius and finite resistivity included, and assuming $\frac{\partial}{\partial r} \gg \frac{1}{r}\frac{\partial}{\partial\theta}, \frac{\partial}{\partial s}$ (s is distance along field line) the vorticity equation and Ohm's law governing the electrostatic potential ϕ, and the vector potential $A_\parallel\,\mathbf{b}$, take the form

$$\frac{\partial}{\partial s}\nabla_\perp^2 A_\parallel = ic\omega\,\boldsymbol{\nabla}_\perp \cdot \frac{1}{v_A^2}\left(1+\frac{3}{8}r_{Li}^2\,\nabla_\perp^2\right)\cdot\boldsymbol{\nabla}_\perp\phi \tag{37}$$

$$E_\parallel \equiv -\frac{\partial\phi}{\partial s} + i\frac{\omega}{c}A_\parallel = -\frac{\omega}{c}\delta^2\,\nabla_\perp^2 A_\parallel \tag{38}$$

with $\delta^2 = c^2/4\pi\omega\sigma$, with σ the parallel electrical conductivity (here we take $4\pi\sigma = i\omega_{pe}^2/[\omega + i\nu_{\mathrm{eff}} - k_\parallel^2 v_e^2/2\omega]$, where ω_{pe} is the electron plasma frequency, $v_{the}^2 = 2T_e/m_e$ and ν_{eff}, the effective collision frequency, is to be determined from kinetic theory; typically the inequality $v_{the}^2 \gg \omega^2/k_\parallel^2,\ \nu_{\mathrm{eff}}^2/k_\parallel^2$, applies).

Now substituting Eq. (38) into Eq. (37) yields

$$\frac{\partial}{\partial s}\nabla_\perp^2\frac{\partial\phi}{\partial s} + \nabla_\perp\cdot\frac{\omega^2}{v_A^2}\nabla_\perp\phi = \delta^2\frac{\omega}{c}\nabla_\perp^4\frac{\partial A_\parallel}{\partial s} - \frac{3}{8}\frac{\omega^2}{v_A^2}r_{Li}^2\,\nabla_\perp^4\phi\,. \tag{39}$$

The left-hand side of Eq. (39) is the ideal MHD operator. For the right-hand side, which is most significant for $r \approx r_m$, where the ideal equation has near singular structure, we may use lowest order estimates specifically, $i\omega\,A_\parallel/c = \partial\varphi/\partial s$, $\frac{\partial}{\partial s} \to ik_\parallel \equiv i(n - m/q(r))/R_0$, $\frac{\omega^2 R_0^2}{v_A^2(0)} \equiv \Omega^2 = \Omega_m^2 \equiv \frac{1}{4q_m^2\,\rho(r_m)}$. Careful manipulations are needed to obtain the correct toroidal

coupling of the left-hand side of Eq. (39) and they are presented in Ref. 5. Using these results near the TAE resonant structure then gives

$$\frac{\partial}{\partial r}\left[\Omega^2\rho(r)-\left(\frac{m}{q(r)}-n\right)^2\right]\frac{\partial\phi_m}{\partial r}+\widehat{\varepsilon}_m\Omega^2\rho(r)\,\frac{\partial\phi_{m+1}}{\partial r}=-\frac{r_{LT}^2\,\Omega_m^2}{2}\,\frac{\partial^4\phi_m}{\partial r^4}$$

$$\frac{\partial}{\partial r}\left[\Omega^2\rho(r)-\left(\frac{m+1}{q(r)}-n\right)^2\right]\frac{\partial^2\phi_{m+1}}{\partial r}+\widehat{\varepsilon}_m\Omega^2\rho(r)\,\frac{\partial\phi_m}{\partial r}=-\frac{r_{LT}^2\,\Omega_m^2}{2}\,\frac{\partial^4\phi_{m+1}}{\partial r^4} \qquad (40)$$

where $r_{LT}^2=\frac{3}{4}r_{Li}^2+\widetilde{r}_{Ls}^2$,

$$\widetilde{r}_{Ls}^2=\frac{m_e}{M_i}\,\frac{v_{the}^2}{\omega_{ci}^2}\left[1-\frac{2v_A^2}{v_{the}^2}\left(1+\frac{i\nu_{\text{eff}}}{|k_\parallel|v_A}\right)\right],$$

and $\widehat{\varepsilon}_m=\frac{5}{2}\frac{r_m}{R_0}$.

Near $r=r_m$ we can use

$$\frac{(m+1)}{q(r)}-n\doteq\frac{1}{2q_m}-\frac{(m+1)(q-q_m)}{q_m^2},$$

$$\frac{m}{q(r)}-n\doteq-\frac{1}{2q_m}-\frac{m(q-q_m)}{q_m^2}$$

$$\Omega^2\rho(r)=\frac{1}{4q_m^2}\left[1+\widehat{\varepsilon}_m\,g_m+(q-q_m)\delta_m/q_m\right]$$

with g_m and δ_m defined in Sec. II. Now rescaling the independent variable so that $x=4n(q-q_m)/\widehat{\varepsilon}_m$, we find that Eq. (40) can be written as

$$\frac{\partial}{\partial x}\left[\Big(g-x(1-\lambda)\Big)\frac{\partial\phi_1}{\partial x}+\frac{\partial\phi_2}{\partial x}\right]=-\eta\,\frac{\partial^4\phi_1}{\partial x^4}$$

$$\frac{\partial}{\partial x}\left[\Big(g+x(1+\lambda)\Big)\frac{\partial\phi_2}{\partial x}+\frac{\partial\phi_1}{\partial x}\right]=-\eta\,\frac{\partial^4\phi_2}{\partial x^4} \qquad (41)$$

where $\phi_{m+1}^-\to\phi_2$, $\phi_m^+\to\phi_1$, the subscript m is deleted from other locally evaluated quantities (e.g. $g_m, q_m\to g, q$, etc.), $\eta=8n^2\,s^2q^2\left(\widetilde{r}_{Ls}^2+\frac{3}{4}r_{Li}^2\right)/\widehat{\varepsilon}^3\,r^2$, and $s=\partial\ln q/\partial\ln r$.

Equation (41) can be integrated once to yield

$$\begin{aligned}
&[g - x(1-\lambda)]\,\chi_1 + \eta\,\frac{\partial^2 \chi_1}{\partial x^2} + \chi_2 = -C_1(1-\lambda) \\
&[g + x(1+\lambda)]\,\chi_2 + \eta\,\frac{\partial^2 \chi_2}{\partial x^2} + \chi_1 = C_2(1+\lambda)
\end{aligned} \tag{42}$$

with C_1 and C_2 constant of integration (the normalized fluxes of the previous section) and $\chi = \partial\phi/\partial x$.

We now take the Fourier transform of Eq. (42) with $\psi(k) = \int_{-\infty}^{\infty} \frac{dx}{2\pi} \exp(-ikx)\chi(x)$. Then Eq. (42) becomes

$$\begin{aligned}
&\left[-i(1-\lambda)\frac{\partial}{\partial k} + g - \eta k^2\right]\psi_1 + \psi_2 = -(1-\lambda)\delta(k)C_1, \\
&\left[i(1+\lambda)\frac{\partial}{\partial k} + g - \eta k^2\right]\psi_2 + \psi_1 = (1+\lambda)\delta(k)C_2.
\end{aligned} \tag{43}$$

With the definition of $\Delta\Phi_m$ used in Sec. II (see for example Eq. (7)) we note that

$$\pi\Delta\,\Phi_{1,2} \equiv \phi_{1,2}(x=\infty) - \phi_{1,2}(x=-\infty) = \pi\left(\psi_{1,2}(0^+) + \psi_{1,2}(0^-)\right)\ . \tag{44}$$

We need to solve Eq. (43) for the values of ψ at $k = 0^{\pm}$ in terms of the flux C. It is convenient to symmetrize Eq. (43) by introducing the transformation

$$\Psi_1(k) = \frac{\psi_2(k)}{(1+\lambda)^{1/2}} \exp\left[\frac{i\lambda}{1-\lambda^2}\int_0^k dk'(g - \eta k'^2)\right]$$

$$\Psi_2(k) = \frac{\psi_1(k)}{(1-\lambda)^{1/2}} \exp\left[\frac{i\lambda}{1-\lambda^2}\int_0^k dk'(g - \eta k'^2)\right]$$

The equation for $\Psi(k)$ then takes the form

$$\left(\frac{d}{dk} + i\,\frac{g-\eta k^2}{1-\lambda^2}\right)\Psi_1 + \frac{i}{(1-\lambda^2)^{1/2}}\,\Psi_2 = \frac{-iC_1\,\delta(k)}{(1+\lambda)^{1/2}} \tag{45a}$$

$$\left(\frac{d}{dk} - i\,\frac{g-\eta k^2}{1-\lambda^2}\right)\Psi_2 - \frac{i}{(1-\lambda^2)^{1/2}}\,\Psi_1 = \frac{-iC_2\,\delta(k)}{(1-\lambda)^{1/2}} \tag{45b}$$

These equations are similar to those given in Ref. 10 and identical to those derived in Ref. 11 for $\lambda = 0$. The physically relevant solution of Eqs. (45) decays as $k \to \pm\infty$, or, for η real, incoming phase velocity (outgoing group velocity). Because the transformation $k \to -k$ transforms the homogeneous equations for (Ψ_{1h}, Ψ_{2h}) into those for (Ψ_{2h}, Ψ_{1h}), we have the symmetry relation

$$\Psi_1(k)\Big|_{k>0} = A^+\Psi_{1h}(k) \ , \qquad \Psi_2(k)\Big|_{k>0} = A^+\Psi_{2h}(k) \ , \tag{46a}$$

$$\Psi_1(k)\Big|_{k<0} = A^-\Psi_{2h}(-k) \ , \qquad \Psi_2(k)\Big|_{k<0} = A^-\Psi_{1h}(-k) \ , \tag{46b}$$

where A^+ and A^- are constants. The constants are determined by integrating Eqs. (45) across the origin and substituting Eqs. (46). We find

$$A^+ = -i\,\frac{C_1\Psi_{1h}(0^+)/(1+\lambda)^{1/2} - C_2\Psi_{2h}(0^+)/(1-\lambda)^{1/2}}{\Psi_{1h}^2(0^+) - \Psi_{2h}^2(0^+)} \tag{47a}$$

$$A^- = -i\,\frac{C_1\Psi_{2h}(0^+)/(1+\lambda)^{1/2} - C_2\Psi_{1h}(0^+)/(1-\lambda)^{1/2}}{\Psi_{1h}^2(0^+) - \Psi_{2h}^2(0^+)} \tag{47b}$$

We are now in a position to write the α's and β's in terms of $\Psi_{1h}(0^+)$ and $\Psi_{2h}(0^+)$. From Eqs. (35), we see, by definition,

$$\Delta\Phi_1 = -\left(\alpha_1^+ C_1 + \beta_1^+ C_2\right) \ , \tag{48a}$$

$$\Delta\Phi_2 = \alpha_2^- C_2 + \beta_2^- C_1 \ , \tag{48b}$$

At the same time, it follows from our definitions that

$$\Delta\Phi_1 = (1+\lambda)^{1/2}\left[\Psi_1(0^+) + \Psi_1(0^-)\right] \ , \tag{49a}$$

$$\Delta\Phi_2 = (1-\lambda)^{1/2}\left[\Psi_2(0^+) + \Psi_2(0^-)\right] \ , \tag{49b}$$

Comparison of Eqs. (48) with the result of substituting Eqs. (46) and Eqs. (47) into Eqs. (49) yields

$$\alpha = i\,\frac{f + 1/f}{f - 1/f} = \alpha_2^- = \alpha_1^+ \ , \tag{50a}$$

$$\beta = \frac{-2i}{f - 1/f} = \left(\frac{1-\lambda}{1+\lambda}\right)^{1/2} \beta_1^+ = \left(\frac{1+\lambda}{1-\lambda}\right)^{1/2} \beta_2^- \ , \tag{50b}$$

where $f = \Psi_{1h}(0^+)/\Psi_{2h}(0^+)$. Thus the inner layer problem has been reduced to one of finding the values at the origin of the well-behaved homogeneous solutions of Eqs. (45). The α's and β's are obviously independent of the scale factor multiplying the solution (Ψ_{1h}, Ψ_{2h}). It is easily verified that Eqs. (50) satisfy the constraints given by Eqs. (22) and (23), discussed in the previous section, for any f. It may also be verified that these expressions reduce to those given by Eqs. (36) in the ideal limit $\eta \to 0$, in which case Ψ_{1h} and Ψ_{2h} are easily obtained analytically.

In general, the solutions Ψ_{1h} and Ψ_{2h} must be obtained numerically. For numerical purposes, it is convenient to set up the problem as a coupled system to be solved for $k > 0$,

$$(1-\lambda^2)^{1/2} i \frac{d}{dk} \begin{pmatrix} \Psi_{1h} \\ \Psi_{2h} \end{pmatrix} = \begin{pmatrix} h - \tilde{\eta}k^2 & 1 \\ -1 & -h + \tilde{\eta}k^2 \end{pmatrix} \begin{pmatrix} \Psi_{1h} \\ \Psi_{2h} \end{pmatrix} \tag{51}$$

where $h = g/(1-\lambda^2)^{1/2}$ and $\tilde{\eta} = \eta/(1-\lambda^2)^{1/2}$. The appropriate solutions for $k \to +\infty$ are selected by using the WKB boundary condition of the spatially damped solution (assuming $\mathrm{Im}\ \tilde{\eta} < 0$)

$$\frac{\Psi_{1h}}{\Psi_{2h}} = -\left[(\tilde{\eta}\,k^2 - h)^2 - 1\right]^{1/2} - h + \tilde{\eta}k^2 \ , \tag{52}$$

for a sufficiently large $k = k_{\max}$. If the imaginary part of η is small, $k_{\max}$ must be chosen to be past the largest turning point in order to extract the correct damping due to tunneling. A numerical code has been implemented that produces α and β values independent of $k_{\max}$.

For analytical purposes, it is convenient to consider the second order equation formed by combining the homogeneous Eqs. (45a) and (45b),

$$\left\{\frac{d^2}{dk^2} + \frac{1}{1-\lambda^2}\left[(h - \tilde{\eta}k^2)^2 \mp 2i\tilde{\eta}(1-\lambda^2)^{1/2}k - 1\right]\right\} \Psi_{ih} = 0 \ , \tag{53}$$

with either

$$\Psi_{2h} = \left[i(1-\lambda^2)^{1/2}\frac{d}{dk} - h + \tilde{\eta}k^2\right] \Psi_{1h} \ , \tag{54a}$$

or

$$\Psi_{1h} = \left[-i(1-\lambda^2)^{1/2}\frac{d}{dk} - h + \tilde{\eta}k^2\right]\Psi_{2h}\ . \tag{54b}$$

In Eq. (53), $i = 1,2$ and we associate the upper sign with 1 and the lower sign with 2. It follows that if one of the Eqs. (54) are satisfied, the other one will also be if Eq. (53) is satisfied.

The character of the modes is determined by the form of the potential of Eq. (53), which has the form

$$\left[\frac{d^2}{dk^2} - V(k)\right]\Psi = 0.$$

The gross features of the potential may be seen by neglecting the $\pm 2i\tilde{\eta}k$ term, which is justified if $|\tilde{\eta}| \ll 1$. Note that the potential is then $V(k) = [1-(h-\tilde{\eta}\,k^2)^2]/(1-\lambda^2)$. It is nearly real for h and $\tilde{\eta}$ nearly real. Now for this discussion only, we take $\tilde{\eta}$ and h real. For all values of h, the potential is negative for large enough k, specifically when $\tilde{\eta}\,k^2 > h+1$, and eigenfunctions will be in the form of a propagating wave. At infinity the propagating waves are given by $\exp(-i\tilde{\eta}\,k^3/3(1-\lambda^2)^{1/2})$ as these waves spatially localize when Im $\eta < 0$ (a condition that follows from any finite resistive model in a stable plasma).

When $h < -1$, the potential is negative, which gives wave propagation for all k values. In this case the inhomogeneous terms at the origin of Eq. (45) excites the outgoing waves. These waves propagate along the k-axis without appreciable reflection. As a result the character of the solution at the origin is insensitive to the shape of the potential, and the ideal theory, which is for a flat potential, with $\tilde{\eta} = 0$, is not strongly affected by finite $\tilde{\eta}$.

When $h^2 < 1$, $V(k)$ is positive in the region $\tilde{\eta}\,k^2 < 1+h$. Thus in this region we are guaranteed an evanescent structure for sufficiently small k. However, as $\tilde{\eta}$ is finite, for $\tilde{\eta}\,k^2 > 1+h$ the wave becomes propagating. Thus, at finite $\tilde{\eta}$ there will always be an effect from tunnelling through the evanescent region, that gives rise to damping. This damping does not appear in the ideal theory.

Note that for $h > 0$, the potential at the origin dips, giving at a concave upward form. As h increases this dip at the origin gives a smaller value for $V(k = 0)$. Finally, the potential becomes negative for $h > 1$, and a new propagating region forms for k near the origin. Now, however, as h increases, there are additional turning points at $\tilde{\eta}^{1/2}k = \pm(h-1)$, which completely change the character of the solution at small k values. The wave character for $|k| < (h-1)/\tilde{\eta}^{1/2}$ are no longer simply outgoing as in the ideal theory, but a near standing wave. It is not a perfect standing wave because the evanescent region, defined by $h - 1 < \tilde{\eta}k^2 < h + 1$, is finite, and the wave leakage gives rise to dissipation. The character of the ideal solution can only be recovered if Im $\tilde{\eta}$ is sufficiently large, so that the wave amplitude that emanates from the origin, reflects from the turning point at $\tilde{\eta}k^2 = h-1$, and propagates back to the origin, is sufficiently small due to damping along the path.

It is also interesting to note that the $\pm 2i\tilde{\eta}k$ term of the potential does not in itself produce a dissipative response when $\tilde{\eta}$ is real. This will be seen from the character of the solutions we obtain in our analysis.

Equation (53) simplifies when $\tilde{\eta} \ll 1$ and $|h^2 - 1| \ll 1$ so that the $(\tilde{\eta}k^2)^2$ term can be neglected. In this case the solutions $\Psi_{1h}(k)$ and $\Psi_{2h}(k)$ can be expressed in terms of parabolic cylinder functions $U(a, x)$, and analytic forms of α and β in terms of these functions as well as gamma functions, can be obtained. In Appendix C we discuss these solutions. A solution to Eq. (53) can also be given in the WKB approximation when $|(h^2-1)/\tilde{\eta}| \gg 1$. The details of this solution is given in Appendix D. The WKB solution is worked out to sufficiently high accuracy to capture the dissipation from wave tunneling and from finite Im$(\tilde{\eta})$.

The analytic approximations in terms of cylinder functions and gamma functions for α and β are

$$\alpha = \frac{i + ix_0 \dfrac{U'(a,-x_0)}{U(a,-x_0)} - ix_0 \dfrac{U'(a,x_0)}{U(a,x_0)}}{x_0 \dfrac{U'(a,-x_0)}{U(a,-x_0)} + x_0 \dfrac{U'(a,x_0)}{U(a,x_0)}}, \tag{55a}$$

$$\simeq \frac{1+\left(\frac{x_0}{G}\right)^2 - ax_0^2}{2i\,\frac{x_0}{G}}\,, \tag{55b}$$

$$\underset{\mathrm{Re}[(h^2-1)/\tilde{\eta}]\gg 1}{\longrightarrow} \begin{cases} \dfrac{i(h-\sigma_1)}{(h^2-1)^{1/2}}\,, & \mathrm{Re}(h)<-1 \\ \dfrac{-h+\sigma_2}{(1-h^2)^{1/2}}\,, & -1<\mathrm{Re}(h)<0 \\ \dfrac{-h+\sigma_3}{(1-h^2)^{1/2}}\,, & 0<\mathrm{Re}(h)<1 \\ \dfrac{-h\cos 2\theta-1}{(h^2-1)^{1/2}\sin 2\theta}\,, & \mathrm{Re}(h)>1 \end{cases} \tag{55c}$$

$$\beta = -\mathrm{isgn}(\mathrm{Re}(-h))\,\frac{\left[1+2x_0\,\dfrac{U'(a,-x_0)}{U(a,-x_0)}\right]^{1/2}\left[1-2x_0\,\dfrac{U'(a,x_0)}{U(a,x_0)}\right]^{1/2}}{x_0\,\dfrac{U'(a,-x_0)}{U(a,-x_0)}+x_0\,\dfrac{U'(a,x_0)}{U(a,x_0)}}\,, \tag{56a}$$

$$\cong \frac{\left[\left(1-\frac{x_0}{G}\right)^2 - ax_0^2\right]^{1/2}\left[\left(1+\frac{x_0}{G}\right)^2 - ax_0^2\right]^{1/2}}{-2\,\mathrm{isgn}(\mathrm{Re}(-h))\,\dfrac{x_0}{G}}\,, \tag{56b}$$

$$\underset{\mathrm{Re}[(h^2-1)/\tilde{\eta}]\gg 1}{\longrightarrow} \begin{cases} \dfrac{i(1-\sigma_1 h)}{(h^2-1)^{1/2}}\,, & \mathrm{Re}(h)<-1 \\ \dfrac{-1+\sigma_2 h}{(1-h^2)^{1/2}}\,, & -1<\mathrm{Re}(h)<0 \\ \dfrac{-1+\sigma_3 h}{(1-h^2)^{1/2}}\,, & 0<\mathrm{Re}(h)<1 \\ \dfrac{h+\cos 2\theta}{(h^2-1)^{1/2}\sin 2\theta}\,, & \mathrm{Re}(h)>1 \end{cases} \tag{56c}$$

where $x_0 = i[h\tilde{\eta}(1-\lambda^2)/2]^{1/4}/h, a = [1-h^2+(1-\lambda^2)\tilde{\eta}/2h]/[8\tilde{\eta}h(1-\lambda^2)]^{1/2}$ (note that the branch of the square root is chosen so that $h^{1/2} \propto i$ when h is real and negative), $G = 2^{-1/2}\Gamma\left(\frac{1}{4}+\frac{a}{2}\right)/\Gamma\left(\frac{3}{4}+\frac{a}{2}\right)$, $\theta = -\pi\left(\frac{1}{4}+\frac{a}{2}\right)$, and

$$\sigma_1 = i\exp\left[-\pi(-ia)\right] + \frac{\tilde{\eta}(1-\lambda^2)}{2(1-h^2)^2}\,, \qquad \mathrm{Re}(h)<-1 \tag{57a}$$

$$\sigma_2 = i\exp(-i\pi a) + \frac{\tilde{\eta}(1-\lambda^2)}{2(1-h^2)^2}\,, \qquad -1<\mathrm{Re}(h)<0 \tag{57b}$$

$$\sigma_3 = \frac{\widetilde{\eta}(1-\lambda^2)}{2(1-h^2)^2}\ , \qquad \mathrm{Re}(h) > 0 \tag{57c}$$

Note that the argument of the exponential terms in Eqs. (57a) and (57b) are nearly negative real when h is nearly real. The σ term for $\mathrm{Re}(h) < -1$ captures the dissipation due to collisions if $\mathrm{Im}(\widetilde{\eta}) \neq 0$, and due to radiation of kinetic Alfvén waves (KAW). The KAW arise from the large k solution of Eq. (53), which are outgoing waves. The parabolic cylinder functions only exhibit outgoing waves for $\mathrm{Re}(h) < 0$ due to the neglect of the k^4 term. For $\mathrm{Re}(h) > 1$ it is important to note that, unlike for the other regions, the leading order dissipation due to $\mathrm{Im}(\widetilde{\eta})$ comes from imaginary θ (which scales as $\widetilde{\eta}^{-1/2}$) and is proportional to $\mathrm{Im}(\widetilde{\eta}^{1/2}) \sim \mathrm{Im}(\widetilde{\eta})/\,\mathrm{Re}(\widetilde{\eta}^{1/2})$. Hence it is unnecessary to go to $\mathcal{O}(\widetilde{\eta})$ here. This is discussed further in Sec. IV.

In the limit $\mathrm{Re}[(h^2-1)/\widetilde{\eta}] \gg 1$, the above asymptotic forms overlap with the solutions of the WKB approximation, where we keep the k^4 term. With the definition $\widetilde{h} = h - \widetilde{\eta}(1-\lambda^2)/[2(1-h^2)]$, these approximate solutions have the form

$$\alpha = \frac{i\widetilde{h}}{(\widetilde{h}^2-1)^{1/2}} \doteq \frac{i(h-\sigma_3)}{(h^2-1)^{1/2}}\ ; \qquad \mathrm{Re}(h) < -1 \tag{58a}$$

$$\beta = \frac{i}{(\widetilde{h}^2-1)^{1/2}} \doteq \frac{i(1-\sigma_3 h)}{(h^2-1)^{1/2}}\ ; \qquad \mathrm{Re}(h) < -1 \tag{58b}$$

$$\alpha = \frac{-\widetilde{h}-ir}{(1-\widetilde{h}^2)^{1/2}} \doteq \frac{-h+\sigma_3-ir}{(1-h^2)^{1/2}}\ ; \qquad -1 < \mathrm{Re}(h) < 1 \tag{59a}$$

$$\beta = \frac{-1-i\widetilde{h}r}{(1-\widetilde{h}^2)^{1/2}} \doteq \frac{-1+h(\sigma_3-ir)}{(1-h^2)^{1/2}}\ ; \qquad -1 < \mathrm{Re}(h) < 1 \tag{59b}$$

$$\alpha = \frac{\widetilde{h}\cos 2\overline{\theta}+1}{(\widetilde{h}^2-1)^{1/2}\sin 2\overline{\theta}} - \frac{it(\widetilde{h}+\cos 2\overline{\theta})}{2(\widetilde{h}^2-1)^{1/2}\sin^2 2\overline{\theta}}\ ; \qquad \mathrm{Re}(h) > 1 \tag{60a}$$

$$\beta = \frac{\widetilde{h}+\cos 2\overline{\theta}}{(\widetilde{h}^2-1)^{1/2}\sin 2\overline{\theta}} - \frac{it(\widetilde{h}\cos 2\overline{\theta}+1)}{2(\widetilde{h}^2-1)^{1/2}\sin^2 2\overline{\theta}}\ ; \qquad \mathrm{Re}(h) > 1 \tag{60b}$$

where

$$r = \exp\left\{-2[(1-\lambda^2)\widetilde{\eta}]^{-1/2} I_1(h)\right\}\ , \tag{61a}$$

$$\overline{\theta} = -\frac{\pi}{4} + [(1-\lambda^2)\tilde{\eta}]^{-1/2} I_2(h) \tag{61b}$$

$$t = \exp\left\{-2[(1-\lambda^2)\tilde{\eta}]^{-1/2} I_3(h)\right\} , \tag{61c}$$

With $I_1(h) = \int_0^{(h+1)^{1/2}} dz[1-(h-z^2)^2]^{1/2}$; $I_2(h) = \int_0^{(h-1)^{1/2}} dz[(h-z^2)^2-1]^{1/2}$; $I_3(h) = \int_{(h-1)^{1/2}}^{(h+1)^{1/2}} dz[1-(h-z^2)^2]^{1/2}$. Plots of the integrals $I_1(-1+x), I_2(x+1)$ and $I_3(x+1)$ are shown in Fig. 1, in the interval $0 < x < 2$.

The results from WKB and those from the large argument expansions of the parabolic cylinder functions given in Eqs. (55c) and (56c) correlate as follows.

The results are the same for $\mathrm{Re}(h) < 1$ with only a discrepancy of $\mathcal{O}(\tilde{\eta}^2)$ when the tunneling terms are neglected. The tunneling terms for $\mathrm{Re}(h) > -1$ are similar for $|h+1| \ll 1$, but Eq. (57b) gives an inaccurate estimate of the tunneling for $|h+1| \cong \mathcal{O}(1)$. From Eq. (61a) we can reproduce the tunneling term in Eq. (57b) by dropping the z^4 term and changing the upper limit of the integral to the zero of the altered integrand. Then the integral for r can be analytically evaluated to give $r = e^{-i\pi a}$ for $-1 < \mathrm{Re}(h) < 0$ when the $\mathcal{O}(\tilde{\eta})$ term in a is dropped.

For $\mathrm{Re}(h) > 1$, Eqs. (55c) and (56c) have the same form as the WKB result, Eqs. (60a) and (60b) with $t = 0$. The results match for $|h-1| \ll 1$, where the z^4 term in Eq. (61b) can be neglected and the upper limit of the integral is replaced by the zero of the altered integrand, in which case $\overline{\theta} = \theta$ when the $\mathcal{O}(\tilde{\eta})$ term in a is dropped. However, for $|h-1| \cong \mathcal{O}(1)$ significant deviation (phase slippage) of θ from $\overline{\theta}$ arises.

Estimates of the errors in the various approximations are given in Appendices B and C.

A comparison of the numerical result and the various approximations for α are given in Fig. 2(a)–(d). We see that the parabolic cylinder functions accurately describe $\mathrm{Re}(\alpha)$ for $\mathrm{Re}(h) < 1$. For $\mathrm{Re}(h) > 1$, the cylinder functions have a phase slippage with increasing $|h^2-1|$ caused by the lack of the k^4 term. Also, while the effect of tunnelling is captured by the cylinder functions for $\mathrm{Re}(h) < 0$, it is completely lost for $\mathrm{Re}(h) > 0$, again due to the

lack of the k^4 term. The tunnelling is accurately described by the cylinder functions only if $h+1 \ll 1$. However, the cylinder functions accurately describe the dissipation due to $\mathrm{Im}(\widetilde{\eta})$ for all h. The gamma functions only approximates the cylinder function if $|h^2-1|$ is not too large. We can also see from Figs. 2(a)–(d) that the WKB approximation correctly describes the effect of finite, though small $|\widetilde{\eta}|$ (that due to tunnelling as well as $\mathrm{Im}(\widetilde{\eta})$), when $|h^2-1|$ is not small. For $\mathrm{Re}(h) > 1$, the WKB approximations are phase synchronized to the exact solutions and exhibit an accurate form for $\mathrm{Im}(\alpha)$ due to wave tunnelling.

V. Analysis of $n = 1$ Mode

The mathematical machinery established here leads to a description of a rich spectrum of Alfvén waves. Roughly, with each gap there is a TAE mode and a denumerable number of KTAE modes. When gap structures are in near alignment, the modes from different resonant surfaces interact, and give mode structures that extend over several resonant surfaces. To give a sample of results we discuss some aspects of the spectrum for the $n = 1$ mode.

We consider the $n = 1$ case where we account for the $m = 1, m = 2$ interaction near $q = 3/2$, and the $m = 2, m = 3$, interaction near $q = 5/2$. We use the results of Table I, (see also Appendix A) which shows that $\overline{\Delta}_1^+ = \widetilde{\Delta}_1^+ = \widetilde{\Delta}_3^- = 0$. The three-term recursion relation then reduces to

$$\left[\left(\overline{\Delta}_1^+ + \alpha_1\right)\left(\overline{\Delta}_2^- + \alpha_1\right) - \beta_1^2\right] C_1^+ + \left(\frac{1+\lambda_1}{1-\lambda_1}\right)^{1/2} \beta_1 \widetilde{\Delta}_2^+ C_2^+ = 0 \,, \tag{67a}$$

$$\left(\frac{1-\lambda_1}{1+\lambda_1}\right)^{1/2} \frac{\beta_1 \widetilde{\Delta}_2^- C_1^+}{\overline{\Delta}_2^- + \alpha_1} + \left[\overline{\Delta}_2^+ + \alpha_2 - \frac{\beta_2^2}{\overline{\Delta}_3^- + \alpha_2} - \frac{\widetilde{\Delta}_2^+ \widetilde{\Delta}_2^-}{\overline{\Delta}_2^- + \alpha_1}\right] C_2^+ = 0 \,. \tag{67b}$$

The determinant of this equation, using $\alpha_i^2 - \beta_i^2 = -1$, gives the result

$$D(\Omega) \equiv \left[\overline{\Delta}_1^+ + \overline{\Delta}_2^- - \frac{1+\overline{\Delta}_1^{+2}}{\overline{\Delta}_1^+ + \alpha_1}\right]\left[\overline{\Delta}_2^+ + \overline{\Delta}_3^- - \frac{1+\overline{\Delta}_3^{-2}}{\overline{\Delta}_3^- + \alpha_2}\right] - \widetilde{\Delta}_2^+ \widetilde{\Delta}_2^- = 0 \,. \tag{68}$$

We now consider the case where $\widehat{\epsilon}$ is sufficiently small, so that the two gaps are strongly mismatched (an exception occurs when there is a degeneracy where $\Omega_1^2 = \Omega_2^2$). If we then

look for a mode near the first gap, we can take $\alpha_2 = -i$; similarly for a mode near the second gap, we have $\alpha_1 = -i$. Thus, the dispersion relations when the gaps are misaligned are:

$$\alpha_1(h_1) + \mathbf{\Delta}_1 = 0$$

$$\alpha_2(h_2) + \mathbf{\Delta}_2 = 0 \tag{69}$$

with

$$\mathbf{\Delta}_1 = \frac{(\overline{\Delta}_1^+\overline{\Delta}_2^- - 1)\left[\overline{\Delta}_2^+\overline{\Delta}_3^- - 1 - i(\overline{\Delta}_2^+ + \overline{\Delta}_3^-)\right] - f\overline{\Delta}_1^+(\overline{\Delta}_3^- - i)}{(\overline{\Delta}_1^+ + \overline{\Delta}_2^-)\left[\overline{\Delta}_2^+\overline{\Delta}_3^- - 1 - i(\overline{\Delta}_2^+ + \overline{\Delta}_3^-)\right] - f(\overline{\Delta}_3^- - i)}\,, \tag{70a}$$

$$\mathbf{\Delta}_2 = \frac{(\overline{\Delta}_2^+\overline{\Delta}_3^- - 1)\left[\overline{\Delta}_1^+\overline{\Delta}_2^- - 1 - i(\overline{\Delta}_1^+ + \overline{\Delta}_2^-)\right] - f\overline{\Delta}_3^-(\overline{\Delta}_1^+ - i)}{(\overline{\Delta}_2^+ + \overline{\Delta}_3^-)\left[\overline{\Delta}_1^+\overline{\Delta}_2^- - 1 - i(\overline{\Delta}_1^+ + \overline{\Delta}_2^-)\right] - f(\overline{\Delta}_1^+ - i)}\,, \tag{70b}$$

and $f = \widetilde{\Delta}_2^+\widetilde{\Delta}_2^- > 0$ as is proved in Appendix B. We note that

$$\text{Im } \mathbf{\Delta}_1 = -\frac{f\overline{\Delta}_1^{+2}(1 + \overline{\Delta}_3^{-2})}{\left|(\overline{\Delta}_1^+ + \overline{\Delta}_2^-)\left(\overline{\Delta}_2^+\overline{\Delta}_3^- - 1 - i(\overline{\Delta}_2^+ + \overline{\Delta}_3^-)\right) - f(\overline{\Delta}_3^- - i)\right|^2} < 0 \tag{71a}$$

$$\text{Im } \mathbf{\Delta}_2 = -\frac{f\overline{\Delta}_3^{-2}(1 + \overline{\Delta}_1^{+2})}{\left|(\overline{\Delta}_2^+ + \overline{\Delta}_3^-)\left(\overline{\Delta}_1^+\overline{\Delta}_2^- - 1 - i(\overline{\Delta}_2^- + \overline{\Delta}_1^+)\right) - f(\overline{\Delta}_1^+ - i)\right|^2} < 0 \tag{71b}$$

Equation (69) is the dispersion relation for the TAE and KTAE roots when the gaps are not aligned so that only a single TAE pair interaction need be accounted for. However, possible continuum damping at the other resonant surface (where toroidal coupling can be neglected) is taken into account by the complex nature of $\mathbf{\Delta}_i$. We note that further simplification in $\mathbf{\Delta}_i$ occurs for the TAE mode at $q = 3/2$, where $\overline{\Delta}_1^+ \gg \overline{\Delta}_2^-$ (note that $\overline{\Delta}_1^+ \to \infty$ if there is no density variation in the profile inside the $q = 3/2$ surface). In this case $\mathbf{\Delta}_1 \doteq \overline{\Delta}_2^-$ which is essentially real. Then Eq. (69) reduces to the dispersion relation determined in Ref. 5.

We also point out that in the dispersion relation given by Eq. (69), $\alpha(\omega)$ is determined by the inner layer equations and $\mathbf{\Delta}_i$ (in general a complex number with Im $\mathbf{\Delta}_i < 0$) is

determined by the global eigenvalue properties. The precise value of this number is unimportant for seeing the qualitative structure of modes. In the Mett-Mahajan work,[9,10] the inner layer equations are quite similar to our theory. In fact, their theory [see e.g. Eqs. (12) of Ref. 10] can be synchronized with the noninteracting gap limit of the present theory with the replacement

$$\frac{-2}{\Delta_i}\frac{1}{1+\sqrt{1+\frac{1}{\Delta_i^2}}} \to G$$

where G of the Mett-Mahajan model was determined by the mode number and the plasma parameters local to the gap [$G = 2\pi/(4n^2q^2 - 1)$ neglecting a density gradient]. Hence, the spectrum of their theory can be described by ours with an appropriate choice of Δ_i. The present theory indicates how Δ_i is systematically evaluated in the large aspect ratio limit.

Now let us analytically consider the spectrum of modes when the imaginary parts of Δ_i and α_i (for real h_i) are small. We look for the root $h_i = h_{i0} + h_{i1}$ that satisfies Eq. (69), where

$$\alpha_{i0}(h_{i0}) + \mathrm{Re}\,\Delta_i = 0 \tag{72a}$$

$$h_{i1} = \frac{-\,\mathrm{Im}\,\Delta_i - \alpha_{i1}(h_{i0})}{\frac{\partial \alpha_{i0}(h_{i0})}{\partial h}} \tag{72b}$$

with $\alpha_{i0}(h_{i0})$ the lowest order part of α_i and α_{i1} the extra part of α_i which we specify below. If we look for a TAE root between $-1 < \mathrm{Re}\ h < 1$, and use Eq. (59b) for α, where we neglect the σ_3 and r terms in α_{i0}, we find,

$$h_{i0} = \frac{\mathrm{Re}\,\Delta_i}{[1+(\mathrm{Re}\,\Delta_i)^2]^{1/2}} \tag{73a}$$

$$h_{i1} = \frac{-ir(h_{i0}) + \tilde{\eta}\frac{1-\lambda^2}{2}\left[1+(\mathrm{Re}\,\Delta_i)^2\right]^2 + \frac{i\,\mathrm{Im}\,\Delta_i}{[1+(\mathrm{Re}\,\Delta_i)^2]^{1/2}}}{1+(\mathrm{Re}\,\Delta_i)^2} \tag{73b}$$

where

$$r(h_{i0}) = \exp\left\{\frac{-2}{[\tilde{\eta}_i(1-\lambda_i^2)]^{1/2}}\, I_1(h_{i0})\right\}$$

with $I_1(-1+x)$ plotted in Fig. 1. For $-1 < h < 0$, we can use an interpolation formula,

$$I_1(h) \simeq \frac{.874\pi(1-h^2)}{3.50(2h)^{1/2} + \pi(1-h^2)} .$$

We also used $\partial\alpha/\partial h = -(1-h^2)^{-3/2}$.

The three sources of damping in Eq. (73b) are respectively due to radiation of kinetic Alfvén waves, collisional damping (Im $\tilde{\eta} < 0$), and continuum damping from the neighboring resonance. Equation (73b) is accurate for small $\tilde{\eta}$. As $\tilde{\eta}$ increases to order unity, our analytic approximations fail, and Eq. (72) needs to be solved numerically. Now let us first evaluate the dispersion relation when $\tilde{\Delta}_2^+ = \tilde{\Delta}_2^- = 0$ so that there is no continuum damping from m-mode coupling. Physically we achieve $\tilde{\Delta}_2^{\pm} = 0$ if $q(a)$ is sufficiently small, e.g., $q(a) < 3$ for a constant density profile. In Figs. 3(a) and 3(b), we show two numerical solutions for $n = 1$, $m = 1, 2$ corresponding to the TAE and the lowest KTAE for the h_1 as a function of $|\eta|$ for $\boldsymbol{\Delta}_1 \doteq \overline{\Delta}_2^- = -0.3$, -0.6 and -1.2, with $\eta = |\eta| \exp(-i0.1)$. Note that the TAE is most strongly affected by changes in $\boldsymbol{\Delta}_1$. For small enough $|\eta|$, the linear dissipation dominates the damping, while at larger, though still moderately small $|\eta|$, the dissipation due to tunneling becomes the more important mechanism. It increases the damping of the TAE by almost an order of magnitude over the linear extrapolation obtained when tunneling is neglected.

In Figs. 4(a) and (b) we compare the two numerical solutions (the TAE and lowest KTAE) for h_1 as a function of $|\eta|$ for $\boldsymbol{\Delta}_1 = -0.6$ with $\eta = |\eta| e^{-0.1i}$, to the solutions obtained using the WKB approximation for α (shown as dashed lines). We see that WKB is very good for $|\eta| \lesssim 0.3$ for both real and imaginary parts. For the KTAE the WKB root deviates slowly and monotonically from the exact solution as $|\eta|$ increases beyond 0.3. Surprisingly, for the TAE, the WKB solution gives a substantial descerpency for $|\eta| \sim 1$ and then seems to track back to the true solution for $|\eta| \gg 1$.

As $|\tilde{\eta}|$ becomes larger than unity, a different analytic approximation can be formulated.

In this regime, as previously reported,[9] radiation damping dominates the TAE description and Im h scales as $\widetilde{\eta}^{1/3}$. In Appendix E we confirm this result and obtain a logarithmic correction. We find

$$h = \sqrt{1-\lambda^2}\, e^{-i\pi/3} \left(\frac{\widetilde{\eta}}{4\sqrt{1-\lambda^2}}\right)^{1/3} \left\{\frac{3}{2} \ln\left(-\frac{if a\sqrt{1-\lambda^2}}{\sqrt{\pi}}\right)\right\}^{2/3},$$

with $a = (\frac{2i\widetilde{\eta}}{\sqrt{1-\lambda^2}})^{1/3}$, $f = \pm\,[(\mathbf{\Delta}_1 - i)/(\mathbf{\Delta}_1 + i)]^{1/2}$ and the upper sign corresponding to TAE and the lower KTAE. It is interesting to note that our WKB form gives the same dominant scaling without the logarithmic correction, even though formally our derivation was valid for small $|\widetilde{\eta}|$. This explains the large $|\widetilde{\eta}|$ WKB behavior illustrated in Figs. 4(a) and 4(b).

In addition to the TAE mode, roots of Eq. (69) can be found corresponding to KTAE modes. We can infer this graphically in Fig. 2(a) and 2(c), which plots Re α_i as a function of h_i. To the extent dissipation can be neglected there are a series of poles, $h_i^{(n)}$ on the real axis for $h_i > 1$, and $\alpha_i(h_i)$ decreases monotonically between the poles. From Eq. (60a), the poles in WKB approximation arise where $\overline{\theta} = -n\pi/2$ [if $h_i - 1 \ll 1$ this is equivalent to $h_i^{(n)} \doteq 1 + (1-\lambda^2)^{1/2}(n + 1/2)(2\widetilde{\eta})^{1/2}$]. Roots arise for h values between the poles, where

$$\alpha_i(h_i) = -\,\mathrm{Re}\ \mathbf{\Delta}_i\ .$$

As long as the imaginary part is small, there will in general be additional KTAE roots between the poles $h_i^{(n)}$ and $h_i^{(n+1)}$.

An explicit description of the eigenvalue can be given when $|h-1| \ll 1$ and $|\eta| \ll 1$. In this case α_i can be approximated as,

$$\alpha_i = \frac{\cos 2\theta + (h-1)\cos 2\theta + 1}{\sqrt{2(h-1)}\sin 2\theta}$$

with $\theta \doteq \frac{\pi(h-1)}{[8\widetilde{\eta}(1-\lambda^2)]^{1/2}} - \frac{\pi}{4}$. Roots occur near the zeroes of $\sin 2\theta$ when $\cos 2\theta \doteq -1$, i.e. where $2\theta = (2p+1)\pi \equiv 2\theta_p$ with p an integer ($p \geq 0$). Hence, writing $h = h_p + \delta h_p$, with $h_p - 1 = [2\widetilde{\eta}(1-\lambda^2)]^{1/2}(2p + 3/2)$ the h value at the poles, and by expanding θ about θ_p,

i.e. $\theta = \theta_p + \delta\theta_p$, we find that the dispersion relation can be written as,

$$\alpha_i + \Delta_i \doteq \frac{-\delta\theta_p^2 + (h_p - 1)/2}{2^{1/2}(h_p - 1)^{1/2}\delta\theta_p} + \Delta_i = 0$$

with $\delta\theta_p = \pi\delta h_p/(8\tilde{\eta}(1-\lambda^2))^{1/2}$. The solution to this equation is

$$\delta\theta_p = \frac{\pi\delta h_p}{[8\tilde{\eta}(1-\lambda^2)]^{1/2}} = \left(\frac{h_p - 1}{2}\right)^{1/2}\left[\Delta_i \pm (1+\Delta_i^2)^{1/2}\right] .$$

Hence we explicitly see that with $|\tilde{\eta}| \ll 1$, $\delta\theta_p$ is small for sufficiently small p with the roots slightly shifted to either side of the poles where $2\theta_p = (2p+1)\pi$. It is also interesting to note that the poles of α correspond to the eigenvalues of the homogeneous equation given by Eq. (53). For small $\tilde{\eta}$ these roots are $h - 1 = [2\tilde{\eta}(1-\lambda^2)]^{1/2}(n + 1/2)$ with n an integer ($n \geq 0$). Thus the actual roots lie close to the odd n-values and the smallest actual root is not close to the ground state of the homogeneous equation, but close to the excited state.

An estimate for the damping can be obtained by treating the imaginary part of Eq. (60a) as small. If $\mathrm{Im}\ \tilde{\eta} \ll \mathrm{Re}\ \tilde{\eta}$, to leading order, we need only expand $\bar{\theta}$ to linear order in $\mathrm{Im}\ \tilde{\eta}/\mathrm{Re}\ \tilde{\eta}$, keep the tunneling term, and it suffices to use the lowest order WKB form. We then find

$$\alpha_i(h_{i0}) \doteq \frac{h_{i0}\cos 2\bar{\theta}_0 + 1}{(h_{i0}^2 - 1)^{1/2}\sin 2\bar{\theta}_0} - i\left(\frac{t}{2} - \frac{\mathrm{Im}\ \tilde{\eta}}{\mathrm{Re}\ \tilde{\eta}}\bar{\theta}_0\right)\frac{h_{i0} + \cos 2\bar{\theta}_0}{(h_{i0}^2 - 1)^{1/2}\sin 2\bar{\theta}_0} \tag{74}$$

where $\bar{\theta}_0$ is given by Eq. (61b) with $\mathrm{Re}\ \tilde{\eta}$ replacing $\tilde{\eta}$. The shift of the eigenfrequency, h_{i1} due to dissipation is then

$$h_{i1} = i\left(\frac{t}{2} - \frac{\mathrm{Im}\ \tilde{\eta}\bar{\theta}_0(h_{i0})}{\mathrm{Re}\ \tilde{\eta}}\right)\frac{h_{i0} + \cos 2\bar{\theta}_0}{(h_{i0}^2 - 1)^{1/2}\sin 2\bar{\theta}_0}\Big/\frac{\partial\alpha_{i0}(h_{i0})}{\partial h} \tag{75}$$

where h_{i0} satisfies the real part of the dispersion relation. Now

$$\frac{\partial\alpha_{i0}(h_{i0})}{\partial h} \doteq -\frac{2I_4(h_{i0})}{[(1-\lambda^2)\tilde{\eta}]^{1/2}}\frac{h_{i0} + \cos 2\theta_0}{\sin^2 2\theta_0(h_{i0}^2 - 1)^{1/2}} \tag{76}$$

where

$$I_4(h) = \int_0^{(h-1)^{1/2}} dz\,\frac{h - z^2}{[(h-z^2)^2 - 1]^{1/2}} ,$$

is plotted in Fig. 1 for $h = 1 + x$. Hence we find

$$h_{i1} = -\frac{i}{2}\frac{[(1-\lambda^2)\,\mathrm{Re}\,\tilde{\eta}]^{1/2}}{I_4(h_{i0})}\left[\frac{t(h_{i0})}{2} - \frac{\mathrm{Im}\,\tilde{\eta}}{\mathrm{Re}\,\tilde{\eta}}\bar{\theta}_0(h_{i0}) - \frac{\sin^2 2\theta_0 (h_{i0}^2-1)^{1/2}}{h_{i0}+\cos 2\theta_0}\,\mathrm{Im}\,\Delta_i\right] . \quad (77)$$

Recall that $t(h_{i0})$ and $\theta_0(h_{i0})$ is given by Eqs. (61b) and (61c). Note that if $\tilde{\Delta}_2^+\tilde{\Delta}_2^- > 0$, Im $h_{i1} < 0$, which corresponds to damping.

This pairing of the KTAE roots for $|\eta| \ll 1$ is readily seen in the numerical solutions of Eqs. (69a) and (69b) shown in Fig. 5(a) using the numerical values of $\overline{\Delta}_i$ and $\tilde{\Delta}_i$ listed in Table I. The corresponding imaginary frequencies are shown in Fig. 5(b). The solid lines correspond to roots of gap 1 with $\alpha_2 = -i$ while the dashed lines depict roots of gap 2 with $\alpha_1 = -i$. Note that the damping of the TAE roots plateau for decreasing $|\eta|$ due to continuum damping. It is interesting to note that the KTAE do not experience this effect. The KTAE damping is much smaller for $|\tilde{\eta}| \ll 1$ because the modes become very localized in this limit. The KTAE are not strongly affected by Im $\boldsymbol{\Delta}_i$; the imaginary character of $\tilde{\eta}$ is more important to the damping.

We note in passing that there is another set of KTAE modes near $h = -1$. They are associated with the poles of $\alpha(h_i)$ in the complex plane. When $\tilde{\eta}$ is real, these poles are in the complex plane, and when $|h+1| \ll 1$, we can use Eqs. (B10a) and (B8) to see that the poles occur where $\frac{1}{4} + \frac{a}{2} = -n$ with $n = 0, 1, 2, \ldots$, and $a = -i(1-h^2)/[-8\tilde{\eta}h(1-\lambda^2)]^{1/2}$. For $h \doteq -1$, the poles are approximately given by $h = -1 - i[2\tilde{\eta}(1-\lambda^2)]^{1/2}(n+1/2)$. The eigenvalues to the dispersion relation, given by Eq. (69), are slightly shifted from the poles. These roots are much more damped than the first KTAE modes we discussed, and hence seem less important to consider. This structure of these poles have also been discussed by Candy and Rosenbluth.[11] It should be noted that the similar pole structure was found in Ref. 3 for the resistive TAE case. However, as they treated a purely resistive parallel conductivity, the pole structure is rotated in the complex plane, from what is found in Candy-Rosenbluth and here.

Finally, we consider the case where two TAE gaps are nearly aligned. In this case Eq. (68) is more difficult to analyze analytically, though one can easily show that stability is guaranteed if $\widetilde{\Delta}_2^+ \widetilde{\Delta}_2^- > 0$ (see the last part of Appendix B). Instead, we show numerical solutions in Figs. 6(a) and 6(b) as a function of $\eta \equiv |\eta| \exp(-i\theta)$ are $\theta = 0$ and $\theta = .1$ with $\overline{\Delta}$ and $\widetilde{\Delta}$ taken from Table I. We clearly see the branches of the TAE modes for each gap, and that the modes become more strongly damped with increasing $|\eta|$. When the gaps are in alignment, continuum mode damping disappears, and hence the TAE mode is much less damped than in the misaligned case shown in Figs. 5(a) and (b). In addition, the real frequencies of the TAE are significantly affected by the interaction of the two gaps. The KTAE branches are also seen, with the coalescence of mode to the same eigenvalue as $|\eta|$ decreases including the fine structure pairing that is seen when there is no alignment. We also observe the interesting interaction when frequencies try to cross. Figures 6(c) and (d) give an expanded view of this region. Usually, the Re Ω curves do not cross while the imaginary curves cross. However, in the case that the real frequencies cross, the correspondingly Im Ω curves maintain a gap. One can show that as we follow $|\eta|$ continuously, continuous modes frequently switch polarization from say predominantly $m = 1, 2$ to $m = 2, 3$. Otherwise the shape of the KTAE spectrum with two resonant regions, is quite similar to the KTAE spectrum obtained when one neglects the interaction of $m = 1, 2$ modes with $m = 2, 3$ modes.

VI. Acknowledgments

We are indebted to M.N. Rosenbluth, J. Candy, B. Breizman, J.W. Van Dam, and S. Mahajan for important discussions. We are particularly thankful to M.N. Rosenbluth and J. Candy for making available to us their work in preliminary form. This work was supported by the U.S. Department of Energy contract #DE-FG05-80ET-53088.

Appendix A – Numerical Evaluation of $\overline{\Delta}_m$ and $\widetilde{\Delta}_m$

The cylindrical equations are of the form

$$\begin{aligned} \frac{d\widehat{C}_m(r)}{dr} &= (m^2-1)\left(\Omega^2\rho(r) - k_m^2(r)\right)\phi_m - r\Omega^2\frac{\partial\rho}{\partial r}\phi_m \\ r^3\Big(\rho(r)\Omega^2 - k_m^2(r)\Big)\frac{\partial(\phi_m/r)}{\partial r} &= \widehat{C}_m(r) \end{aligned} \tag{A1}$$

with $k_m^2(r) = [m/q(r) - n]^2$.

Let us first assume both r_{m-1} and r_m exist. Then we integrate between $0 < r < r_{m-1}$ to evaluate $\phi_m^{(a)}(r)$. Numerically, we start at a point $r = \delta_i$ with $\delta_i \ll 1$, set $\Omega^2 = \Omega_{m-1}^2$ and integrate to $r = r_m(1-\delta)$ with $\delta \ll 1$. Numerically, we take the well-behaved boundary condition as $\phi_m^{(a)}(\delta_i) = \delta_i^m$ and $\widehat{C}_m^{(a)}(\delta_i) = \delta_i^{m+1}(m-1)\left(\rho(0)\Omega_{m-1}^2 - k_m^2(0)\right)$, which is exact as $\delta_i \to 0$.

We now integrate Eq. (A1) to $r = r_m(1-\delta)$, and determine $\phi_m\Big(r_{m-1}(1-\delta)\Big)$ and $\widehat{C}_m\Big(r_m(1-\delta)\Big)$. We also define

$$a_m = \left| r_{m-1}^2 \frac{\partial}{\partial r}\Big(\rho(r_{m-1})\Omega_{m-1}^2 - k_m^2(r_{m-1})\Big)\right| = \frac{nr_{m-1}^2}{q_{m-1}^2} q'_{m-1}\left(1+\lambda_{m-1}\right) .$$

In the vicinity of $r = r_{m-1}$, the solution for $\phi_m^{(a)}(r)$ then matches to

$$\phi_m^{(a)}(r) = \frac{\widehat{C}_m(r_{m-1}-\delta)}{a_m}\left[\ln\Big(n[q_{m-1}-q(r)]\Big) + \pi\Delta_m^{(a)}\right] . \tag{A2}$$

Recall that $\widehat{C}_m^{(a)}(r_{m-1})/a_m = C_m^-$.

We now determine $\phi_m^-(r)$ in the region $r_{m-1}+\delta < r < r_m^+ - \delta$ for $\Omega^2 = \Omega_{m-1}^2$. The point r_m^+ is defined by $\rho^{1/2}(r_m^+)\Omega_{m-1} = n - m/q(r_m^+)$. For now we assume r_m^+ exists and is close to $r = r_m$ (i.e. $n|q_m - q(r_m^+)| \ll 1$). With an initial condition, $\phi^-(r_m^+ - \delta) = 1$ and $\widehat{C}^-(r_m^+ - \delta) = 0$ (note that $\phi^-(r)$ is regular at $r = r_m^+$), we integrate to $r = r_{m-1} + \delta$ thereby

finding $\widehat{C}_m^-(r_{m-1}+\delta)$ and $\phi_m^-(r_{m-1}+\delta)$. Then in the vicinity of $r = r_{m-1}+\delta$, the analytic form for $\phi_m^-(r)$ is

$$\phi_m^-(r) = \frac{\widehat{C}_m^-(r_{m-1}+\delta)}{a_m}\left[\ln\Big(n(q-q_m)\Big) + \pi\Delta_m^-\right] . \tag{A3}$$

The quantities $\overline{\Delta}_m^-$ and $\widetilde{\Delta}_m^-$, defined by Eq. (12), are then given by

$$\lim_{\delta\to 0}\left[\frac{\phi_m^{(a)}(r_{m-1}-\delta)}{\widehat{C}_m^{(a)}(r_{m-1}-\delta)} - \frac{\phi_m^-(r_{m-1}+\delta)}{\widehat{C}_m^-(r_{m-1}+\delta)}\right] = \pi\left(\Delta_m^{(a)} - \Delta_m^-\right) \equiv \pi\overline{\Delta}_m^- . \tag{A4}$$

$$\widetilde{\Delta}_m^- = \frac{a_m}{\pi\widehat{C}_m^-(r_{m-1}+\delta)} + \mathcal{O}(\delta) . \tag{A5}$$

We note that, if desired, higher order accuracy in δ can be achieved with straightforward analytic analysis.

We now integrate Eq. (A1) for $\phi_m^+(r)$ from $r = r_m^- + \delta$ to $r_m - \delta$ with $\Omega^2 = \Omega_m^2$, and with the boundary conditions $\phi_m^+(r_m^-+\delta) = 1$ and $\widehat{C}_m^+(r_m^-+\delta) = 0$, where $\rho^{1/2}(r_m^-)\Omega_m = -n + m/q(r_m^-)$ [again we assume r_m^- exists and $n|q_{m-1} - q(r_m^-)| \ll 1$]. We also integrate $\phi_m^{(b)}(r)$ from $r = a$ to $r_m + \delta$, with the boundary condition $\phi_m^{(b)}(a) = 0$ and $\widehat{C}_m^{(a)}(r = a) = 1$. We define

$$b_m = r_m^2\left|\frac{\partial}{\partial r}\Big(\rho(r_m)\Omega_m^2 - k_m^2(r_m)\Big)\right| = \frac{nr_m^2}{q_m^2}q_m'(1-\lambda_m) .$$

As before, we find

$$\begin{aligned}\overline{\Delta}_m^+ &= \frac{b_m}{\pi}\left[\frac{\phi^{(b)}(r_m+\delta)}{\widehat{C}_m^{(b)}(r_m+\delta)} - \frac{\phi^+(r_m-\delta)}{\widehat{C}_m^+(r_m-\delta)}\right] \\ \widetilde{\Delta}_m^+ &= \frac{b_m}{\pi\widehat{C}_m^+(r_m-\delta)} .\end{aligned} \tag{A6}$$

In calculating a "string" of poloidal harmonics from $m_i \le m \le m_f$ with $\dfrac{m_i - 1/2}{n} < q(0) < \dfrac{m_i + 1/2}{n}$, and $\dfrac{m_f - 1/2}{n} < q(a) < \dfrac{m_f + 1/2}{n}$, the first member of the string and the last member of the string will have only one toroidal Alfvén resonance. For these cases, the resonance point r_m^- or r_m^+ may or may not exist. If $r_m^+(r_m^-)$ does not exist, then $\widetilde{\Delta}_m^-(\widetilde{\Delta}_m^+)$ is zero.

To be concrete let us consider two examples. First let $m = m_i$. Then the resonant surface $q = q_{m_i} = (m_i + 1/2)/n$ is in the plasma and $q = (m_i - 1/2)/n$ is not in the plasma. Likewise let us assume that the point $r^-_{m_i}$ is not in the plasma [in principle, this assumption can be violated, e.g. when the density variation is negligible $q(r^-_{m_i}) = \dfrac{m_i(2m_i+1)}{2n(m_i+1)} > \dfrac{m_i - 1/2}{n}$ and it is possible that $\dfrac{m_i - 1/2}{n} < q(0) < q(r^-_{m_i})$; however, for simplicity we restrict the choice of parameters so that $q(r^-_{m_i}) < q(0)$]. Then for $m = m_i$ there is only one resonant point at $q = q_{m_i}$. We then integrate the differential equation with $\Omega^2 = \Omega^2_{m_i}$ from the origin to $r_m - \delta$ for $\phi^{(a)}_m(r)$, and from $r = a$ to $r = r_m + \delta$ for $\phi^{(b)}_m(r)$. We then have $\widetilde{\Delta}^{\pm}_{m_i} = 0$, $\overline{\Delta}^-_{m_i} = 0$ and $\overline{\Delta}^+_{m_i}$ given by Eq. (A6) with $\phi^{(a)}_m(r - \delta)$ replacing $\phi^+_m(r - \delta)$. A second example is when we choose $m = m_f$, only one TAE resonance, at $q = q_{m_f}$ is present. Then $\widetilde{\Delta}^{\pm}_{m_f} = \overline{\Delta}^+_{m_f} = 0$, and $\overline{\Delta}^-_{m_f}$ is constructed in the obvious way.

Another point regarding the validity of the three-term recursion relation needs to be noted. The accuracy of the recursion relation requires both $|n[q(r_m) - q(r^+_m)]|$ and $|n[q(r_{m-1}) - q(r^-_m)]|$ to be small. Formally, these inequalities are only automatically fulfilled for n large. However, even for $n \approx 1$, these numbers tend to be less than unity, so that they are in practice sufficiently well satisfied for even low n. Nonetheless, if there is a strong mismatch of TAE toroidal coupling, an alternative termination and initiation procedures of the three-term recursion relation needs to be formulated (though in practice we have not found it necessary to implement such an alternative method). For example, we may wish to terminate a string in the three-term recursion relation at $m = m_\ell + 1$ because $|n[q(r^+_{m_{f+1}}) - q(r_{m_\ell+1})]|$ is too large, so that toroidal coupling is negligible (note, $m_{\ell+1}$ need not necessarily the largest possible m value). In this case we take $\beta_{m_\ell+1} = 0$, as we assume there is negligible toroidal coupling to $C^-_{m_\ell+2}$. In addition, in calculating $\widetilde{\Delta}^+_{m_\ell+1}$ and $\overline{\Delta}^+_{m_\ell+1}$ we use, in integrating Eq. (A1), $\Omega^2 = \Omega^2_{m_\ell}$ with the singular points of the $m = m_\ell + 1$ mode at $r = r_{m_\ell}$ and $r = r^+_{m_{\ell+1}}$. Similar considerations apply if an alternative initiation of a string is needed. Then if an initial m at $m = m_k$ is taken, we should set $\beta_{m_k-1} = 0$, and use $\Omega^2 = \Omega^2_{m_k}$ in integrating

Eq. (A1) when calculating $\overline{\Delta}^{-}_{m_k}$ and $\tilde{\Delta}^{-}_{m_k}$. For $m_k + 1 \leq m \leq m_\ell$, the $\overline{\Delta}$'s and $\tilde{\Delta}$'s are calculated in the standard way discussed earlier. There is then a three-term recursion relation defined for $m_k + 1 \leq m \leq m_\ell$, and a two-term relation for $m = m_k$ and $m = m_\ell + 1$. This truncation at the ends allows for a properly posed eigenvalue problem for the three-point recursion relation.

Finally, we present numerical results of the calculated $\overline{\Delta}$ and $\tilde{\Delta}$ values in Table I, and compare them to $\overline{\Delta}^{\infty}$ and $\tilde{\Delta}^{\infty}$, that would be calculated for the high-n equations used in Ref. 8. We see that there is a strong tendency for $\overline{\Delta}^{+}_{m} > \overline{\Delta}^{\infty}_{m} > \overline{\Delta}^{-}_{m}$, and that appropriately compared values approach each other as n increases. However, near $r = 0$ and $r = a$, there can be significant differences in the $\overline{\Delta}$-values, even in the sign of $\overline{\Delta}$. In all these cases, the three-term recursion relation terminates by having $\tilde{\Delta} = 0$ at the first and last allowed m values.

Appendix B – Proof of Stability

We consider the case where the kinetic terms on the right-hand side of Eq. (1) are neglected. We then follow the manipulations from Eqs. (15)–(21), with $\phi^*_m(r)$ chosen as the adjoint trial function. It then straightforwardly follows that Eq. (21) is altered to the following form

$$\sum_m \frac{r_m\, q'_m}{q_m^2}$$

$$\left[(1+\lambda_m) C^-_{m+1}\, C^{*-}_{m+1} \left(\overline{\Delta}^-_{m+1} + \alpha_m \right) + (1-\lambda_m) C^{+*}_m C^+_m \left(\overline{\Delta}^+_m + \alpha_m \right) \right.$$

$$\left. + \beta_m (1+\lambda_m)^{1/2} (1-\lambda_m)^{1/2} \left(C^{+*}_m\, C^-_{m+1} + C^{-*}_{m-1}\, C^+_m \right) \right]$$

$$-\frac{1}{2} \sum_m \left[\frac{r_m\, q'_m}{q_m^2} (1+\lambda_m)\, \tilde{\Delta}^+_{m+1}\, C^{+*}_{m+1}\, C^-_{m+1} + \frac{r_{m+1}\, q'_{m+1}}{q_m^2} (1-\lambda_{m+1}) \tilde{\Delta}^-_{m+1}\, C^+_{m+1}\, C^*_{m+1} \right.$$

$$\left. + \frac{r_m\, q'_m}{q_m^2} (1-\lambda_m) \tilde{\Delta}^-_m\, C^+_m\, C^{-*}_m + \frac{r_{m-1}\, q'_{m-1}}{q^2_{m-1}} (1+\lambda_{m-1}) \tilde{\Delta}^+_m\, C^{+*}_m\, C^-_m \right]$$

$$= 0. \tag{B1}$$

We now assume that the Wronskian relation, given by Eq. (14) is exactly satisfied (in practice, in our numerical scheme, this is only approximately true and to the extent it is not satisfied spurious instability cannot in principle be ruled out; however we have not found any such cases with our numerical searches and as we will see below, we conjecture that it will not occur; at any event the numerical scheme can be altered to have the near identity given by Eq. (14) exactly satisfied, e.g. $\tilde{\Delta}^-_m$ can be defined by Eq. (14), with $\tilde{\Delta}^+_m$ calculated by the methods described in the text). Hence the sum of the last bracket is real. If we now take the

imaginary part of Eq. (B1) we find, with $D^-_{m+1} = (1+\lambda_m)^{1/2}\, C^-_{m+1}$, $D^+_m = (1-\lambda_m)^{1/2}\, C^+_m$,

$$\frac{1}{2}\sum_m \frac{r_m q'_m}{q_m^2}\left[\begin{array}{l} (\mathrm{Im}\ \alpha_m + \mathrm{Im}\ \beta_m)\left(D^-_{m+1}+D^+_m\right)\left(D^-_{m+1}+D^+_m\right)^* \\ \\ +(\mathrm{Im}\ \alpha_m - \mathrm{Im}\ \beta_m)\left(D^-_{m+1}-D^+_m\right)\left(D^-_{m+1}-D^+_m\right)^* \end{array}\right] = 0. \tag{B2}$$

If $q'_m > 0$, as we have implicitly assumed throughout this work, we note that Eq. (B2) cannot be satisfied if $\mathrm{Im}\ \alpha < 0$, $-\mathrm{Im}\ \alpha_m > |\mathrm{Im}\ \beta_m|$. These inequalities are indeed satisfied as has been proved by Candy and Rosenbluth,[10] for the case $\lambda = 0$, and readily follows in our case from Eqs. (45) using the same arguments as Ref. 10.

It is also of interest to note that $\tilde{\Delta} < 0$ is guaranteed from Eqs. (1) and (2) in the $\hat{\varepsilon} = 0$ limit. From Eq. (10) it is clear that $\phi^-_m(r) < 0$ as $q \to q_{m-1}$. However, $\phi^-_m(r)$ cannot change sign between $r_{m-1} < r < r_m$. If it did change sign a contradiction would follow from an identity formed from the quadratic form obtained from Eqs. (1) and (2),

$$r\phi_m(r)\frac{d\phi_m(r)}{dr}\bigg|_{r_1}^{r_2} = \int_{r_1}^{r_2} dr\left\{r\left(\rho(r)\Omega^2 - k_m^2(r)\right)\left[\left(\frac{d\phi_m}{dr}\right)^2 + m^2\phi_m\right] + k_m^2\, r\phi_m^2\right\}. \tag{B3}$$

Now suppose $\phi_m(r)$ changed sign at $r = r_T$ with $r_{m-1} < r_T < r_m$. Then choosing $r_1 = r_T$, $r_2 = r_m$ and $\phi_m = \phi^-_m(r)$, we find, that since $\phi^-_m(r)$ is regular at $r = r_m$, that the left-hand side of Eq. (B3) vanishes, while the right-hand side is positive definite. To avoid a contradiction $\phi^-_m(r)$ cannot change sign; hence $\phi^-_m(r)$ is negative in the interval $q_{m-1} \le q < q_m$, and therefore $\tilde{\Delta}^-_m \equiv \phi^-_m(r = r_{m-1})/\pi < 0$. From the same arguments we also conclude $\tilde{\Delta}^+_m < 0$, and $\tilde{\Delta}^+_m\,\tilde{\Delta}^-_m > 0$.

The actual difference scheme that we employed numerically, does not exactly satisfy Eq. (14), and the stability proof does not strictly apply to it. However, the condition $\tilde{\Delta}^+_m\,\tilde{\Delta}^-_m > 0$ does apply. For the $n = 1$ analysis of Sec. V, we essentially show below that the stability of the equations only required $\alpha_m^2 - \beta_m^2 = -1$, $\mathrm{Im}\ \alpha_m < 0$, and $\tilde{\Delta}^+_m\,\tilde{\Delta}^-_m \ge 0$. We conjecture that the condition $\tilde{\Delta}^\pm_m \le 0$ together with the conditions on α_m is all that is

required for the stability of the general 3-point recursion relation for the actual numerical scheme used in this work.

To see that stability seems to only require these conditions for the system given by Eq. (67), we adopt the following perturbative procedure. First, we look for roots of Eq. (68) when, to lowest order, α_m is real for real h. We will now show that these roots are real (hence to lowest order stable). In the text we have already shown, at least perturbatively, that the imaginary parts of α_m induces a damping component to the roots [see Eqs. (73b) and (77)]. Hence, the demonstration of reality of the lowest order roots is tantamount to stability of the system.

When α_m is taken as real for real h, the dispersion relation, $D(\Omega) = 0$, in Eq. (68) is a real function of real Ω. Hence, if a complex root can arise, both Ω and Ω^* would be roots. At marginal stability a double root must occur, so that $\partial D(\Omega)/\partial\Omega = 0$. When $\tilde{\Delta}_2^- \tilde{\Delta}_2^+ = 0$, it is straightforward to solve Eq. (68) and show that Ω is real. Then consider the evolution of the roots as $\tilde{\Delta}_2^+ \tilde{\Delta}_2^-$ increases (note both $\tilde{\Delta}_2^+$ and $\tilde{\Delta}_2^-$ are negative in an MHD stable plasma). If instability is to arise, two Ω roots have to coalesce at a critical value of $\tilde{\Delta}_2^+ \tilde{\Delta}_2^-$. At this value $\frac{\partial D(\Omega)}{\partial\Omega} = D(\Omega) = 0$. However, if we get $\frac{\partial D(\Omega)}{\partial\Omega} = 0$, we find the relation

$$\begin{aligned}&\left[\overline{\Delta}_2^+ + \overline{\Delta}_3^- - \frac{1+\overline{\Delta}_3^{-2}}{\overline{\Delta}_3^- + \alpha_2}\right] \frac{\partial\alpha_1}{\partial h_1}(1+\overline{\Delta}_1^{+2})\hat{\epsilon}_1\,\Omega_1^2(\alpha_2+\overline{\Delta}_3^-)\\ &= -\left[\overline{\Delta}_1^+ + \overline{\Delta}_2^- - \frac{1+\overline{\Delta}_1^{+2}}{\overline{\Delta}_1^+ + \alpha_1}\right] \frac{\partial\alpha_2}{\partial h_2}(1+\overline{\Delta}_3^{-2})\hat{\epsilon}_2\,\Omega_2^2(\alpha_1+\overline{\Delta}_1^+).\end{aligned} \tag{B4}$$

Substituting this relation into $D(\Omega) = 0$, yields

$$D(\Omega) = -\frac{\dfrac{\partial\alpha_2}{\partial h_2}}{\dfrac{\partial\alpha_1}{\partial h_1}} \frac{(\overline{\Delta}_1^+ + \alpha_1)^2}{(\overline{\Delta}_3^- + \alpha_2)^2}\left[\overline{\Delta}_1^+ + \overline{\Delta}_2^- - \frac{1+\overline{\Delta}_1^{+2}}{\alpha_1+\overline{\Delta}_1^+}\right]^2 \frac{\hat{\epsilon}_2\,\Omega_2^2}{\hat{\epsilon}_1\,\Omega_1^2}\frac{1+\overline{\Delta}_3^{-2}}{1+\overline{\Delta}_1^{+2}} - \tilde{\Delta}_2^+\tilde{\Delta}_2^- < 0. \tag{B5}$$

The inequality follows as we have previously showed that $\tilde{\Delta}_2^+ \tilde{\Delta}_2^- > 0$ and $\partial\alpha_2/\partial h_2 < 0$ and $\partial\alpha_1/\partial h_1 < 0$ [see just after Eq. (73) and Eq. (76)]. Hence, we can never have marginal

stability. Thus, as the roots are real for $\tilde{\Delta}_2^+ \tilde{\Delta}_2^- = 0$, they remain real for all positive values of $\tilde{\Delta}_2^+ \tilde{\Delta}_2^-$. Q.E.D.

It is interesting to note that if $\tilde{\Delta}_2^+ \tilde{\Delta}_2^+ < 0$ (which as we have seen, can only occur in a MHD unstable system) then an unstable TAE root may occur, as $D(\Omega)$ can then vanish for a double root.

Appendix C – Gamma Function Approximations

For $\tilde{\eta} \ll 1$ and $|h^2 - 1| \ll 1$, it is a good approximation to drop the k^4 term in the potential of Eq. (53). The resulting equation may be cast into the standard form of the parabolic cylinder equation[13]

$$\frac{d^2\Psi_{ih}}{dx^2} - \left(\frac{1}{4}x^2 + a\right)\Psi_{ih} = 0 \ , \tag{C1}$$

where $x = [8\tilde{\eta}h/(1-\lambda^2)]^{1/4}[k \pm i(1-\lambda^2)^{1/2}/2h]$ and $a = [1-h^2+(1-\lambda^2)\tilde{\eta}/2h]/(8\tilde{\eta}h(1-\lambda^2))^{1/2}$ (note that the branch of the square root is chosen so that $h^{1/2} \propto i$ when h is real and negative). Decaying solutions for large k are given by [see Ref. 13]

$$\Psi_{ih} = BU(a,x) \ , \tag{C2}$$

where B is an arbitrary constant and $U(a,x)$ the standard parabolic cylinder function that is well behaved at positive infinity. Substituting Eq. (C2) into Eq. (54a) yields

$$\frac{\Psi_{1h}(0^+)}{\Psi_{2h}(0^+)} = \left\{-h\left[1 - 2x_0\frac{U'(a,x_0)}{U(a,x_0)}\right]\right\}^{-1} \tag{C3}$$

where $x_0 \equiv i[h\tilde{\eta}(1-\lambda^2)/2]^{1/4}/h$. Although the ratio f is now determined, it is important to realize that Eq. (C3) is approximate, and more accurate approximation to f can be obtained if Ψ_{1h} and Ψ_{2h} are treated in identical ways (e.g. we would like to maintain the condition $Im(\alpha) < 0$ for real h). Then starting with the second order equation for Ψ_{2h}, writing $\Psi_{2h} \propto U(a,x)$ and using Eq. (54b), we find, at $k = 0$,

$$\frac{\Psi_{1h}(0^+)}{\Psi_{2h}(0^+)} = -h\left[1 + 2x_0\frac{U'(a,-x_0)}{U(a,-x_0))}\right] \ . \tag{C4}$$

To treat the two approximate forms equally, we multiply together Eqs. (C3) and (C4) and take the square root, to obtain

$$\frac{\Psi_{1h}(0^+)}{\Psi_{2h}(0^+)} = \mathrm{sgn}(\mathrm{Re}(-h))\left\{\frac{1 + 2x_0\dfrac{U'(a,-x_0)}{U(a,-x_0)}}{1 - 2x_0\dfrac{U'(a,x_0)}{U(a,x_0)}}\right\}^{1/2} \ . \tag{C5}$$

Then from Eqs. (50a) and (50b) we find

$$\alpha = \frac{i + ix_0 \dfrac{U'(a,-x_0)}{U(a,-x_0)} - ix_0 \dfrac{U'(a,x_0)}{U(a,x_0)}}{x_0 \dfrac{U'(a,-x_0)}{U(a,-x_0)} + x_0 \dfrac{U'(a,x_0)}{U(a,x_0)}} , \tag{C6a}$$

$$\beta = -\text{isgn}(\text{Re}(-h)) \frac{\left[1 + 2x_0 \dfrac{U'(a,-x_0)}{U(a,-x_0)}\right]^{1/2} \left[1 - 2x_0 \dfrac{U'(a,x_0)}{U(a,x_0)}\right]^{1/2}}{x_0 \dfrac{U'(a,-x_0)}{U(a,-x_0)} + x_0 \dfrac{U'(a,x_0)}{U(a,x_0)}} . \tag{C6b}$$

Equations (C5) and (C6) may be simplified by expanding U in a power series [see Ref. 13] as

$$U(a,x) = Gy_1 - y_2 , \tag{C7}$$

where

$$G = 2^{-1/2}\Gamma\left(\frac{1}{4} + \frac{a}{2}\right) / \Gamma\left(\frac{3}{4} + \frac{a}{2}\right) , \tag{C8}$$

and

$$y_1 = 1 + \frac{1}{2!}ax^2 + \frac{1}{4!}\left(a^2 + \frac{1}{2}\right)x^4 + \frac{1}{6!}\left(a^3 + \frac{7}{2}a\right)x^6 + \frac{1}{8!}\left(a^4 + 11a^2 + \frac{15}{4}\right)x^8 + \ldots$$

$$y_2 = x + \frac{1}{3!}ax^3 + \frac{1}{5!}\left(a^2 + \frac{3}{2}\right)x^5 + \frac{1}{7!}\left(a^3 + \frac{13}{2}a\right)x^7 + \frac{1}{9!}\left(a^4 + 17a^2 + \frac{63}{4}\right)x^9 + \ldots$$

Making the appropriate substitutions, we can then write, to a reasonable degree of accuracy,

$$\frac{\Psi_{1h}(0^+)}{\Psi_{2h}(0^+)} = \text{sgn}(\text{Re}(-h)) \left\{ \frac{\left(1 - \dfrac{x_0}{G}\right)^2 - ax_0^2}{\left(1 + \dfrac{x_0}{G}\right)^2 - ax_0^2} \right\}^{1/2} + \mathcal{O}\left[\frac{x_0}{G}(ax_0^2)^2\right] + \mathcal{O}\left(\frac{x_0}{G}x_0^4\right) . \tag{C9}$$

The series expansions contain two small parameters, $\nu \equiv (1-h^2)^{1/2}/h$ and $\tilde{\eta}$. The ordering in Eq. (C9) is apparent from $\frac{x_0}{G} = \mathcal{O}(\nu) + \mathcal{O}(\nu\tilde{\eta})$, $ax_0^2 = \mathcal{O}(\nu^2) + \mathcal{O}(\tilde{\eta})$, and $x_0^4 = \mathcal{O}(\tilde{\eta})$. Substituting Eq. (C9) into Eqs. (50a) and (50b) we find

$$\alpha = -i \frac{1 + \left(\dfrac{x_0}{G}\right)^2 - ax_0^2}{2\dfrac{x_0}{G}} + \mathcal{O}\left[\frac{G}{x_0}(ax_0^2)^2\right] + \mathcal{O}\left(\frac{G}{x_0}x_0^4\right) , \tag{C10a}$$

$$\beta = \mathrm{isgn}(\mathrm{Re}(-h))\frac{\left[\left(1-\frac{x_0}{G}\right)^2 - ax_0^2\right]^{1/2}\left[\left(1+\frac{x_0}{G}\right)^2 - ax_0^2\right]^{1/2}}{2\frac{x_0}{G}}$$

$$+\mathcal{O}\left[\frac{G}{x_0}(ax_0^2)^2\right] + \mathcal{O}\left(\frac{G}{x_0}x_0^4\right) . \qquad \text{(C10b)}$$

Further insight into Eqs. (C9) and (C10) is provided by examining the form of G when (formally) $|a| \gg 1$. There are four regimes of interest; each one for a in a different quadrant in the complex plane. We assume h is nearly real.

(1) $\mathrm{Re}(h) < -1$. Here $-ia$ is nearly real and has positive real and imaginary parts. The reflection formula then exactly gives [see Ref. 13]

$$\frac{\Gamma\left(\frac{1}{4}+\frac{i(-ia)}{2}\right)}{\Gamma\left(\frac{3}{4}+\frac{i(-ia)}{2}\right)} = \pi^{-1}\sin\left[\pi\left(\frac{3}{4}+\frac{i(-ia)}{2}\right)\right]\Gamma\left(\frac{1}{4}+\frac{i(-ia)}{2}\right)\Gamma\left(\frac{1}{4}-\frac{i(-ia)}{2}\right) . \qquad \text{(C11)}$$

Since the last two terms on the right-hand side of Eq. (C11) are complex conjugates of each other when $-ia$ is real, the *sin* term captures all of the imaginary contributions. This is essential for capturing the radiative or tunneling contribution to the damping, which is present in case (2). Hence this contribution is more important in region (2), $-1 < \mathrm{Re}(h) < 0$, but we treat it here for completeness. Application of Stirling's formula [Ref. 13] to the last two terms in Eq. (C11) yields

$$\Gamma\left(\frac{1}{4}+\frac{i(-ia)}{2}\right)\Gamma\left(\frac{1}{4}-\frac{i(-ia)}{2}\right) = 2\pi\left\{\frac{2}{-ia\,\mathrm{sgn}\,[\mathrm{Re}(-ia)]}\right\}^{1/2}\exp\left\{-\frac{\pi}{2}(-ia)\,\mathrm{sgn}\,[\mathrm{Re}(-ia)]\right\}$$

$$\times\left\{1+[4(-ia)]^{-2}+\mathcal{O}[(-ia)^{-4}]\right\} , \qquad \text{(C12)}$$

where we have expanded accurately with a fourth order error. This is necessary to ultimately exhibit dissipation proportional to $\mathrm{Im}(\tilde{\eta})$. Equation (C12) also holds with the replacement $-ia \to ia$. Combining Eq. (C11) and Eq. (C12) gives

$$G = (-ia)^{-1/2}e^{-i\pi/4}\left[1+ie^{-\pi(-ia)}\right]\left\{1+[4(-ia)]^{-2}+\mathcal{O}[(-ia)^{-4}]\right\} . \qquad \text{(C13)}$$

We point out that the accuracy of this approximation up to and including $\mathcal{O}[(-ia)^{-2}]$ increases with increasing $|a|$, and is accurate to within 15% for $|a| = 0.5$ with h real. The same is true in regions (2)–(4), with Eqs. (C17), (C21), and (C25) (for $\mathrm{Re}(h) > 1$). With Eq. (C13), we find, using Eq. (C9),

$$\frac{\Psi_{1h}(0^+)}{\Psi_{2h}(0^+)} = -\left[h + (h^2-1)^{1/2}\right]\left[1 + \sigma(h^2-1)^{1/2}\right] + \mathcal{O}(\nu^5\sigma) + \mathcal{O}(\sigma^2)\ , \tag{C14}$$

where, in region (1),

$$\sigma = i\exp[-\pi(-ia)] + \frac{\tilde{\eta}(1-\lambda^2)}{2(1-h^2)^2}\ . \tag{C15}$$

It has been verified from Eqs. (C5), (C7) and (C8) that Eq. (C14) is correct to all orders in ν in the limit $\tilde{\eta} \to 0$, which is the ideal limit. This is to be expected since the parabolic cylinder equation reduces to the same ideal limit as the exact inner layer equation, Eq. (53). We conjecture that the $\tilde{\eta}$ correction term in Eq. (C14) is also accurate to all orders in ν because the k^4 term in Eq. (53) contributes an $\tilde{\eta}^2$ correction. Substitution of Eq. (C14) into Eqs. (50a) and (50b) give

$$\alpha = \frac{i(h-\sigma)}{(h^2-1)^{1/2}} + \mathcal{O}(\nu^3\sigma) + \mathcal{O}(\sigma^2)\ , \tag{C16a}$$

$$\beta = \frac{i(1-\sigma h)}{(h^2-1)^{1/2}} + \mathcal{O}(\nu^3\sigma) + \mathcal{O}(\sigma^2)\ . \tag{C16b}$$

(2) $-1 < \mathrm{Re}(h) < 0$. Here ia is nearly real with positive real and imaginary parts. Then an application of the reflection formula and Eq. (C12) gives

$$G = (ia)^{-1/2}e^{i\pi/4}\left[1 - ie^{-\pi(ia)}\right]\left\{1 + [4(ia)]^{-2} + \mathcal{O}[(ia)^{-4}]\right\}\ . \tag{C17}$$

With this form of G we find, using Eq. (C9),

$$\frac{\Psi_{1h}(0^+)}{\Psi_{2h}(0^+)} = -\left[h - i(1-h^2)^{1/2}\right]\left[1 - i\sigma(1-h^2)^{1/2}\right] + \mathcal{O}(\nu^5\sigma) + \mathcal{O}(\sigma^2)\ , \tag{C18}$$

where, in region (2),

$$\sigma = -i\exp(-\pi i a) + \frac{\tilde{\eta}(1-\lambda^2)}{2(1-h^2)^2}\ . \tag{C19}$$

As in region (1), Eq. (C18) holds to all orders in $\tilde{\eta}$ in the limit $\tilde{\eta} \to 0$ and we conjecture that the $\tilde{\eta}$ correction term is also accurate to all orders in ν. Substitution of Eq. (C18) into Eqs. (50a) and (50b) gives

$$\alpha = \frac{-h+\sigma}{(1-h^2)^{1/2}} + \mathcal{O}(\nu^3\sigma) + \mathcal{O}(\sigma^2) \ , \tag{C20a}$$

$$\beta = \frac{-1+\sigma h}{(1-h^2)^{1/2}} + \mathcal{O}(\nu^3\sigma) + \mathcal{O}(\sigma^2) \ , \tag{C20b}$$

(3) $0 < \mathrm{Re}(h) < 1$. Here a is nearly real with positive real and imaginary parts. Then we can apply Stirling's formula directly to obtain

$$G = (a)^{-1/2}\left[1 - (4a)^{-2} + \mathcal{O}(a^{-4})\right] \ . \tag{C21}$$

Note that in this case the gamma functions (and therefore also the parabolic cylinder functions) do not capture the damping due to tunneling, which is now due to the k^4 term. With this form of G we find, using Eq. (C9),

$$\frac{\Psi_{1h}(0^+)}{\Psi_{2h}(0^+)} = -\left[h - i(1-h^2)^{1/2}\right]\left[1 - i\sigma(1-h^2)^{1/2}\right] + \mathcal{O}(\sigma^2) \ , \tag{C22}$$

where, in region (3),

$$\sigma = \frac{\tilde{\eta}(1-\lambda^2)}{2(1-h^2)^2} \ . \tag{C23}$$

As in regions (1) and (2), Eq. (C22) holds to all orders in ν in the limit $\tilde{\eta} \to 0$ and we conjecture that the $\tilde{\eta}$ correction term is also accurate to all orders in ν. Substitution of Eq. (C22) into Eqs. (50a) and (50b) give

$$\alpha = \frac{-h+\sigma}{(1-h^2)^{1/2}} + \mathcal{O}(\sigma^2) \ , \tag{C24a}$$

$$\beta = \frac{-1+\sigma h}{(1-h^2)^{1/2}} + \mathcal{O}(\sigma^2) \ , \tag{C24b}$$

(4) $\mathrm{Re}(h) > 1$. Here $-a$ is nearly real with positive real and imaginary parts. Then we must apply the reflection formula to both gamma functions before using Stirling's formula.

The final result is

$$G = (-a)^{-1/2} \cot\left[\pi\left(\frac{1}{4} - \frac{(-a)}{2}\right)\right]\left\{1 - [4(-a)]^{-2} + \mathcal{O}[(-a)^{-4}]\right\} . \tag{C25}$$

With this form of G we find, using Eqs. (C5), (C7) and (C8) and after considerable algebra,

$$\frac{\Psi_{1h}(0^+)}{\Psi_{2h}(0^+)} = -\frac{e^{-i\theta} + e^{i\theta}[h + (h^2-1)^{1/2}]}{e^{-i\theta}[h + (h^2-1)^{1/2}] + e^{i\theta}} + \mathcal{O}(\nu^7) + \mathcal{O}(\sigma) , \tag{C26}$$

where

$$\theta = -\pi\left(\frac{1}{4} + \frac{a}{2}\right) = \frac{\pi}{4}\left\{[h^2 - 1 + \mathcal{O}(\tilde{\eta})][2h(1-\lambda^2)\tilde{\eta}]^{-1/2} - 1\right\} , \tag{C27}$$

and σ is given by Eq. (C23). We note that, unlike the other regions, the leading order dissipation due to $\mathrm{Im}(\tilde{\eta})$ comes from imaginary θ (which scales as $\tilde{\eta}^{-1/2}$) and is proportional to $\mathrm{Im}(\tilde{\eta}^{1/2}) \sim \mathrm{Im}(\tilde{\eta})/\mathrm{Re}(\tilde{\eta}^{1/2})$. This is discussed further in Sec. V. We also note that Eq. (C26) has a similar property to the other regions only when $\mathrm{Im}(\theta)$ becomes large and positive, which makes $\tan\theta \to i$, and then Eq. (C26) holds to all orders in ν in the ideal limit. Unlike in the other regions, we note that if the phase θ is nearly real when $\tilde{\eta}$ is small, the amplitude terms in Eq. (C26) break down at $\mathcal{O}(\nu^7)$. That is, Eq. (C26) disagrees at $\mathcal{O}(\nu^7)$ in the amplitudes compared to the WKB form of the exact equation, which will be derived below; see Eq. (D23). There are additional discrepancies related to the tunneling and phase, which are discussed below, Eqs. (61). We conjecture that the ν^7 "errors" arise from applying Eqs. (54a) and (54b), which are not exactly compatible with each other when the parabolic cylinder functions, obtained by dropping the k^4 term, are used as solutions. It is interesting to note that the unsymmetrized forms, Eqs. (C3) and (C4) are in error by $\mathcal{O}(\nu^2)$ if one retains the phase as $\tilde{\eta} \to 0$. Thus, apart from the phase slippage and tunneling, our symmetrization increases the accuracy by five orders in ν.

Substitution of Eq. (C26) into Eqs. (50a) and (50b) give

$$\alpha = \frac{h\cos 2\theta + 1}{(h^2-1)^{1/2}\sin 2\theta} + \mathcal{O}(\nu^5) + \mathcal{O}(\sigma) , \tag{C28a}$$

$$\beta = \frac{h + \cos 2\theta}{(h^2 - 1)^{1/2} \sin 2\theta} + \mathcal{O}(\nu^5) + \mathcal{O}(\sigma) \ , \tag{C28b}$$

Finally we note that although the $\tilde{\eta}$ correction is simple in the asymptotic forms Eqs. (C14), (C16), (C18), (C20), (C22), (C24), (C26), (C28), it enters the calculation in several places due to its presence in a. The $[4(-ia)]^{-2}$ terms in Eqs. (C13), (C17), (C21), and (C25), which come from higher order terms in Stirling's formula, are essential to capture the total $\mathcal{O}(\tilde{\eta})$ correction.

Appendix D: WKB Approximations

We now develop the WKB theory, in order to obtain analytic formulas for α and β, directly from Eqs. (53) and (54). We wish to exhibit the dissipative effects from wave tunneling and imaginary η. To obtain the effects of tunneling we need only exhibit results to lowest order in WKB theory. To exhibit dissipation due to imaginary η we will need to go to higher order in WKB theory.

From Eq. (53), the second order equation for Ψ_{1h} and Ψ_{2h} are

$$\left\{\frac{d^2}{dk^2} - V_i(k)\right\}\Psi_{ih} = 0 \ , \tag{D1}$$

with

$$V_i(k) = \frac{1}{1-\lambda^2}\left[1 - (h - \tilde{\eta}k^2)^2 \pm 2i\tilde{\eta}(1-\lambda^2)^{1/2}k\right] \ , \tag{D2}$$

where $i = 1, 2$ and we associate the upper sign with 1 and the lower sign with 2. The WKB solutions for Ψ_{ih} are

$$\Psi_{ih}(k) = \frac{A_i}{Q_i^{1/2}(k)} \exp\left[-\int_0^k dk' Q_i(k')\right] \ , \tag{D3}$$

with A_i a constant amplitude and $Q_i(k)$ is exactly given by

$$Q_i^2 - \frac{Q_i^{1/2}}{2}\left(\frac{Q_i'}{Q_i^{3/2}}\right)' = V_i(k) \ , \tag{D4}$$

where the primes denote d/dk. In the WKB limit we assume $Q_i^{-3/2}(Q_i'/Q_i^{3/2})' \ll 1$ and iterate Eq. (D4) to obtain

$$Q_i^2 = V_i(k) + \frac{1}{4}V_i^{1/4}\left(\frac{V_i'}{V^{5/4}}\right)' = V_i(k) + \frac{1}{4}\frac{V_i''}{V_i} - \frac{5}{16}\left(\frac{V_i'}{V_i}\right)^2 \ . \tag{D5}$$

Near the origin this iteration is justified if $\tilde{\eta}h/(1-h^2) \ll 1$. In order for the WKB solution to be valid between the origin and the nearest turning points, we also require $\tilde{\eta} \ll 1$. We

shall assume these inequalities throughout this discussion. If in Eq. (D4) we evaluate the correction term, we find

$$Q_i^2(k=0) = (1-h^2+\tilde{\eta}h)/(1-\lambda^2) \ , \tag{D6}$$

(independent of i). Now substituting Eq. (D3) into the first mode coupling equation (given by Eq. (54)) and using $Q_i'(k=0) = \pm i\tilde{\eta}/(1-\lambda^2)^{1/2}$, we find

$$\frac{A_2}{A_1} = -i\left[1-h^2+\frac{\tilde{\eta}h(1-\lambda^2)}{1-h^2}\right]^{1/2} - h + \frac{\tilde{\eta}(1-\lambda^2)}{2(1-h^2)} \cong -i(1-\tilde{h}^2)^{1/2} - \tilde{h} + \mathcal{O}\left[\left(\frac{\tilde{\eta}}{1-h^2}\right)^2\right] \tag{D7}$$

where

$$\tilde{h} = h - \frac{\tilde{\eta}(1-\lambda^2)}{2(1-h^2)} \ . \tag{D8}$$

Note that the amplitude ratio Ψ_1/Ψ_2 is shifted by higher order WKB theory, but retains an obvious structural form that is manifested by the replacement of h by $\tilde{h}$.

We shall see that the WKB solutions have different structure in three different regions; (1) $\mathrm{Re}(h) < -1$, (2) $-1 < \mathrm{Re}(h) < 1$, and (3) $\mathrm{Re}(h) > 1$. For simplicity we limit ourselves to $\mathrm{Im}(h) \ll \mathrm{Re}(h)$ and $\mathrm{Im}(\eta) \ll \mathrm{Re}(\eta)$.

(1) $\mathrm{Re}(h) < -1$. In this case there are no breakdowns of WKB theory (turning points) along the real axis from $k \to \infty$ to the origin. Then the form of the WKB integrals are

$$\Psi_{ih}(k) = \frac{A_i}{P_i^{1/2}} \exp\left[-i\int_0^k dk' P_i(k')\right] \ , \tag{D9}$$

where $P_i^2 = -Q_i^2$ and P_i is primarily real and positive. The ratio A_1/A_2 is found by substituting the WKB solutions into the mode coupling equations, Eq. (54) at $k=0$, from which we find

$$\frac{A_2}{A_1} = -h + (h^2-1)^{1/2} = \frac{-1}{h+(h^2-1)^{1/2}} \ . \tag{D10}$$

Thus, from Eqs. (50a) and (50b) we find

$$\alpha = \frac{ih}{(h^2-1)^{1/2}} \ , \tag{D11a}$$

$$\beta = \frac{i}{(h^2-1)^{1/2}} \ . \tag{D11b}$$

These are the ideal solutions. Their imaginary character exhibits a strong dissipative behavior. Nonideal effects are obtained by the replacement of h by $\widetilde{h}$.

(2) $-1 < \mathrm{Re}(h) < 1$. As $k \to \infty$ the well-behaved solution (that has $\mathrm{Im}(\widetilde{\eta}) < 0$) goes as

$$\Psi_{ih}(k) = \frac{A_i}{P_i^{1/2}} \exp\left[-i\int_{k_{Ti}}^{k} dk' P_i(k')\right] \ , \tag{D12}$$

where k_{Ti} is the zero of $P_i(k)$ and is approximately given by

$$k_{Ti} \cong [(1+h)/\widetilde{\eta}]^{1/2} \pm i(1-\lambda^2)^{1/2}/2 \equiv \overline{k}_T \pm i(1-\lambda^2)^{1/2}/2 \ . \tag{D13}$$

On the real axis, to the left of $\overline{k}_T$, $\Psi_{ih}(k)$ matches onto

$$\Psi_{ih}(k) = \frac{A_i}{Q_i^{1/2}}\Bigg\{ \exp\left[\frac{i\pi}{4} + \int_0^{k_{Ti}} dk' Q_i(k')\right] \exp\left[-\int_0^k dk' Q_i(k')\right]$$

$$+\frac{1}{2}\exp\left[\frac{-i\pi}{4} - \int_0^{k_{Ti}} dk' Q_i(k')\right] \exp\left[\int_0^k dk' Q_i(k')\right]\Bigg\} \ . \tag{D14}$$

Here we have assumed a close enough alignment of the real axis to the Stokes line emanating from k_{Ti} and heading leftward, that a Stokes factor of $1/2$ can be taken in generating the subdominant part of the WKB solution. At the origin we then have (we neglect common constants in Ψ_{1h} and Ψ_{2h} which do not affect the value of α and β),

$$\Psi_{ih}(k) = A_i \widetilde{f}_i^{-1/2}\left[1 - \frac{i}{2}\widetilde{f}_i\right] \ , \tag{D15}$$

where

$$\widetilde{f}_i = \exp\left[-2\int_0^{k_{Ti}} dk' Q_i(k')\right]$$

$$\cong \exp\left\{-2\int_0^{\overline{k}_{Ti}} dk' \overline{Q}_i(k') \mp 2i\widetilde{\eta}\int_0^{\overline{k}_T} dk' k' \left[1-(h-\widetilde{\eta}k'^2)^2\right]^{-1/2}\right\} + \mathcal{O}(\widetilde{\eta}) = r\left[-h \mp i(1-h^2)^{1/2}\right] \ , \tag{D16}$$

with $r = \exp\left[-2\int_0^{\bar{k}_T} dk' \overline{Q}_i(k')\right]$ and $\overline{Q}_i(k) = \left[1-(h-\tilde{\eta}k^2)^2\right]^{1/2}/(1-\lambda^2)^{1/2}$. Hence, to within a relative constant,

$$\Psi_{ih}(0) = A_i\left[-h+i(1-h^2)^{1/2}\right]^{\pm 1/2}\left\{1-\frac{ir}{2}\left[-h+i(1-h^2)^{1/2}\right]^{\mp 1}\right\}, \tag{D17}$$

We note that the ratio of WKB amplitudes determined from the mode coupling equations at the origin leads to $A_1/A_2 = 1$.

Now calculating α and β, using Eq. (50),

$$\alpha = \frac{-h-ir}{(1-h^2)^{1/2}} + \mathcal{O}(r^2), \tag{D18a}$$

$$\beta = \frac{-(1+ihr)}{(1-h^2)^{1/2}} + \mathcal{O}(r^2), \tag{D18b}$$

The results from higher order WKB theory is affected by replacing h by $\tilde{h}$ where h explicitly appears in Eqs. (D18).

(3) $\mathrm{Re}(h) > 1$. In this region there are two relevant turning points, $k_{Ti}^{(a)} \cong \bar{k}_T^{(a)} \pm i(1-\lambda^2)^{1/2}/2$ with $\bar{k}_T^{(a)} = [(1+h)/\tilde{\eta}]^{1/2}$ and $k_{Ti}^{(b)} \cong \bar{k}_T^{(b)} \mp i(1-\lambda^2)^{1/2}/2$ with $\bar{k}_T^{(b)} = [(h-1)/\tilde{\eta}]^{1/2}$. We introduce a small parameter

$$f_i^{1/2} = \exp\left[-\int_{k_{Ti}^{(a)}}^{k_{Ti}^{(b)}} dk' Q_i(k')\right]. \tag{D19}$$

We then take for Ψ_{ih} to the right of $\bar{k}_{Ti}^{(a)}$,

$$\Psi_{ih}(k) = \frac{A_i f_i^{1/2}}{P_i^{1/2}} \exp\left[-i\int_{k_{Ti}^{(a)}}^{k} dk' P_i(k')\right], \tag{D20}$$

To the left of $\bar{k}_{Ti}^{(a)}$ this solution matches onto

$$\Psi_{ih}(k) = \frac{A_i}{Q_i^{1/2}}\left\{\exp\left[\frac{i\pi}{4} - \int_{k_{Ti}^{(b)}}^{k} dk' Q_i(k')\right] + \frac{1}{2} f_i \exp\left[\frac{-i\pi}{4} + \int_{k_{Ti}^{(b)}}^{k} dk' Q_i(k')\right]\right\}. \tag{D21}$$

To the left of $\bar{k}_{Ti}^{(b)}$, Ψ_{ih} matches onto

$$\Psi_{ih}(k) = \frac{A_i e^{i\pi/4}}{P_i^{1/2}}\Bigg\{(1+f_i/4)\exp\left[-i\int_0^k dk' P_i(k')\right]\exp\left[i\int_0^{k_{Ti}^{(b)}} dk' P_i(k') - \frac{i\pi}{4}\right]$$

$$+ (1 - f_i/4) \exp\left[i \int_0^k dk' P_i(k')\right] \exp\left[-i \int_0^{k_{Ti}^{(b)}} dk' P_i(k') + \frac{i\pi}{4}\right] \Bigg\} . \tag{D22}$$

Then at the origin, we find after discarding common factors, expanding the phase integrals in small η in the manner previously indicated, and matching to the WKB amplitude ratio at the origin,

$$\Psi_{ih}(k=0) = \mp \left\{ \exp(i\bar{\theta}) \left[h \pm (h^2-1)^{1/2}\right]^{1/2} (1 - t/4) + \exp(-i\bar{\theta}) \left[h \mp (h^2-1)^{1/2}\right]^{1/2} (1 + t/4) \right\} , \tag{D23}$$

where

$$\bar{\theta} = -\frac{\pi}{4} + \left[(1-\lambda^2)\tilde{\eta}\right]^{-1/2} \int_0^{z_b} dz [(h - z^2)^2 - 1]^{1/2} , \tag{D24a}$$

$$t = \exp\left\{ -2[(1-\lambda^2)\tilde{\eta}]^{-1/2} \int_{z_b}^{z_a} dz [1 - (h - z^2)^2]^{1/2} \right\} , \tag{D24b}$$

$z_a = (h+1)^{1/2}$, $z_b = (h-1)^{1/2}$. Using Eq. (50), we can now calculate α and β,

$$\alpha = \frac{h \cos 2\bar{\theta} + 1}{(h^2-1)^{1/2} \sin 2\bar{\theta}} - \frac{it(h + \cos 2\bar{\theta})}{2(h^2-1)^{1/2} \sin^2 2\bar{\theta}} + \mathcal{O}(t^2) , \tag{D25a}$$

$$\beta = \frac{h + \cos 2\bar{\theta}}{(h^2-1)^{1/2} \sin 2\bar{\theta}} - \frac{it(h \cos 2\bar{\theta} + 1)}{2(h^2-1)^{1/2} \sin^2 2\bar{\theta}} + \mathcal{O}(t^2) . \tag{D25b}$$

The result of higher order WKB theory is affected by replacing h by $\tilde{h}$ where h explicitly appears in Eqs. (D25). As in the gamma function solutions, the correct ideal limit is recovered from Eqs. (D23), (D25a) and (D25b) when $\mathrm{Im}(\bar{\theta})$ becomes large and positive, which makes the trigonometric functions large with $\cos 2\bar{\theta} / \sin 2\bar{\theta} \to -i$.

Appendix E – Large $|\tilde{\eta}|$ approximation

We start with Eqs. (53) and (54a) and transform to the new variables $\Phi_1(k)$ and $\Phi_2(k)$,

$$\Phi_1(k) = \Psi_{1h}(k) \exp\left[i \int_0^k dk(h - \tilde{\eta}k^2)/(1-\lambda^2)^{1/2}\right] \tag{E1}$$

$$\Phi_2(k) = \Psi_{2h}(k) \exp\left[i \int_0^k dk(h - \tilde{\eta}k^2)/(1-\lambda^2)^{1/2}\right] \tag{E2}$$

Then Eqs. (53) and (54a) become

$$\left[\frac{d^2}{dk^2} - 2i\frac{h - \tilde{\eta}k^2}{(1-\lambda^2)^{1/2}}\frac{d}{dk} - \frac{1}{1-\lambda^2}\right]\Phi_1(k) = 0 \tag{E3}$$

$$\Phi_2(k) = i(1-\lambda^2)^{1/2}\frac{d\Phi_1}{dk} \tag{E4}$$

Note that the f of Eqs. (50a) and (50b) gives $f \equiv \Psi_{1h}(0^+)/\Psi_{2h}(0^+) = \Phi_1(0^+)/\Phi_2(0^+)$. Our $|\tilde{\eta}| \gg 1$ approximation treats the last term on the left hand side of Eq. (E3) as small. Dropping this term, we can solve Eq. (E3) analytically, choosing the decaying solution for $k \to +\infty$. We obtain

$$\Phi_1(k) = \int_\infty^k dk \exp\left[2ik(h - \frac{1}{3}\tilde{\eta}k^2)/\sqrt{1-\lambda^2}\right], \tag{E5}$$

and therefore

$$\Phi_1(0) = -\int_0^\infty dk \exp\left[2ik(h - \frac{1}{3}\tilde{\eta}k^2)/\sqrt{1-\lambda^2}\right], \tag{E6}$$

$$\Phi_1'(0) = 1. \tag{E7}$$

Hence, $f = -i\Phi_1(0)/\sqrt{1-\lambda^2}$. Equation (E6) can be written in terms of the related Airy function,[13]

$$\mathrm{Hi}\,(z) \equiv \frac{1}{\pi}\int_0^\infty dt \exp(-\frac{1}{3}t^3 + zt) \tag{E8}$$

and, when combined with Eqs. (E4) and (E7) gives

$$f = \frac{i\pi \mathrm{Hi}\,(z)}{a\sqrt{1-\lambda^2}}, \tag{E9}$$

where $a = \left(\frac{2i\widetilde{\eta}}{\sqrt{1-\lambda^2}}\right)^{1/3}$ and $z = \frac{2ih}{a\sqrt{1-\lambda^2}}$. This function has the asymptotic form[13]

$$\mathrm{Hi}\,(z) \sim \frac{\exp\left(\frac{2}{3}z^{3/2}\right)}{\sqrt{\pi}z^{1/4}} \tag{E10}$$

for large $|z|$ and $|\arg z| < \frac{\pi}{3}$. Then asymptotically

$$f \sim -e^{\frac{-i\pi}{4}}\left[\frac{\pi^2(1-\lambda^2)}{4\widetilde{\eta}h}\right]^{1/4}\exp\left\{\frac{4i}{3}\frac{h^{3/2}}{[\widetilde{\eta}(1-\lambda^2)]^{1/2}}\right\}. \tag{E11}$$

This result may be compared with the WKB approximation at face value for large $|\widetilde{\eta}|$, which can be extracted from Eq. (D23). Taking $|\widetilde{\eta}|$, $h \gg 1$ gives

$$f_{WKB} \sim \frac{3i}{5}\exp\left\{\frac{4i}{5}\frac{h^{3/2}}{[\widetilde{\eta}(1-\lambda^2)]^{1/2}}\right\}. \tag{E12}$$

Note that the WKB phase is the same as in Eq. (E11), but the numerical factor is not. The fact that WKB picks up the correct phase explains why the WKB approximation, which has been derived only the small $|\widetilde{\eta}|$ limit, tracks the true solution for the TAE branch for $|\widetilde{\eta}| \gg 1$ in Figs. (4a) and (4b). The discrepency in amplitude is important for the KTAE branch, where we see at large $\widetilde{\eta}$ substantial deviation of the WKB and numerical solutions.

Once f is specified, α and β may be calculated from Eqs. (50a) and (50b). Asymptotically, we find

$$\alpha = i\frac{\frac{-i\pi}{2}\sqrt{\frac{1-\lambda^2}{\widetilde{\eta}h}}\exp\left\{\frac{8i}{3}\frac{h^{3/2}}{[\widetilde{\eta}(1-\lambda^2)]^{1/2}}\right\}+1}{\frac{-i\pi}{2}\sqrt{\frac{1-\lambda^2}{\widetilde{\eta}h}}\exp\left\{\frac{8i}{3}\frac{h^{3/2}}{[\widetilde{\eta}(1-\lambda^2)]^{1/2}}\right\}-1}, \tag{E13}$$

$$\beta = \frac{\sqrt{\pi}\left[\frac{4\pi^2(1-\lambda^2)}{\widetilde{\eta}h}\right]^{1/4}e^{\frac{i\pi}{4}}}{\frac{-i\pi}{2}\sqrt{\frac{1-\lambda^2}{\widetilde{\eta}h}}\exp\left\{\frac{8i}{3}\frac{h^{3/2}}{[\widetilde{\eta}(1-\lambda^2)]^{1/2}}\right\}-1}. \tag{E14}$$

In the case of noninteracting gaps the dispersion relation takes the form of Eqs. (69),

$$\alpha(h) + \Delta = 0. \tag{E15}$$

When combined with Eq. (50a), this may be solved for f as

$$f = \pm\left(\frac{\Delta - i}{\Delta + i}\right)^{1/2}. \tag{E16}$$

This, when combined with Eq. (E9), gives a dispersion relation applicable to TAE [for (+) sign in Eq. (E16)] and KTAE [for (−) sign in Eq. (E16)] and accurate to within 10% for $|\widetilde{\eta}| \gtrsim 5$. A more explicit, though less accurate, dispersion relation is obtained from the asymptotic form Eq. (E10), and may be written

$$\frac{2}{3}z^{3/2} = \ln\left(\frac{-if a\sqrt{1-\lambda^2}}{\sqrt{\pi}}\right) + \frac{1}{4}\ln z\,. \tag{E17}$$

Since $|z|$ is of order unity, we can treat the $\frac{1}{4}\ln z$ term perturbatively. Then to leading order

$$h = \sqrt{1-\lambda^2}e^{\frac{-i\pi}{3}}\left(\frac{\widetilde{\eta}}{4\sqrt{1-\lambda^2}}\right)^{1/3}\left[\frac{3}{2}\ln\left(\frac{-if a\sqrt{1-\lambda^2}}{\sqrt{\pi}}\right)\right]^{2/3}, \tag{E18}$$

which recovers the $\eta^{1/3}$ scaling of Ref. 9 with a logarithmic correction.

References

1. C.E. Kieras and J.A. Tataronis, J. Plasma Phys. **28**, 395 (1982).

2. S. Riyopoulos and S. Mahajan, Phys Fluids **29**, 731 (1986).

3. C.Z. Cheng, L. Chen, and M.S. Chance, Ann. Phys. **161**, 21 (1985).

4. C.Z. Cheng and M.S. Chance, Phys. Fluids **29**, 3695 (1986).

5. H.L. Berk, J.W. Van Dam, Z. Guo, and D.M. Lindberg, Phys. Fluids B **4**, 1806 (1992).

6. M.N. Rosenbluth, H.L. Berk, J.W. Van Dam, and D.M. Lindberg, Phys. Rev. Lett. **68**, 596 (1992).

7. F. Zonca and L. Chen, Phys. Rev. Lett. **68**, 592 (1992).

8. M.N. Rosenbluth, H.L. Berk, J.W. Van Dam, and D.M. Lindberg, Phys. Fluids B **4**, 2189 (1992).

9. R.R. Mett and S.M. Mahajan, Phys. Fluids B **4**, 2885 (1992).

10. R.R. Mett and S.M. Mahajan, in Theory of Fusion Plasmas, Proceedings of the Joint Varenna-Lausanne International Workshop, Varenna, Italy, 1992, edited by J. Vaclavik, F. Troyon, and E. Sindoni (Editrice Compositori Società Italiana di Fisica, Bologna, 1992), pp. 243-256. [Also IFSR#572]

11. J. Candy and M.N. Rosenbluth, to be published.

12. M.S. Chu, A.D. Turnbull, J.M. Greene, L.L. Lao, M.S. Chance, H.L. Berk, B.N. Breizman, W.Q. Li, D.M. Lindberg, S.M. Mahajan, R.R. Mett, D.W. Ross, J.W. Van Dam, J.C. Wiley, H. Ye, J. Candy, and M.N. Rosenbluth, to appear in Proceedings of the

Fourteenth International Conference on Plasma Physics and Controlled Nuclear Fusion Research, Würzburg, Germany, 1992 (International Atomic Energy Agency, Vienna, 1993). 1

13. M. Abramowitz and I.A. Stegun, eds., Handbook of mathematical functions with formulas, graphs, and mathematical tables (National Bureau of Standards Applied Mathematics Series 55, Washington, D.C., 1964).

Figure Captions

1. Plots of the integrals used in the WKB approximations: $I_1(x-1), I_2(x+1), I_3(x+1)$, and $I_4(x+1)$ for $0 < x < 2$. These integrals are defined below Eqs. (61) and (76).

2. Comparison of the various analytic approximations of a (these include the parabolic cylinder function U, the gamma function Γ, and the WKB) with the actual numerical result, shown as a solid line, in the range $-2 < h < 2$. To avoid clutter, the analytic approximations were truncated whenever they deviated significantly from the numerical solution. Frequently, the approximations agree so well that it is difficult to distinguish the curves. For example, for $h < 1$ the U and exact curves nearly coincide, while for $h > 1$ the curves for U and Γ nearly coincide and the exact and WKB are very close. (a) Real part of α vs. h for $\eta = 0.05$. (b) Imaginary part of α vs. h for $\eta = 0.05$. In this plot (only), the vertical scale is expanded by a factor of 250 for $h > -0.4$ in order to show the close agreement of the WKB approximation with the numerical result. (c) Real part of α vs. h for $\eta = 0.05e^{-0.1i}$. (d) Imaginary part of α vs. h for $\eta = 0.05e^{-0.1i}$.

3. Influence of varying values of $\mathbf{\Delta}_i$ on the TAE and KTAE eigenfrequencies shown as a function of $|\eta|$ for the non-interacting gap model Eq. (69) when $\mathbf{\Delta}_i = \overline{\Delta_2^-}$. The value $\overline{\Delta_2^-} = -0.6$ is representative of an $n = 1$ mode with $q(r) = 1 + 2(r/a)^2$ and a density profile varying as $[1 - .99(r/a)^4]$. Note that the TAE frequency (both real and imaginary parts) is much more strongly affected by changes in $\overline{\Delta_2^-}$ than the KTAE. We have also taken $\eta = |\eta|e^{-0.1i}$ and $m = 1$, which locates the gap at $q = 1.5$ and makes $\lambda = 0.2674$. (a) Real part of h vs. $|\eta|$. (b) Imaginary part of h vs. $|\eta|$.

4. Comparison of the eigenfrequencies predicted by the WKB approximation (shown as dashed lines) with the exact numerical result for the non-interacting gap model Eq. (69)

for the case $\overline{\Delta}_2^- = -0.6$ and the same profiles used in Fig. 3 with $m = 1$ and $\eta = |\eta|e^{-0.1i}$. (a) Real part of h vs. $|\eta|$. (b) Imaginary part of h vs. $|\eta|$.

5. TAE and KTAE eigenfrequencies Ω (defined below Eq. (1)) as a function of $|\eta|$ for the two-gap case in the limit that the neighboring gap is strongly nonaligned so that the neighboring gap gives continuum damping. Solid lines represent eigenfrequencies of the inner gap ($m = 1$ with $q = 1.5$) with the outer gap $\alpha_2 = -i$, and the dashed lines depict eigenfrequencies of the outer gap ($m = 2$ with $q = 2.5$) with the inner gap $\alpha_1 = -i$. Note the pairing of the KTAE for small $|\eta|$, seen in the real frequencies. This pairing continues for higher order modes, but is not shown in the figure. Here we use the same profiles as in Fig. 3 (which makes $\lambda_1 = 0.2674$, $\lambda_2 = -0.2189$), use an aspect ratio $R/a = 5$, and take $\eta = |\eta|e^{-0.1i}$. (a) Real part of Ω vs. $|\eta|$. (b) Imaginary part of Ω vs. $|\eta|$.

6. Numerically computed TAE and KTAE eigenfrequencies Ω as a function of $|\eta|$ for the two gap case showing the full interaction of the two gaps. Note the intricate interweaving of the real and imaginary parts of the frequencies in the range $10^{-2} < |\eta| < 10^{-1}$. Further discussion appears in the text. Here the profiles, mode numbers, aspect ratio, and phase of h are the same as in Fig. 5. (a) Real part of Ω vs. $|\eta|$. (b) Imaginary part of Ω vs. $|\eta|$. (c) Expanded view of the real part of Ω vs. $|\eta|$ for the range $10^{-2} < |\eta| < 10^{-1}$. (d) Expanded view of the imaginary part of Ω vs. $|\eta|$ for the range $10^{-2} < |\eta| < 10^{-1}$.

Table I: Numerical $\overline{\Delta}$ and $\tilde{\Delta}$ values[1]

	m	$\overline{\Delta}^+$	$\overline{\Delta}^-$	$\overline{\Delta}^\infty$	$\tilde{\Delta}^-$	$\tilde{\Delta}^+$	$\tilde{\Delta}^\infty$
	1	21.15271	0.00000	0.00000	0.00000	0.00000	0.00000
$n=1$	2	2.62165	−0.30201	0.88318	−0.77120	−1.23264	−0.67471
	3	0.00000	0.45850	2.71935	0.00000	0.00000	−2.55784
	2	1.86289	0.00000	0.00000	0.00000	0.00000	0.00000
	3	2.15165	−0.32631	0.38312	−0.30512	−0.91914	−0.16688
$n=2$	4	2.50775	0.95023	1.41002	−1.36689	−1.66860	−1.21901
	5	2.04883	2.05401	2.33551	−2.43010	−1.35978	−2.16696
	6	0.00000	0.71181	3.05639	0.00000	0.00000	−2.90031
	3	1.07274	0.00000	0.00000	0.00000	0.00000	0.00000
	4	1.39604	−0.29507	0.24529	−0.13339	−0.45659	−0.05139
	5	1.95316	0.52063	0.88318	−0.79243	−1.22061	−0.67471
$n=3$	6	2.34720	1.29423	1.57863	−1.52629	−1.73618	−1.39243
	7	2.45968	2.02825	2.19613	−2.24813	−1.92829	−2.02475
	8	1.95382	2.84024	2.71935	−3.07293	−1.38325	−2.55784
	9	0.00000	0.73573	3.15946	0.00000	0.00000	−3.00491
	4	0.77103	0.00000	0.00000	0.00000	0.00000	0.00000
	5	1.01766	−0.25538	0.18317	−0.06480	−0.23871	−0.01711
	6	1.46937	0.31373	0.62236	−0.49852	−0.82662	−0.40539
	7	1.90499	0.89546	1.14902	−1.04536	−1.34697	−0.94977
$n=4$	8	2.24878	1.45572	1.66096	−1.59246	−1.75228	−1.47699
	9	2.46221	1.99461	2.12420	−2.12642	−2.01301	−1.95129
	10	2.46426	2.54951	2.53367	−2.68419	−2.04154	−2.36888
	11	1.92306	3.26849	2.89332	−3.42500	−1.40284	−2.73469
	12	0.00000	0.71919	3.20938	0.00000	0.00000	−3.05556
	5	0.60582	0.00000	0.00000	0.00000	0.00000	0.00000
	6	0.80391	−0.22119	0.14721	−0.03338	−0.12975	−0.00590
	7	1.15157	0.20298	0.47488	−0.33132	−0.57066	−0.25597
	8	1.53540	0.65735	0.88318	−0.75267	−1.02063	−0.67471
	9	1.88819	1.11107	1.30661	−1.19482	−1.42169	−1.11245
$n=5$	10	2.18490	1.54902	1.70969	−1.62779	−1.75661	−1.52699
	11	2.40889	1.97189	2.08032	−2.04881	−2.01223	−1.90646
	12	2.53182	2.39474	2.41632	−2.47286	−2.15999	−2.24934
	13	2.47456	2.86151	2.71935	−2.94653	−2.10876	−2.55784
	14	1.91344	3.53937	2.99242	−3.64829	−1.42193	−2.83535
	15	0.00000	0.69259	3.23883	0.00000	0.00000	−3.08544

[1]computed for $q(r) = 1 + 2(r/a)^2$ and $\rho(r) = 1 - .99(r/a)^4$.

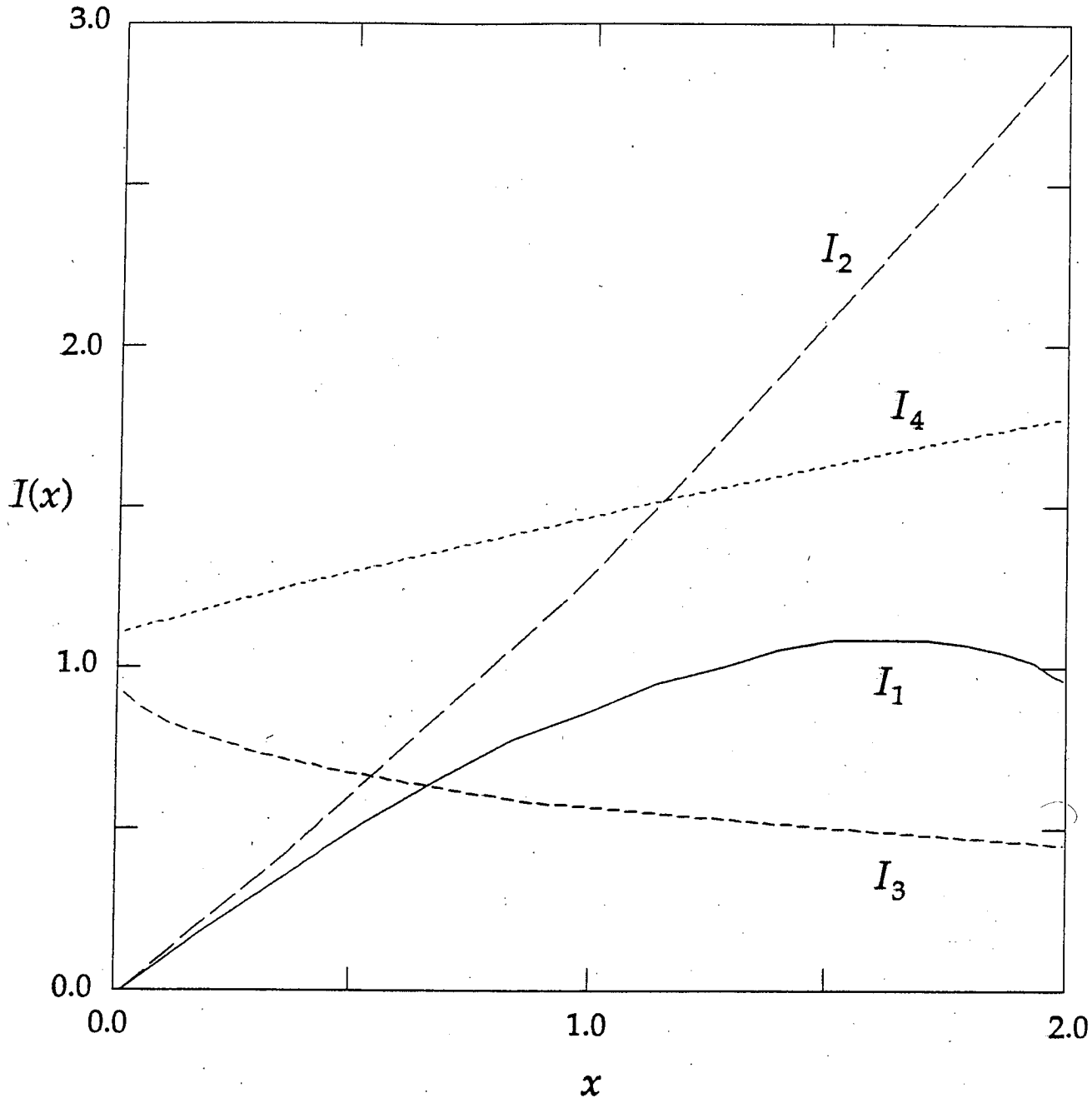

Fig. 1 - Berk et al.

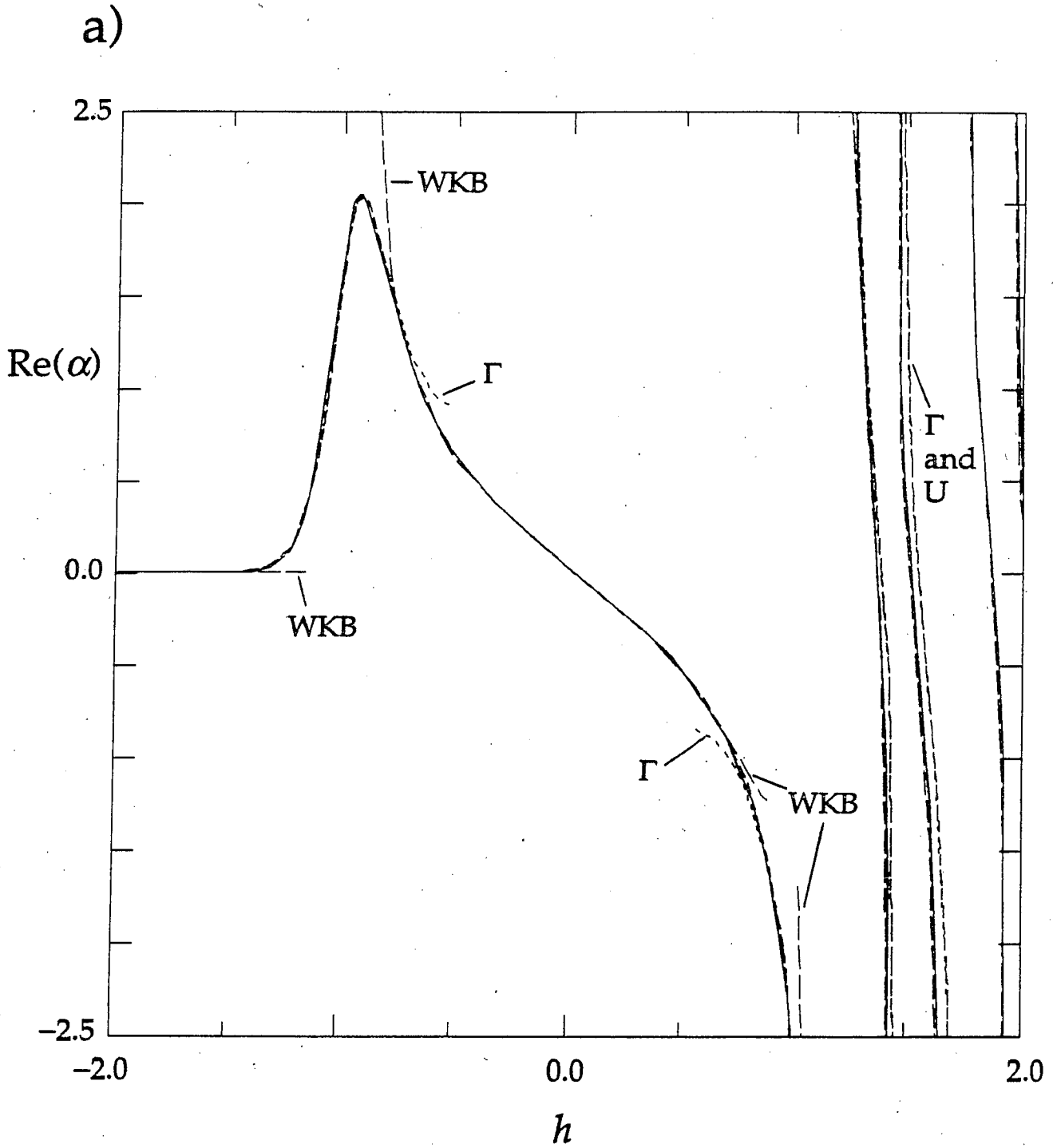

Fig. 2(a) - Berk et al.

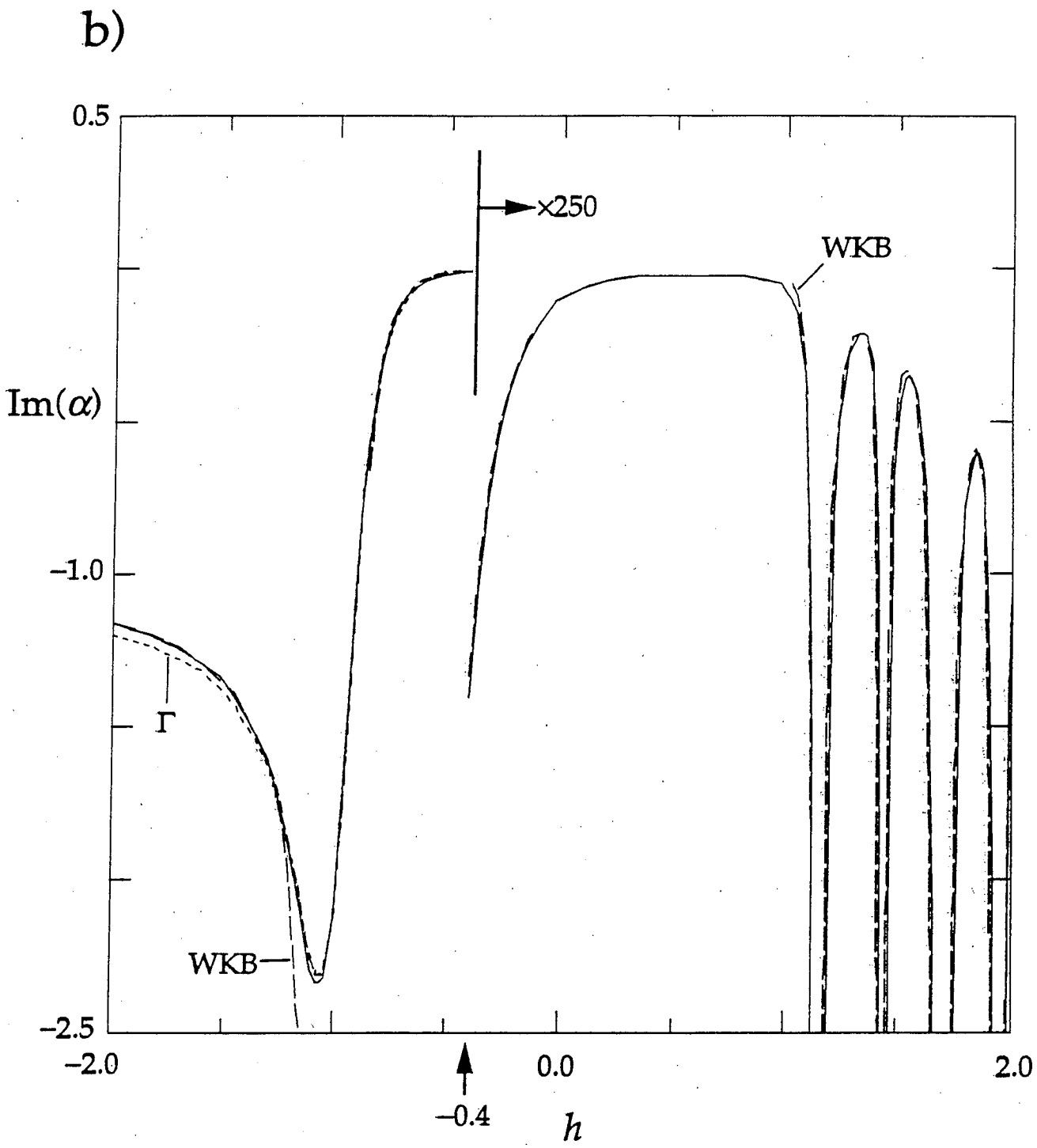

Fig. 2(b) - Berk et al.

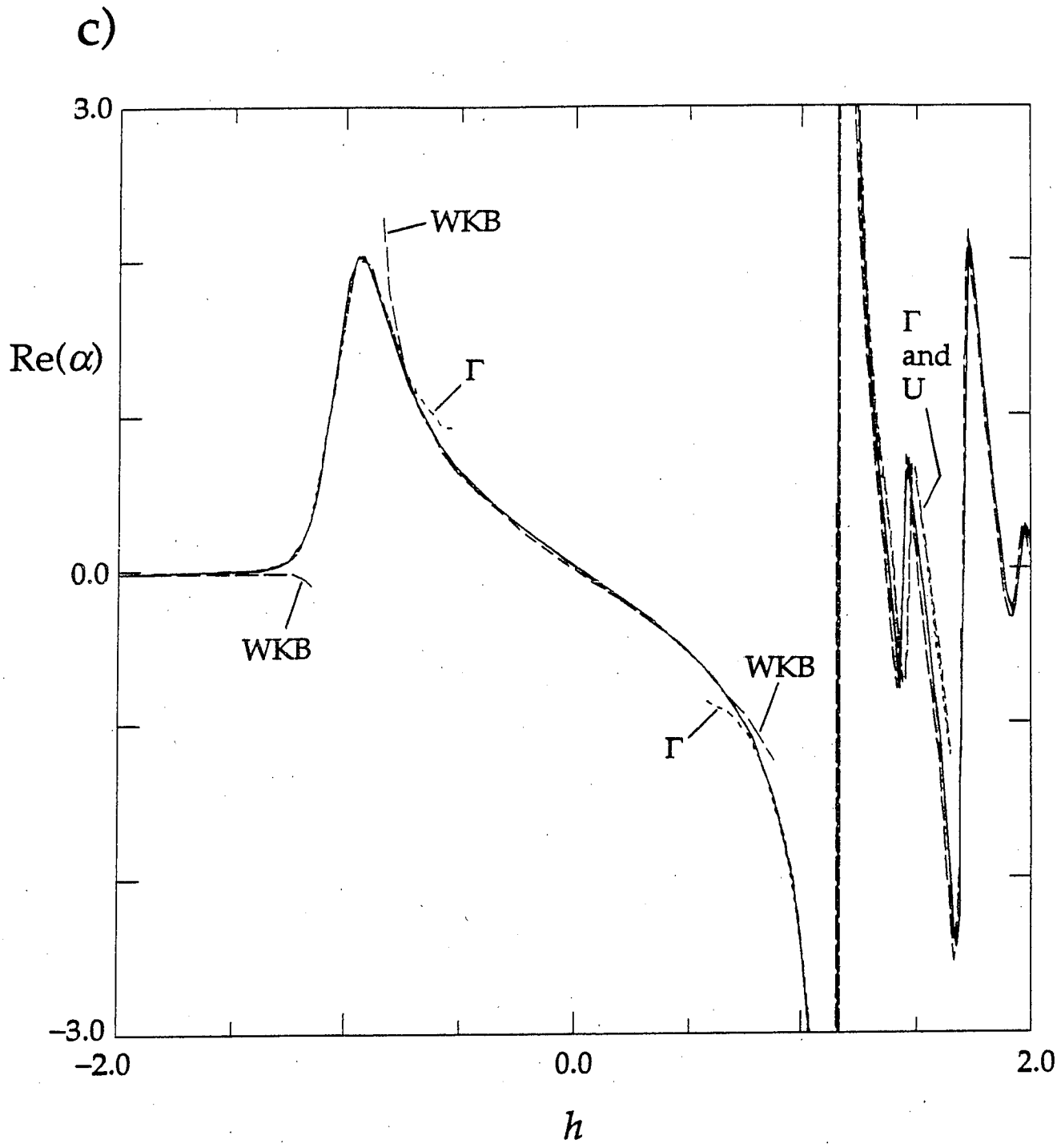

Fig. 2(c) - Berk et al.

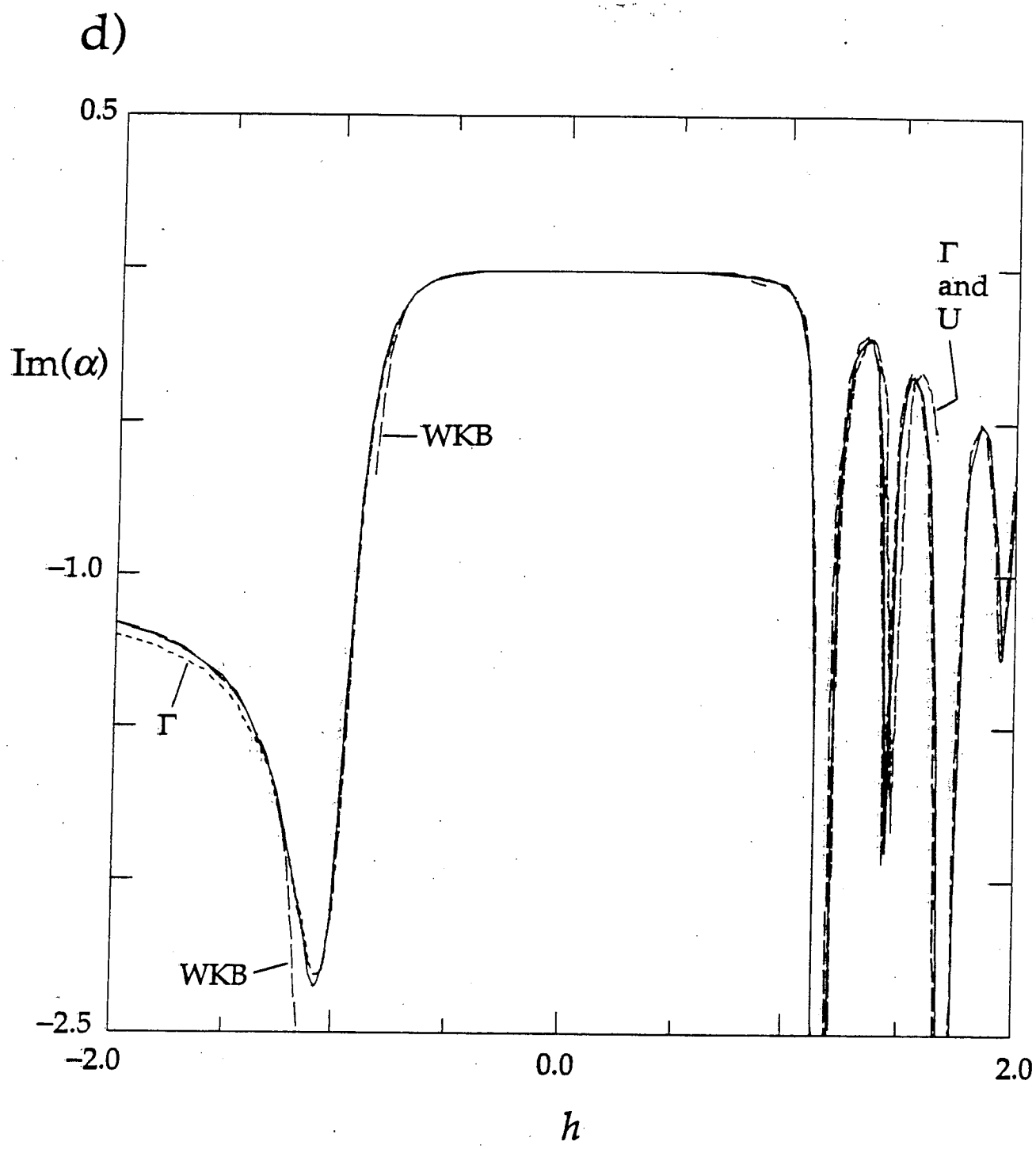

Fig. 2(d) - Berk et al.

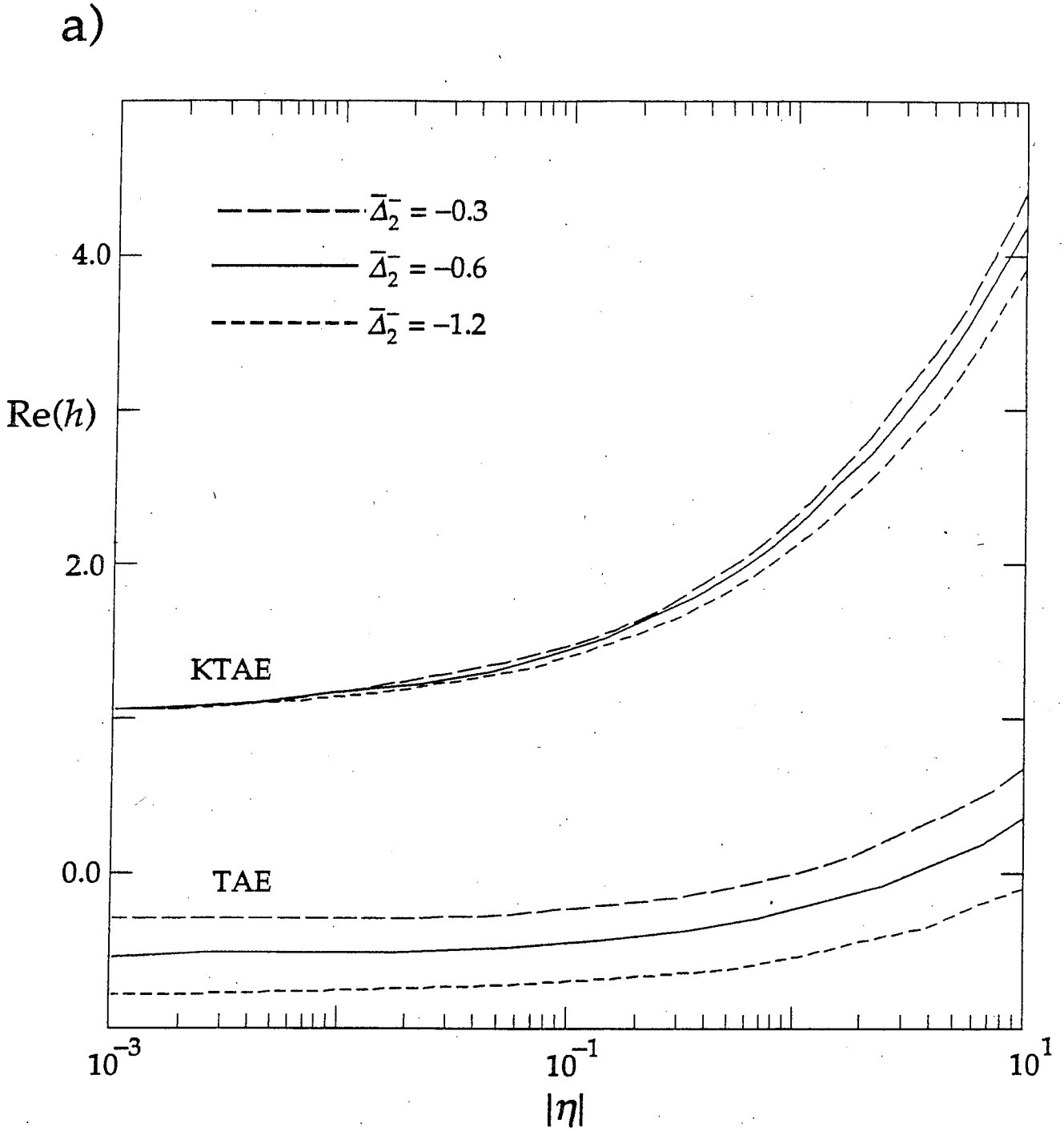

Fig. 3(a) - Berk et al.

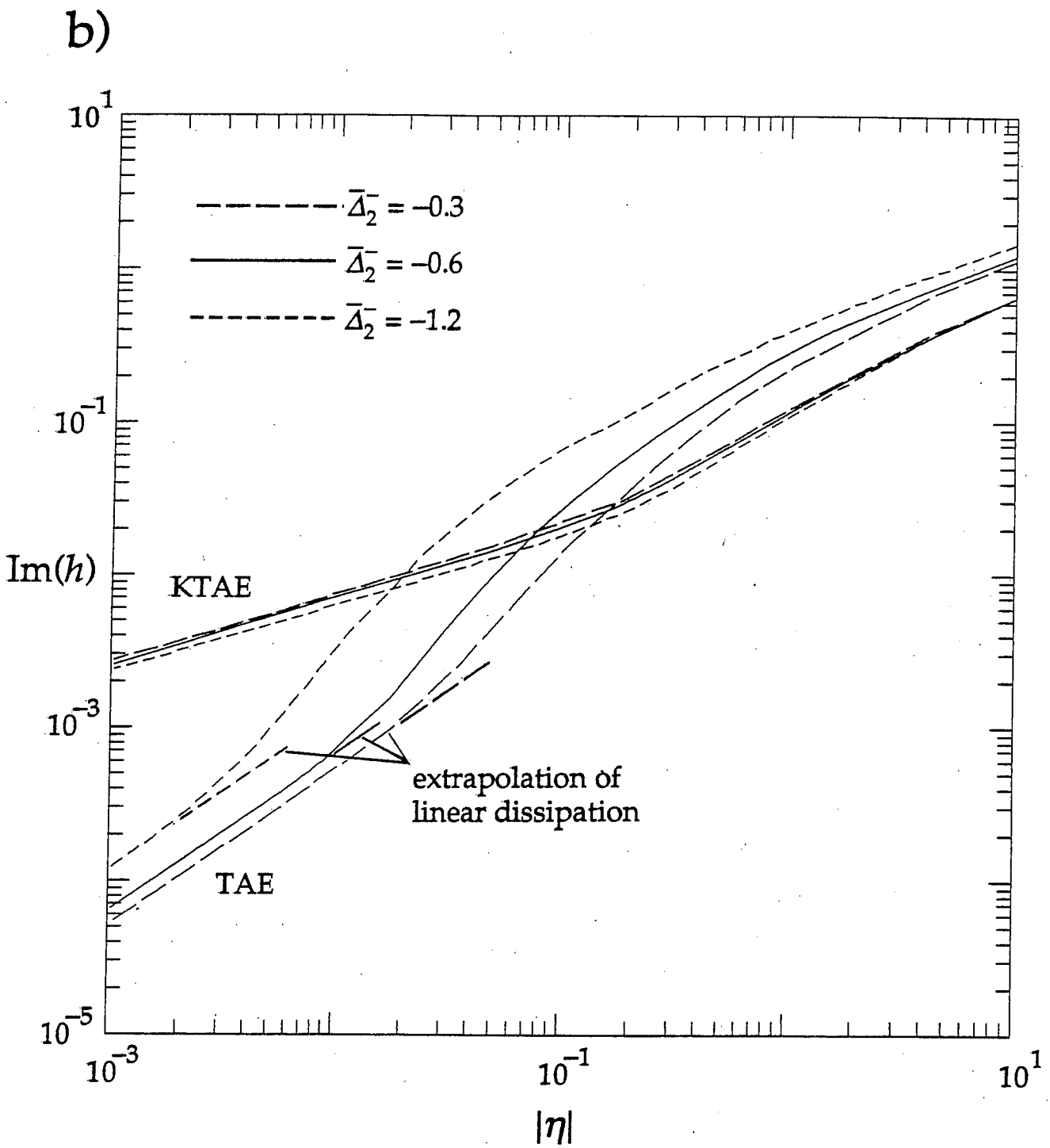

Fig. 3(b) - Berk et al.

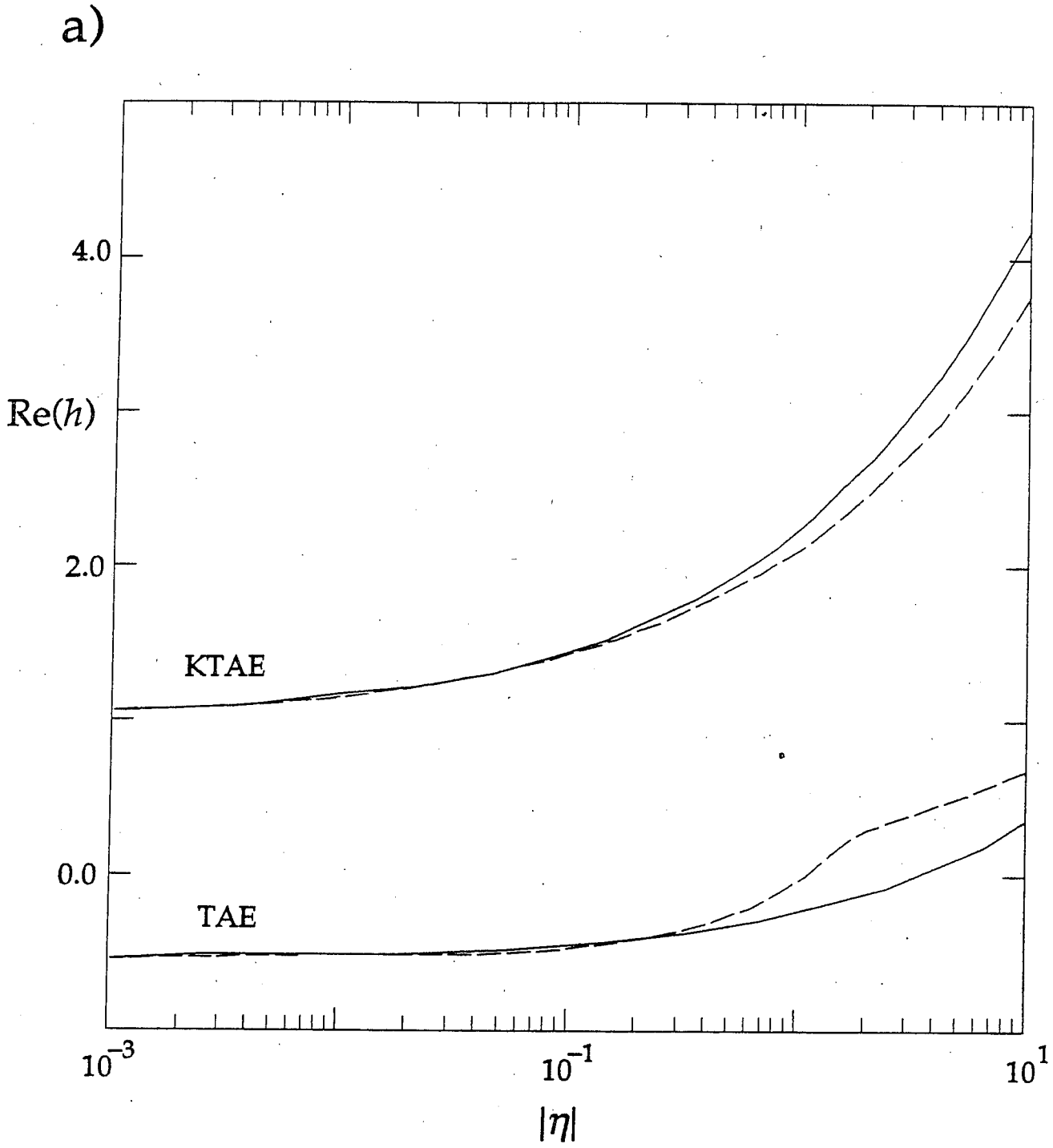

Fig. 4(a) - Berk et al.

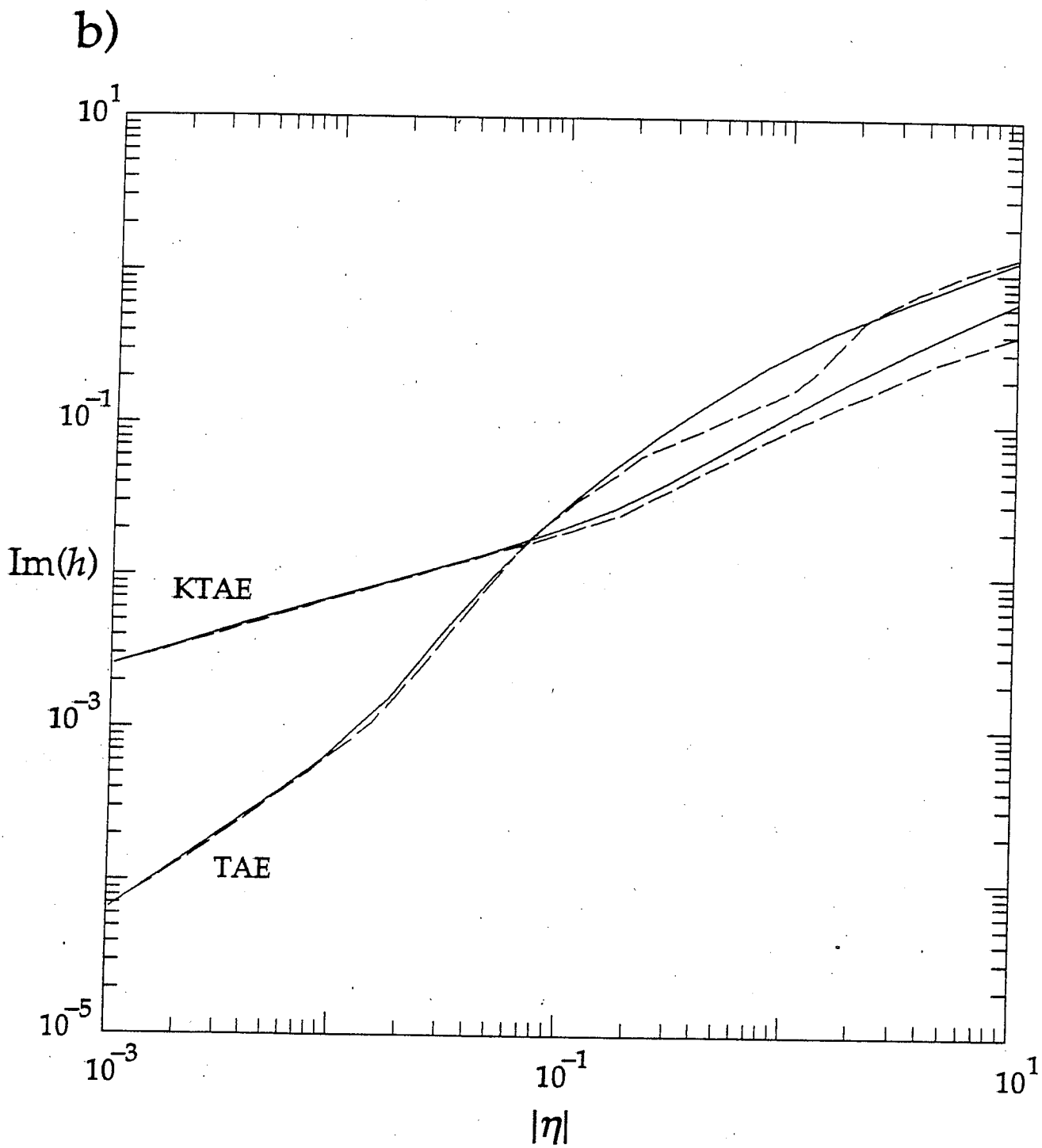

Fig. 4(b) - Berk et al.

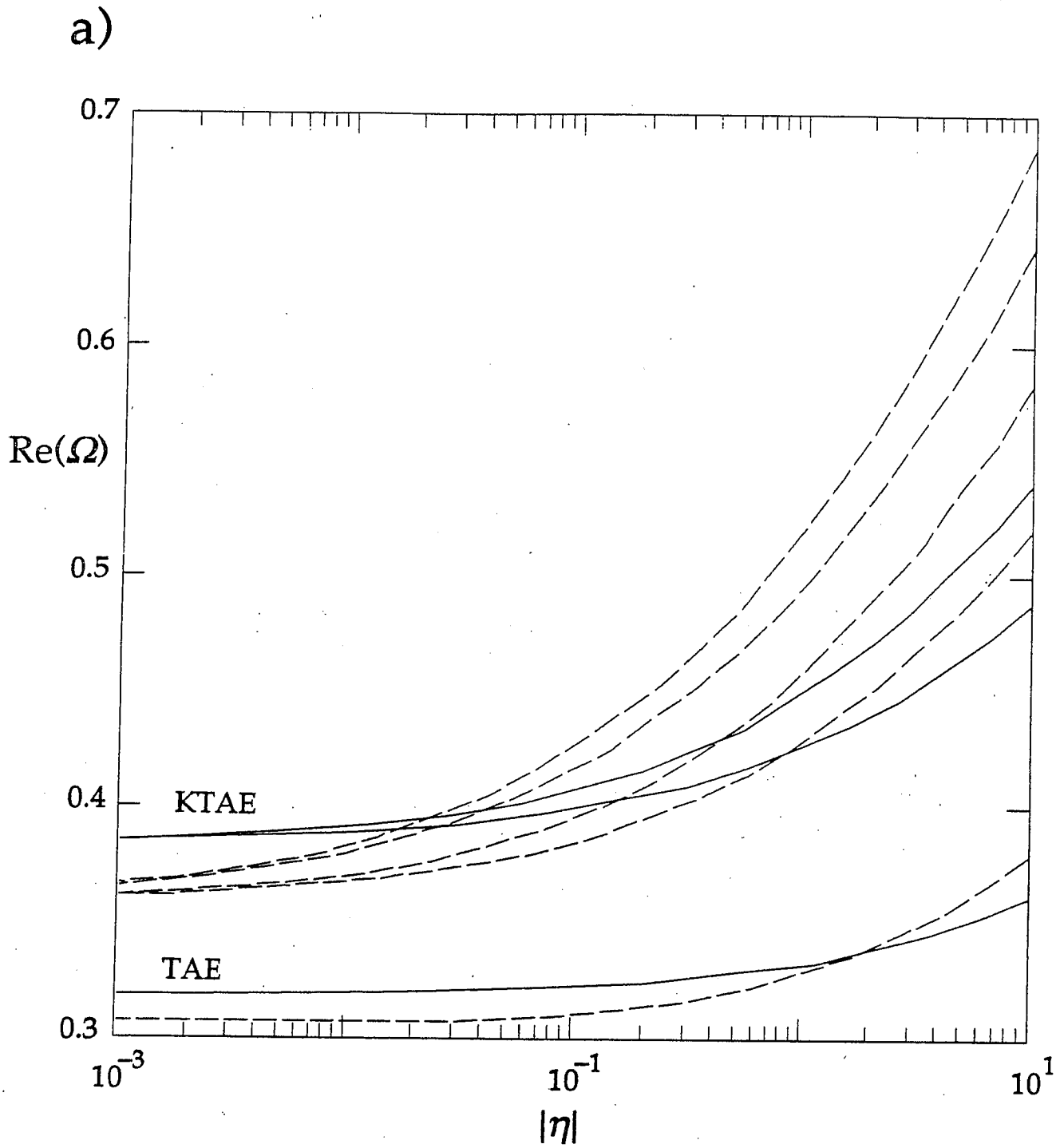

Fig. 5(a) - Berk et al.

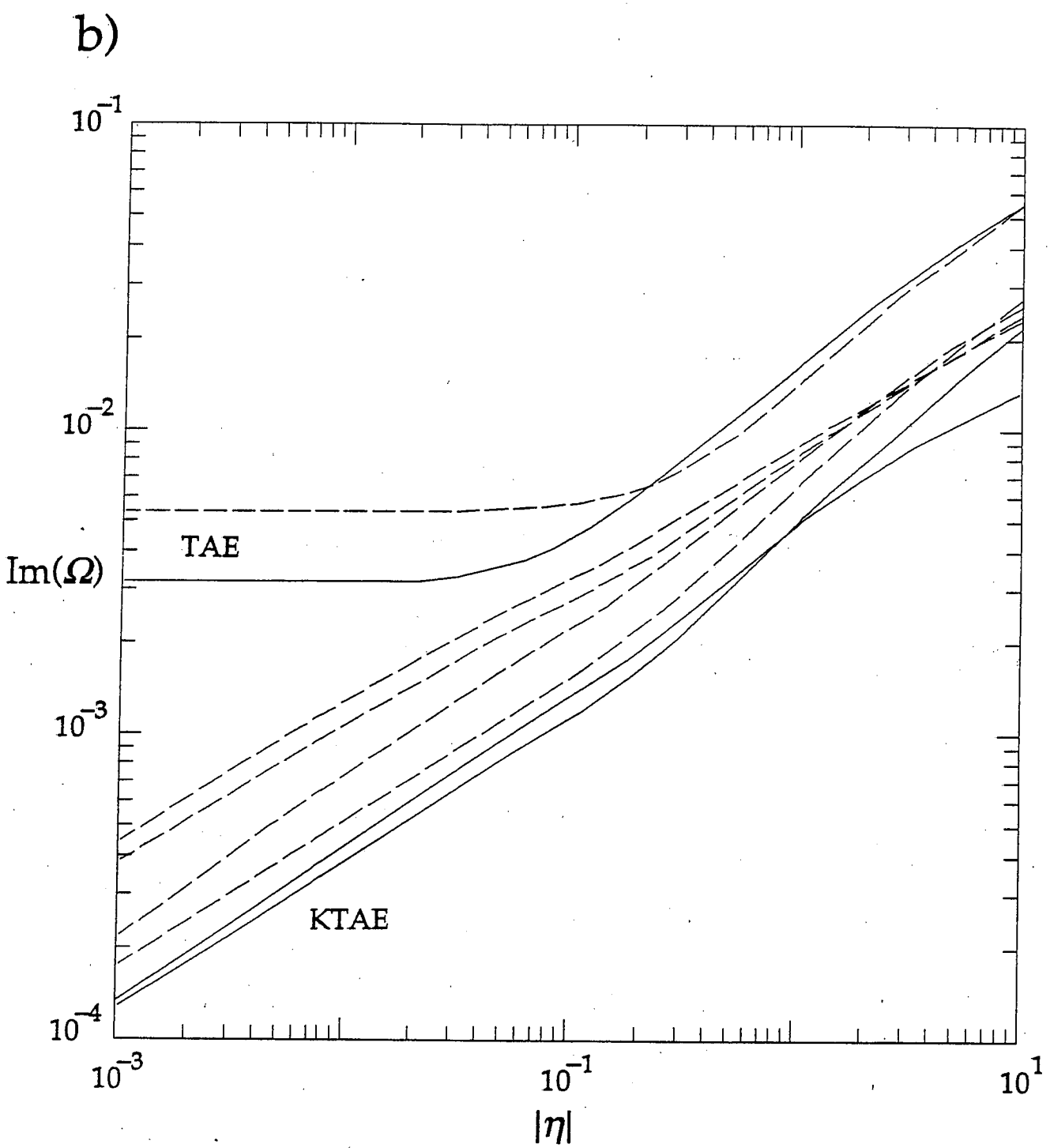

Fig. 5(b) - Berk et al.

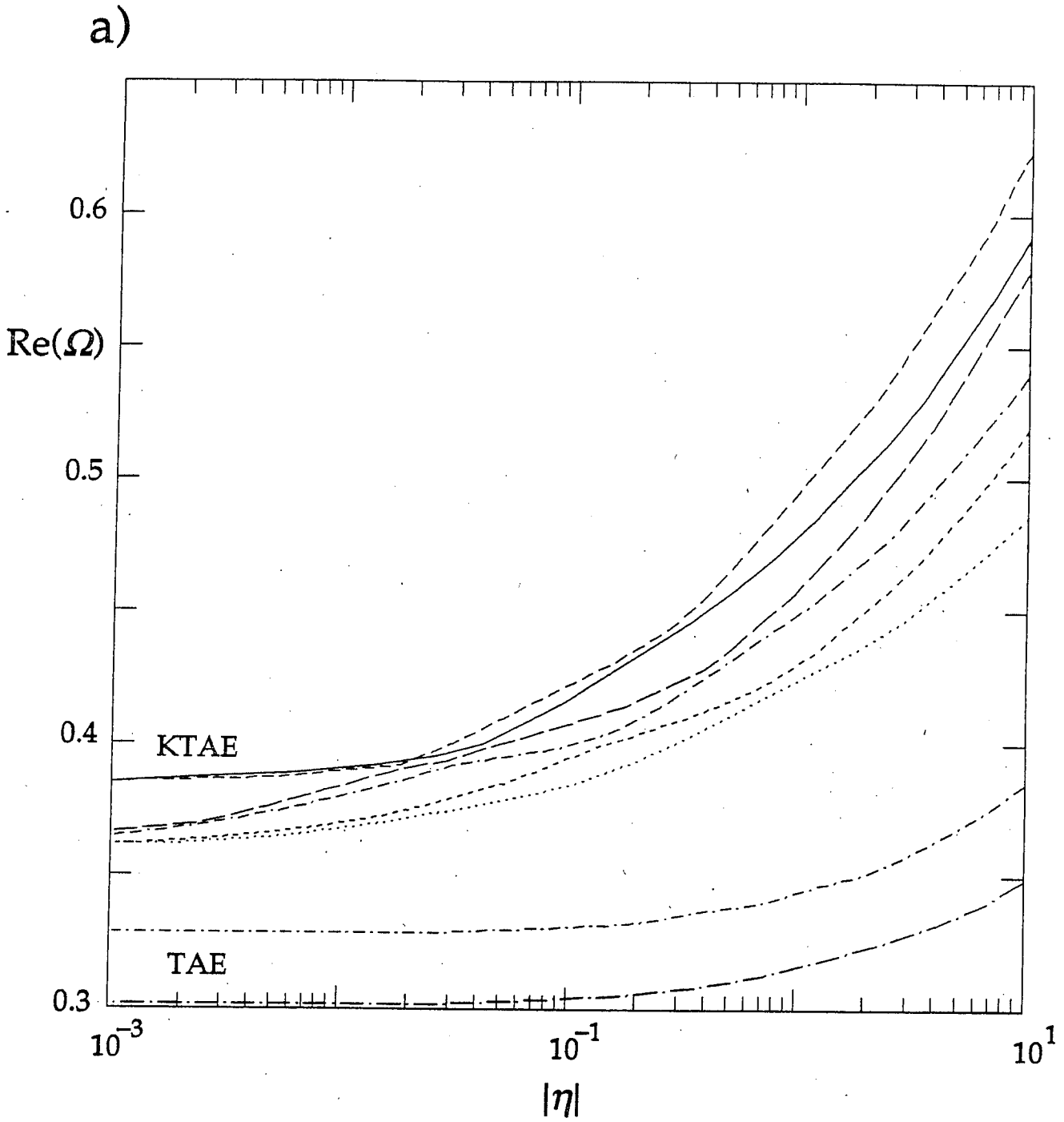

Fig. 6(a) - Berk et al.

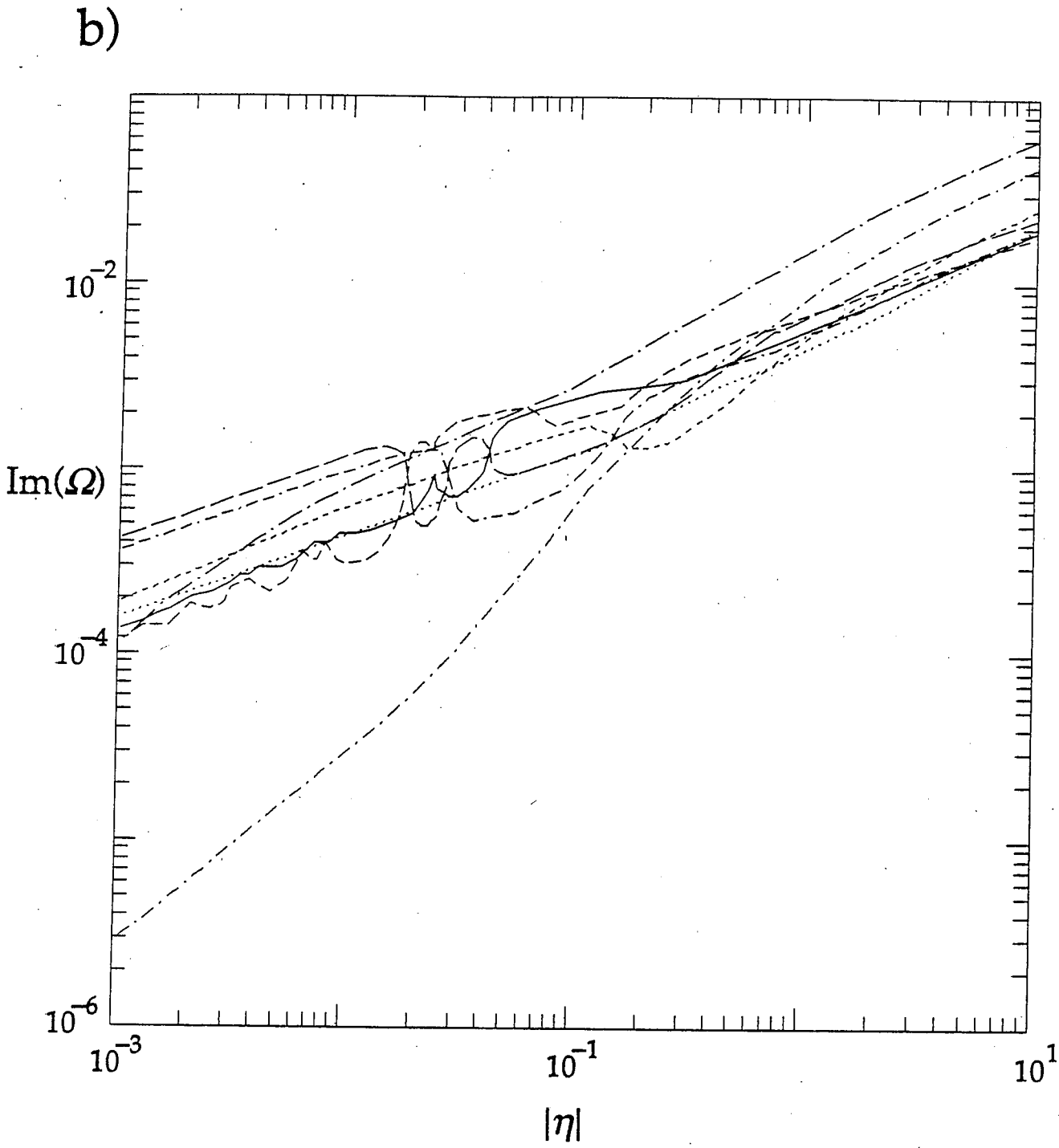

Fig. 6(b) - Berk et al.

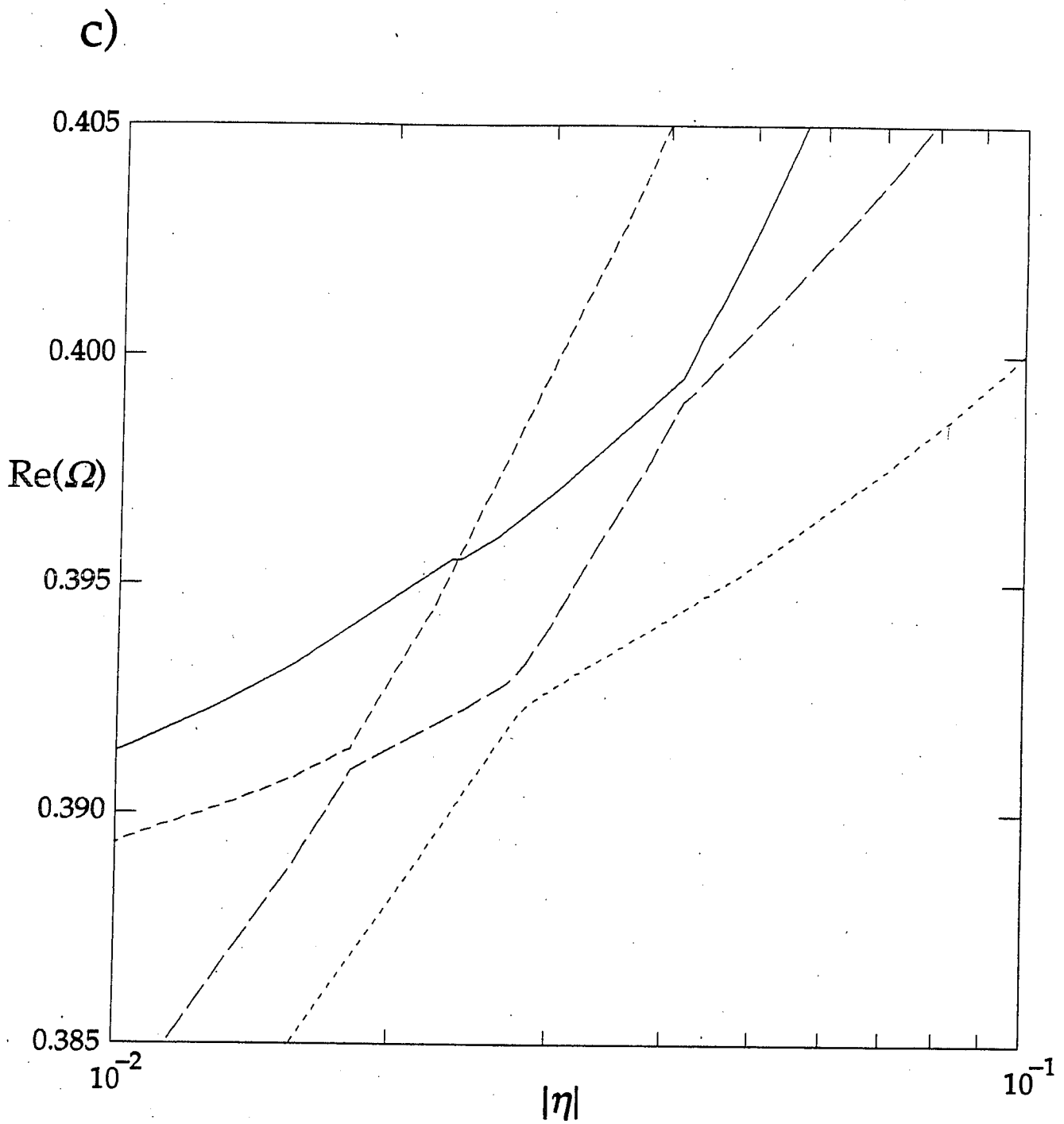

Fig. 6(c) - Berk et al.

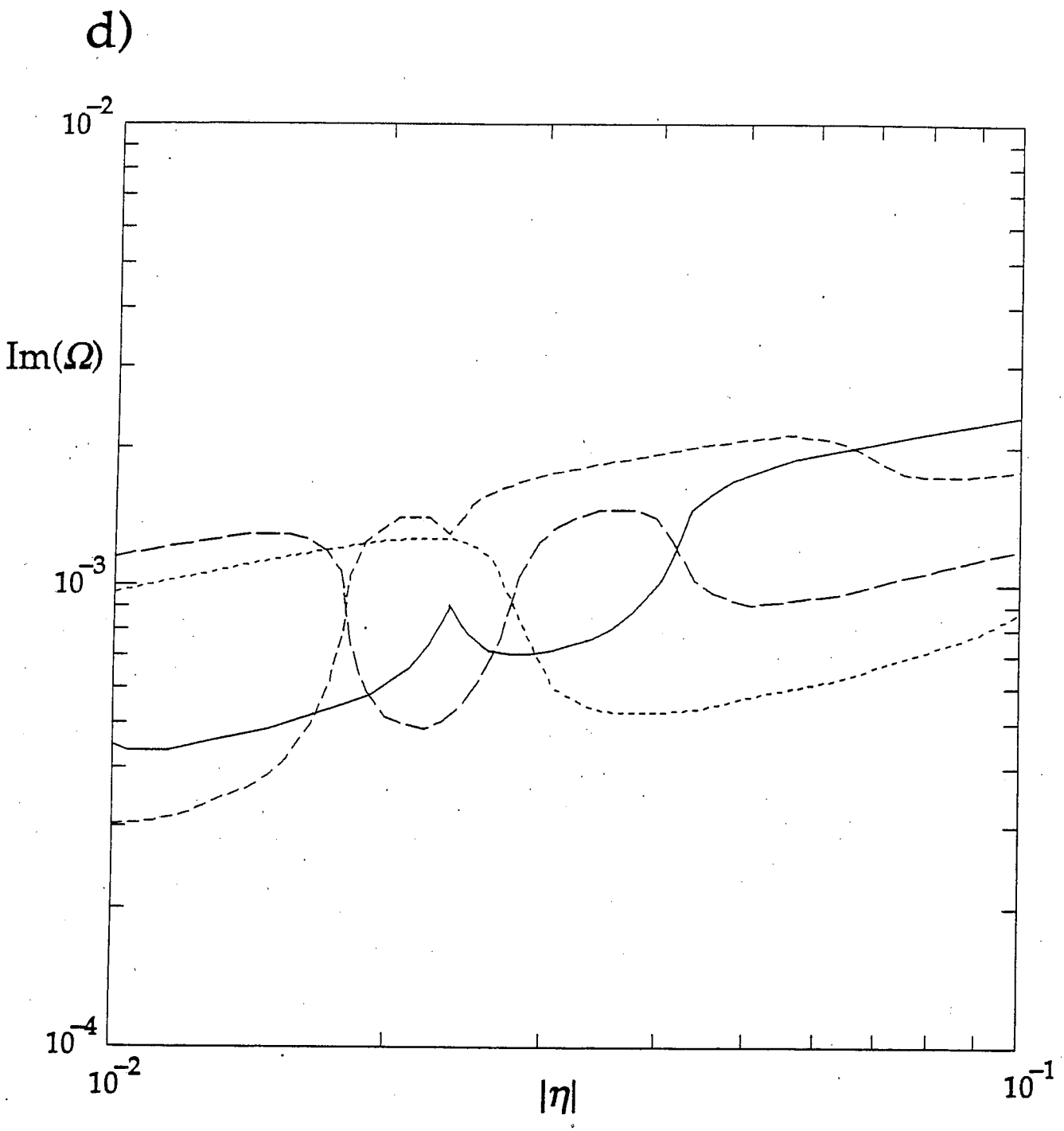

Fig. 6(d) - Berk et al.